ULTRASONIC FIELD MODELING USING DISTRIBUTED POINT SOURCE METHOD (DPSM)

A Thesis report

Submitted in the partial fulfillment of requirements for the award of the degree of

Master of Engineering
in
CAD/CAM & ROBOTICS

Submitted by

SAMEER SHARMA

Roll no.**80781023**

Under the guidance of

Dr. ABHIJIT MUKHERJEE
Director
Thapar University, Patiala

Mr. SANDEEP SHARMA
Sr. Lecturer, MED
Thapar University, Patiala

Mrs. SHRUTI SHARMA
Sr. Lecturer, CED
Thapar University, Patiala

Department of Mechanical Engineering
THAPAR UNIVERSITY PATIALA (PUNJAB)-147004

JUNE-2009

Certificate

This is to certify that the work which is presented in this thesis report entitled, "**Ultrasonic Field Modeling Using Distributed Point Source Method (DPSM)** " being submitted by **Sameer Sharma** in partial fulfillment of requirements for the award of degree of Master of Engineering in CAD/CAM & ROBOTICS, at Mechanical Engineering Department, Thapar University, Patiala, is an authentic record of the initial work carried out by him under the supervision of **Dr. Abhijit Mukherjee , Director,** Thapar University, Patiala, **Mr. Sandeep Sharma,** Sr. Lecturer, Mechanical Engineering Department, Thapar University, Patiala and **Ms. Shruti Sharma**, Sr. Lecturer, Civil Department,Thapar University, Patiala .The matter embodied in this report has not been submitted in part or full to any other university or institute for the award of any degree.

(Dr. Abhijit Mukherjee)
Director
Thapar University, Patiala

(Mr. Sandeep Sharma)
Sr. Lecturer,MED
Thapar University,Patiala

(Ms. Shruti Sharma)
Sr. Lecturer,CED
Thapar University,Patiala

(Dr.S.K.Mohapatra)
Professor & Head, MED
Thapar University,
Patiala.

(Dr.R.K.Sharma)
Dean, Academic Affairs
Thapar University,
Patiala.

ii

Acknowledgement

I take this opportunity to express my sincere gratitude to **Dr. Abhijit Mukherjee, Director**, Thapar University for giving me the opportunity of doing my thesis work under his guidance. I am also thankful to him for his constant supervision and valuable suggestions.

It is my proud privilege to express regards and sincere gratitude to **Mr.Sandeep Sharma, Sr. Lecturer, Mechanical Engineering Department**, Thapar University, Patiala, for his patient listening of my ideas and also suggesting new ways for implementing my ideas by his expert guidance through out my work.

I would like to extend my thanks to **Ms.Shruti Sharma, Sr. Lecturer, Civil Engineering Department,** Thapar University, Patiala, for her guidance and providing necessary information and facilities for the successful completion of my thesis.

I am also thankful to **Dr.S.K.Mohapatra, Head Mechanical Engineering Department,** Thapar University, Patiala, for the motivation and inspiration that triggered me for my thesis work.

I also take this opportunity to thank to the entire faculty and staff of **Mechanical Engineering Deparment,** Thapar University, Patiala, for their help, inspiration and moral support, which went a long way in successfully completion of this report.

Sameer Sharma

(80781023)

Abstract

Modeling of ultrasonic fields in presence of cracks, inclusions in materials is of great interest to the researchers in the field of real time non-destructive evaluation (NDE) and structural health monitoring (SHM). A semi-analytical method Distributed Point Source Method (DPSM) is adopted in this work to model elastic wave field in solid media with and without internal anomalies by using Finite size transducers placed directly on solid and also considering the solid fluid couplant interaction.Trasient state analysis has also been carried out for the same. Present work also contains wave propagation analysis for fluid (homogeneous/non homogeneous) for transducer having non normal incidence.

For transient analysis, tone burst signal is used as input signal and response is observed at different target points and results are found to be matching with the wave velocities in specified media. Ultrasonic field in solid media has been modeled for circular and rectangular shapes of transducer. In later case, fluid-solid interface has been considered and is kept normal as well as non normal angle to wave propagation direction. In both cases, Fast Fourier transformation (FFT) is used to convert time domain signal into frequency domain and inverse FFT is used to again transform results into time domain.

Keywords: DPSM, Tomo-grams, Fluid/Solid Interface, Plates, Anomalies, Wave Propagations, Transducer, Interface

CONTENTS

List of Figures

List of Tables

CHAPTER 1

INTRODUCTION

1.1 Objectives of the present study

Promising gains in the performance and cost-effective maintenance of high-value assets such as aircraft, civil infrastructure and maritime vessels paved the way for recent developments in field of Structural Health Monitoring (SHM).Health of several structures is monitored by recording propagation of stress waves through them. The wave characteristics changes with medium in which waves tend to propagate.

The overall objectives of the present study are:

- Review of literature on propagation of ultrasonic waves through fluid/solid media and ultrasonic field modeling in mentioned mediums using Distributed Point Source Method (DPSM).
- Discretization of transducer surface for source point grid formation.
- Ultrasonic field modeling in homogeneous and non homogeneous fluids when transducer is at non-normal incidence considering both steady state and transient state.
- Field modeling inside a solid when an arbitrary forcing function is applied by transducer in steady and transient states.
- Modeling of ultrasonic field near fluid/solid interface when both steady and transient states have been considered.
- Field modeling inside a plate completely submerged in water with transducer on one side and both sides.
- Ultrasonic field modeling inside plate with an internal defect.
- Modeling Transient wave propagation in plate with and without defect.

1.2 Structural Health Monitoring (SHM) and Non Destructive Testing (NDT)

The process of implementing a damage identification strategy for aerospace, civil and mechanical engineering infrastructure is referred to as structural health monitoring (SHM). Here, damage is defined as changes to the material and/or geometric properties of these systems, including changes to the boundary conditions and system connectivity, which adversely affect the system's performance. A wide variety of highly effective local non-destructive evaluation tools are available for such monitoring. However, the majority of SHM research conducted over the last 30 years has attempted to identify damage in structures on a more global basis. The past 10 years have seen a rapid increase in the amount of research related to SHM as quantified by the significant escalation in papers published on this subject. The increased interest in SHM and its associated potential for significant life-safety and economic benefits has motivated the need of effective testing techniques.Non Destructive Testing emerges as most effective testing technique for SHM because of economical benefits and reduction in testing time (**Joseph L. Rose, 2004[1])**.In next section several NDT techniques have been discussed which are used in different field applications.

NDT signifies the method of testing where testing of specimen is done without changing its geometry and physical properties.NDT is classified into various methods of nondestructive testing, each based on a particular scientific principle. These, due to their particular natures, may lend themselves especially well to certain applications and be of little or no value at all in other applications. Therefore choosing the right method and technique is an important part of the performance of NDT **(Schmerr, L., 1998 [2])**.

Following are the commonly used **NDT** techniques:

1.2.1 Visual and Optical Testing: The most basic NDT method is visual examination. Visual examiners follow procedures that range from simply looking at a part to see if surface imperfections are visible, to using computer controlled camera systems to automatically recognize and measure features of a component.

1.2.2 Penetrant Testing: Test objects are coated with visible or fluorescent dye solution. Excess dye is then removed from the surface, and a developer is applied.

The developer acts as blotter, drawing trapped penetrant out of imperfections open to the surface. Thus making otherwise invisible defects visible.

1.2.3 Magnetic Particle Testing: This method is accomplished by inducing magnetic field in a ferromagnetic material and then dusting the surface with iron particles. Surface and near-surface imperfections distort the magnetic field and the concentrate iron particles near imperfections provide a visual indication of the flaw.

1.2.4 Electromagnetic or Eddy Current testing: Electrical currents are generated in a conductive material by an induced alternating magnetic field. Interruptions in the flow of eddy currents, caused by imperfections, dimensional changes, or changes in the materials conductive and permeability properties, can be detected with the proper equipment.

1.2.5 Radiography: It involves the use of penetrating gamma or X-ray radiation to examine parts and products for imperfections. An X-ray generator or radioactive isotope is used as a source of radiation. Radiation is directed through a part and on to a film. Possible imperfections are indicated as density changes on the film in the same manner as medical X-ray shows broken bones.

1.2.6 Ultrasonic Testing: Ultrasonic use transmission of high-frequency sound waves into a material reflected and transmitted waves are captured for detecting presence of defects. The most commonly used ultrasonic testing techniques are pulse echo and pulse transmission.

1.2.7 Acoustic Emission Testing: When a solid material is stressed, imperfections within the material emit short bursts of acoustic energy called "emissions." as in ultrasonic testing; acoustic emissions can be detected by special receivers. Emission sources can be evaluated through the study of their intensity, rate, and location.

All the mentioned methods have their own application fields. Present work is focused on ultrasonic testing of materials and mathematical modeling of the ultrasonic field generated by piezoelectric transducer in different mediums using DPSM (Distributed point source method) (**Placko and Kundu, 2007 [2]**).

1.3 Basics of Wave Propagation

1.3.1 Introduction:

Wave propagation theory comprises of the study of basic terminology which is used to define wave propagation through different mediums. Propagation generally points to the movement of waves within solid, various modes that can be developed and their conversion to other modes.

1.3.2 Sound Waves (V.Bindal, 1998[19])

Sound is a series of compression waves that moves through air or other materials. These sound waves are created by the vibration of some object, like a radio loudspeaker. The waves are detected when they cause a detector to vibrate. Sound waves have specific properties while propagating in a medium. Following terms are generally used to define the state of sound waves:

a) Frequency (υ): All sound waves oscillate at a specific frequency, or number of vibrations or cycles per second. Ultrasonic flaw detection applications utilize frequencies between 500,000 and 10,000,000 cycles per second (500 kHz to 10 MHz). At frequencies in the megahertz range, sound energy does not travel efficiently through air or other gasses, but it travels freely through most liquids and common engineering materials.

b) Velocity (c): The speed of a sound wave varies depending on the medium through which it is traveling, affected by the medium's density and elastic properties. Different types of sound waves (see modes of propagation, below) travel at different velocities.

c) Wavelength (λ): It is the distance between any two corresponding points in the wave cycle as it travels through a medium. Wavelength is related to frequency and velocity by the simple equation

$\lambda = c/\upsilon$ **W**here,

λ = wavelength, c = sound velocity, υ = frequency

In ultrasonic flaw detection, the generally accepted lower limit of detection for a small flaw is one-half wavelength. Anything smaller than that will be invisible.

d) Acoustic impedance (Z)*:* Sound travels through materials under the influence of sound pressure. Because molecules or atoms of a solid are bound elastically to one another, the excess pressure results in a wave propagating through the solid. The **Acoustic impedance** (**Z**) of a material is defined as the product of its density (ρ) and acoustic speed in medium (c)

$$Z = \rho / c$$

Acoustic impedance is important in determining acoustic transmission and reflection at the boundary of two materials having different acoustic impedances.

As discussed above waves require medium to travel or propagate. There are various modes in which a wave can travel through a medium either fluid or solid. Snell's Law proves the worth of Acoustic impedance.

1.3.2 Snell's Law:

It states that When sound waves travels from one medium to another medium having different acoustic impedances it tends to change its direction depending upon the differences in Acoustic impedances of two mediums. Snell's Law holds true for shear waves as well as longitudinal waves and can be written as follows.

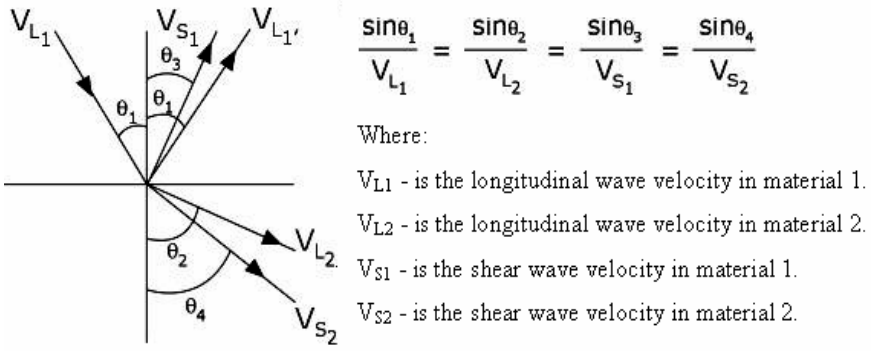

Figure 1.1 Snell's Law Showing Relationship between Velocity and Angle of Waves

1.3.2.1 Reflection and Transmission Coefficient at Oblique Incidence*:*

For a plane wave front incident obliquely on a plane interface between two media, such that the normal to the front and the interface subtend an angle A and where the normal to the interface and the emergent transmitted wave front subtend an angle B,

the simplified corresponding expressions for pressure Reflectivity (R) and Transmissivity (T) are given by:

$$R = \frac{Z_2 \cos A - Z_1 \cos t}{Z_2 \cos A + Z_1 \cos t} \qquad T = \frac{2 Z_2 \cos A}{Z_2 \cos A + Z_1 \cos t}$$

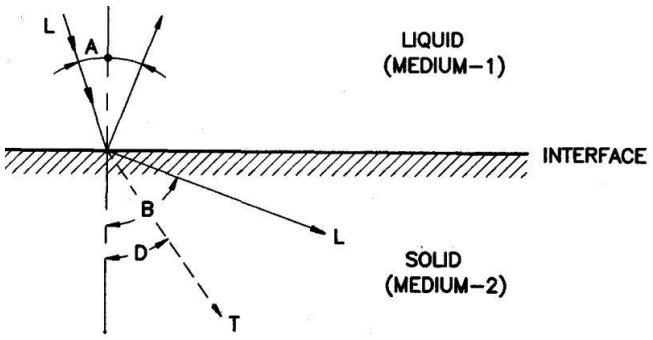

Figure 1.2 Reflection, Refraction and Mode Conversion of Acoustic Wave

For small angles of incidence sound waves traveling at an angle from medium 1 give rise to the longitudinal waves and shear waves in the medium 2. Such a situation is very confusing for NDT inspection, as both of these waves present in the medium 2, travel at different velocities and give rise to separate signals on the flaw detector screen. As a solution to this problem the longitudinal wave is not allowed to enter the test piece and is eliminated by total internal reflection.

1.3.3 Modes of Wave Propagation

In ultrasonic technique for NDT, different types of waves must be studied to understand the undergoing physical phenomena. The objective is to model the wave propagation for different type of ultrasonic sound waves, and use the available software to visualize these waves. Wave is a disturbance that travels, or propagates, from one region of space to another. Depending upon the pattern of motion of particles, waves can be classified as shown in table 1.1

Wave Types in Solids	Direction of motion of Vibrating Particles
Longitudinal	Parallel to wave direction
Transverse (Shear)	Perpendicular to wave direction
Surface - Rayleigh	Elliptical orbit - symmetrical mode
Plate Wave - Lamb	Component perpendicular to surface (extensional wave)
Plate Wave - Love	Parallel to plane layer, perpendicular to wave direction

Table 1.1 Types of Waves Propagation

1.3.3.1 Longitudinal waves,

The oscillations occur in the longitudinal direction or the direction of wave propagation. Since compressional forces are active in these waves, they are also called pressure or compressional waves. They are also sometimes called density waves because their particle density fluctuates as the wave travels. Compression waves can be generated in liquids, as well as solids.

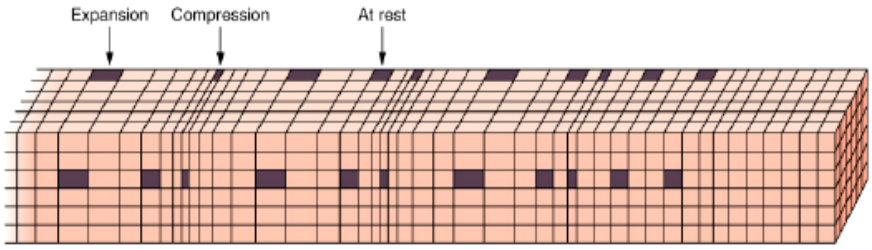

Figure 1.3 Longitudinal Waves

1.3.3.2 Transverse or Shear wave,

The particles oscillate at a right angle to the direction of propagation. Shear waves require an acoustically solid material for effective propagation, and therefore, are not effectively propagated in materials such as liquids or gasses. Shear waves are relatively weak when compared to longitudinal waves. In fact, shear waves are usually generated in materials using some of the energy from longitudinal waves.

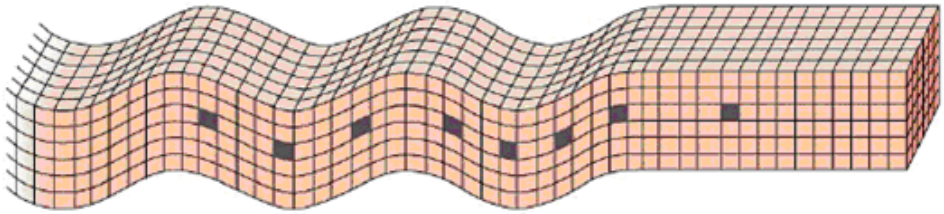

Figure 1.4 Transverse Waves

1.3.3.3 Surface (or Rayleigh) waves

It travels at the surface of a relatively thick solid material penetrating to a depth of one wavelength. Surface waves combine both a longitudinal and transverse motion to create an elliptic orbit motion as shown in the figure 1.5. The major axis of the ellipse is perpendicular to the surface of the solid. As the depth of an individual atom from the surface increases the width of its elliptical motion decreases. Surface waves are generated when a longitudinal wave intersects a surface near the second critical angle and they travel at a velocity between 0.87 and 0.95 of a shear wave. Rayleigh waves are useful because they are very sensitive to surface defects (and other surface features) and they follow the surface around curves. Because of this, Rayleigh waves can be used to inspect areas that other waves might have difficulty reaching.

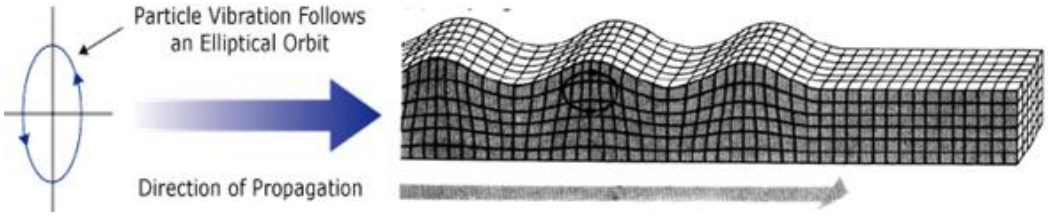

Figure 1.5 Rayleigh Waves

1.3.3.4 Plate waves

These similar to surface waves except they can only be generated in specimen which are a few wavelengths thick. Lamb waves are the most commonly used plate waves in NDT. Lamb waves are complex vibrational waves that propagate parallel to the test surface throughout the thickness of the material. Propagation of Lamb waves depends on the density and the elastic material properties of a component. They are also influenced a great deal by the test frequency and material thickness. Lamb waves are generated at an incident angle in which the parallel component of the velocity of

the wave in the source is equal to the velocity of the wave in the test material. Lamb waves will travel several meters in steel and so are useful to scan plate, wire, and tubes.

1.3.3.5 Lamb waves,

With these waves a number of modes of particle vibration are possible, but the two most common are symmetrical and asymmetrical. The complex motion of the particles is similar to the elliptical orbits for surface waves. Symmetrical Lamb waves move in a symmetrical fashion about the median plane of the plate. This is sometimes called the extensional mode because the wave is "stretching and compressing" the plate in the wave motion direction. Wave motion in the symmetrical mode is most efficiently produced when the exciting force is parallel to the plate. The asymmetrical Lamb wave mode is often called the "flexural mode" because a large portion of the motion moves in a normal direction to the plate, and a little motion occurs in the direction parallel to the plate. In this mode, the body of the plate bends as the two surfaces move in the same direction.

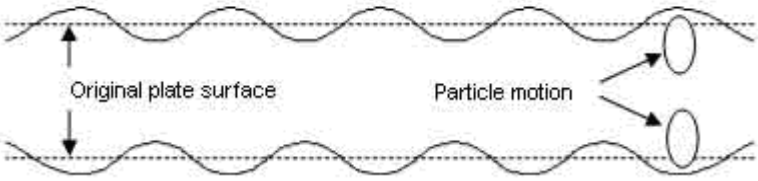

a.) Asymmetric Modes

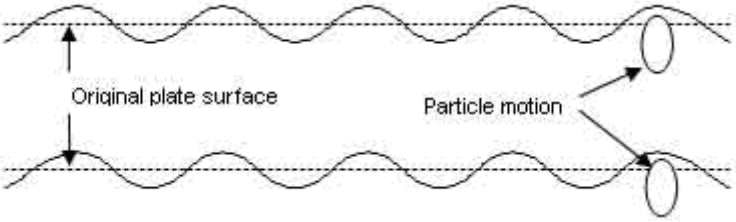

b.) Symmetric Modes

Figure 1.6 Asymmetric and Symmetric Mode Shapes for Plate Waves

1.4 Ultrasonics for NDT

Ultrasonic testing (UT) utilizes high frequency (> 20 kHz) sound energy to conduct examinations and make measurements. A typical UT inspection system consists of several functional units, such as the Pulser/Receiver, transducers, data acquisition instruments and display devices. A Pulser/Receiver is an electronic device that can produce high voltage electrical pulses. Driven by the Pulser, the transducer generates high frequency ultrasonic energy. The sound energy is introduced and propagates through the materials in the form of waves. When there is a discontinuity (such as a crack) in the wave path, part of the energy will be reflected back from the flaw surface. The reflected wave signal is transformed into an electrical signal by the transducer and is displayed on a screen.

As compared to other NDT methods, Ultrasonic testing technique has following advantages,

1. It is sensitive to both surface and subsurface discontinuities.
2. The depth of penetration for flaw detection or measurement is superior to other NDT methods.
3. Only single-sided access is needed when the pulse-echo technique is used.
4. It is highly accurate in determining reflector position and estimating size and shape.

1.4.1 Methods of Ultrasonic Testing:

Following are the three methods generally used:

1. Pulse echo method
2. Through transmission method

1.4.1.1 Pulse Echo Method:

In the pulse-echo method, a piezoelectric transducer with its longitudinal axis located perpendicular to and mounted on or near the surface of the test material is used to transmit and receive ultrasonic energy. The ultrasonic waves are reflected by the opposite face of the material or by discontinuities, layers, voids, or inclusions in the material, and received by the same transducer where the reflected energy is converted into an electrical signal. The electrical signal is computer processed for display on a video monitor or TV screen. The display can show the relative thickness of the material, depth into the material where flaws are located, and (with proper scanning hardware and software), where the flaws are located in the X-Y plane.

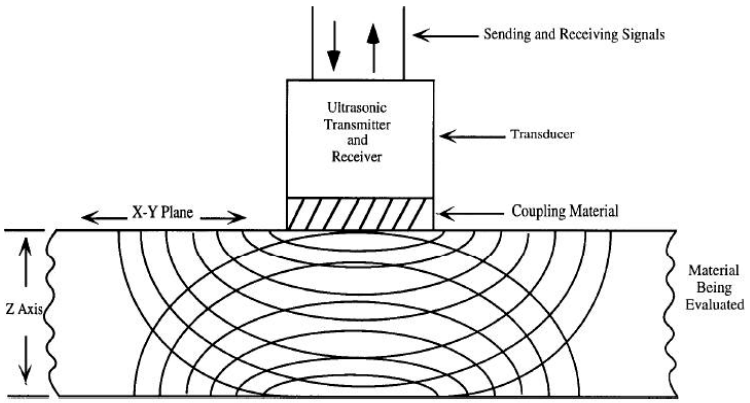

Figure 1.7 Pulse Echo Method

1.4.1.2 Through Transmission Method:

In the through-transmission method, an ultrasonic transmitter is used on one side of the material while a detector is placed on the opposite side. One unit acts as transmitter and the other unit as receiver. Beam from the transmitter T travels through the material to its opposite surface where the receiving transducer R is placed. Scanning of the material using this method will result in the location of defects, flaws and inclusions in the X-Y plane.

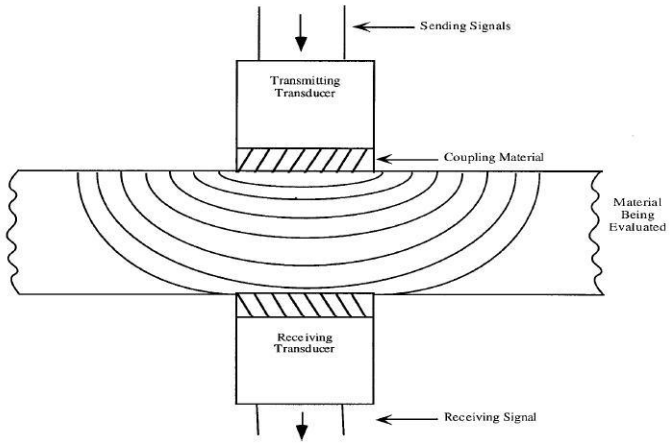

Figure 1.8 Pulse Transmission Method

In this chapter it is concluded that the ultrasonic testing form an important method in NDT technique. For effective use of ultrasonic in NDT. It is important to understand various terms and issues related to it.

1.5 Organization of Work

Present work is subdivided into smaller work elements and these have been compiled into chapters accordingly. Chapter one contains study of ultrasonic testing techniques and basics of wave propagation which has been used to model ultrasonic field. Chapter two discusses prons and cons of various numerical modeling techniques which .can be used to model ultrasonic field in different media. Chapter three comprises of literature review in field of SHM and DPSM.Chapter four presents the basic theory of DPSM technique used to model ultrasonic field in fluid and solid media. Chapter five contains the results and discussion of MATHCAD programs which have been developed for modeling of field in various cases as discussed in objectives. Finally conclusion and future scope of presented work has been discussed.

CHAPTER 2

MODELING OF WAVE PROPAGATION PROBLEMS

There are various methods for numerical modeling of wave propagation problems. These methods either use time based approach or frequency based techniques. Some of them are hybrid. The characteristics of wave propagation problems are that the frequency content of the exciting force is very high. As discussed earlier, at very high frequencies the system becomes mass dominated where inertial effects need to be very accurately modeled. Some popular methods of modeling wave propagation are:

(a) Ray Tracing Method
(b) Spectral Element Method(SEM)
(c) Finite Element Method(FEM)
(d) Distributed Point Source Method(DPSM)

2.1 Ray Tracing Method

In this method, the path of waves emerging out of a point or a group of points is traced as rays through all interfaces. Ray tracing is useful when only a few trains of wave emerge and they traverse through simple interfaces **(Figure 2.1)**.

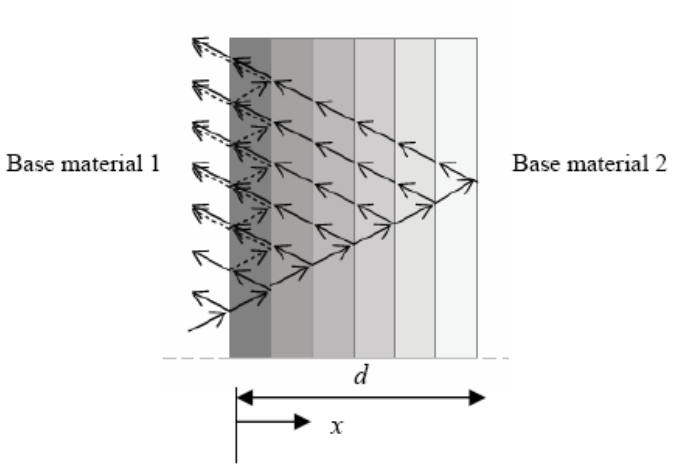

Figure 2.1 One Dimensional Stress Wave Propagation Through Discretely Layered FGM

A simple elegant, one-dimensional model based on ray tracing the path of wave movement was proposed by Bruck (2000) to develop insight into stress wave

management issues in graded materials. The mentioned paper contains excellent validation material for characterization of functionally graded materials (FGM). Time-history profiles of reflected stress waves are presented for Alumina-Aluminum FGM. Amplitude attenuation and time delay in reaching peak reflected stress aspects are also discussed. This method is independent of time or frequency techniques **(Bruck, H., 2000[3])**.

Limitations:

- This method is limited only up to one dimension wave propagation and cannot be extended to two or three dimensions.
- It cannot be used for arbitrary forcing functions.

2.2 Spectral Element Method (SEM)

One of the shortcomings of ray tracing method is its difficulty in extending it to multiple wave trains or multi-dimensions. In the spectral approach (Doyle, 1989), the time forcing function is transformed into frequency function through Fast Fourier Transform (FFT). The problem is solved for one frequency at each time and traversing through a window of frequencies with a small increment. After all the solutions have been obtained in frequency domain an inverse FFT is carried out to obtain the time response of the structure. The response function for a simple material interface can be expressed exactly. Therefore, a super-convergent element is obtained. For multiple interfaces a finite element like discretization can be employed. As a result, a system matrix is developed for the entire structure from the set of linear simultaneous equations. The super-convergence ensures that very few elements are required to model the structure. Moreover, satisfaction of infinite boundary conditions is very easy in this technique. The inertial effects are exactly represented and hence often-exact solutions are obtained for the transformed partial differential equation. However, often-approximate solutions are sought.

The solutions in wave propagation are general functions of space and time. If the time variation of the solution is focused on at a particular point in space, then it has the spectral representation

$$u(x_1, y_1, t) = f_1(t) = \sum C_{1n} e^{i\omega t} \qquad (2.1)$$

In its simplest terms, the solutions to a waves problems is represented as,

$$u(x) = \sum_n \left\{ C_1 e^{ik_1 x} + C_2 e^{ikx} + \ldots + C_{mn} e^{ik_m x} \right\} e^{i\omega t} = \sum \hat{F}_n G(K_{mn} x) e^{i\omega t} \tag{2.2}$$

Where G is the analytically known transfer function of the problems. It is a function of position x and has different numerical values at each frequency. The transform solution is the obtained by evaluating the product,

$$\hat{u}_n = \hat{F}_n G(k_{mn}) \tag{2.3}$$

at each frequency. This is finally reconstructed in the time domain by the use of the inverse FFT. In the process, it is necessary to realize (when using the FFT to perform the inversion) that F_nG is evaluated only up to the Nyquist frequency and the remainder is obtained by imposing that it must be complex conjugate of the initial part, This ensures that reconstructed time history is real only.

Limitations:

- Exact solutions for complex differential equations are difficult to obtain, hence this method becomes inefficient in this case
- Non-linear problems are difficult to solve using this approach.

The above two methods are useful to determine stress wave propagation in the 1-D models; however they prove to be futile when complex models are to be analyzed. In order to analyze linear and non-linear problems, conventional FEM proves to be more useful.

2.3 Finite Element Method (FEM)

This is conventional and versatile method of wave analysis where the domain is discretized in small module called finite element and many professional software can handle this analysis. A very fine mesh of finite elements is necessary to model inertia effect correctly. Also time interval (step) required is also small to model given input signal. Therefore this method is inefficient in modeling semi-infinite elements, whereas for non-linear problems, conventional FEM proves to be more useful.

2.4 Distributed Point Source Method (DPSM)

This method is used specifically for modeling of ultrasonic field .The main originality of DPSM method is that it is not necessary to mesh the totality of the computation volume, but only the surface of interest, in the contrary to a classical finite elements method. The implementation of the model simply requires Discretization of the active surface of the transducer or the interfaces to obtain an array of point sources, so that the initial complexity is changed into a superposition of elementary problems**(Kundu et al ,2000[4]).**

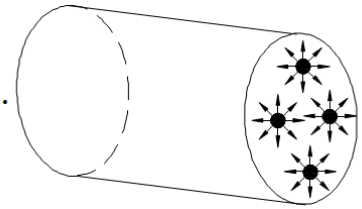

Figure 2.2 Discretization of Transducer Face

First step in DPSM leap towards discritization of transducer surface into number of source points as shown in Figure 2.2.It is based on principle that if the front face of a transducer is considered as the main source of an ultrasonic field, then the ultrasonic field generated by that source can be assumed to be the summation of the ultrasonic fields generated by a number of point sources distributed on transducer source. A harmonic point source, which expands and contracts alternately, can be represented by a point and a sphere as shown in Figure 2.3 a. The point represents the contracted position and the sphere represents the expanded position. When a large number of point sources are placed side by side on a plane surface, then the contacted and expanded positions are shown in Figure 2.3b. The combined effect of a large number of point sources placed side by side is shown in Figure 2.3c. From this figure 2.3 it is clear that the combined effect of a large number of point sources distributed on a plane surface is the vibration of particles in the direction normal to the plane surface. Non-normal components of motion at a point on the surface generated by neighboring source points cancel each other as shown in Figure 2.3d However, non normal components do not vanish along the edge of surface. The particles not only vibrate normal to the surface but also expand to a hemisphere and contract to a point on the edge as shown.

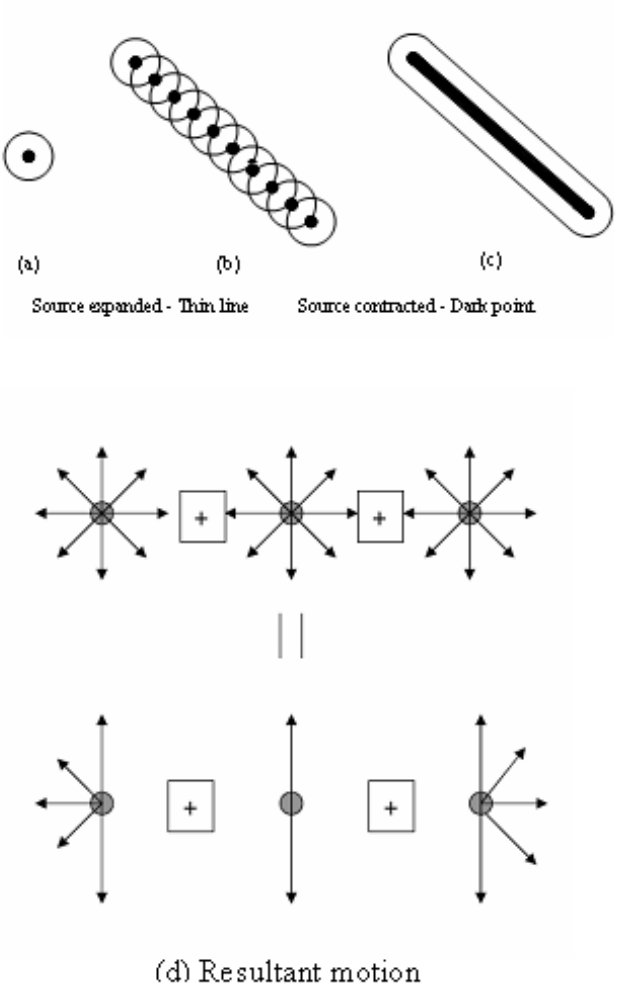

Figure 2.3 Source Point and Resultant Motion of Waveforms

Figure 2.4. shows spherical waves generated by a point source in an infinite medium, cylindrical waves generated by a line source and plane waves generated by an infinite plane. The pressure field due to a finite plane source can be assumed to be the summation of pressure fields generated by a number of point sources distributed over the finite source as shown in Figure 2.3. The finite source can be the front face of the transducer.

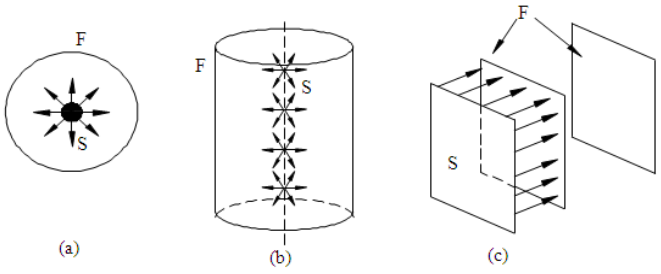

Figure 2.4 Different Types of Wave fronts

CHAPTER 3

LITERATURE REVIEW

This chapter presents a review of literature on propagation of elastic waves through fluids and solids. This gives an idea of study carried out in this area up to this stage.

This work can be classified based on:

1. Historical Overview of SHM
2. Analytical studies focused on wave's application for damage detection.
3. Experimentation done in ultrasonic testing areas.
4. Work done in DPSM area.

3.1 Brief historical overview of SHM

More recently, the development of SHM approaches has been closely coupled with the evolution, miniaturization and cost reductions of digital computing hardware. In conjunction with these developments, SHM has received considerable attention in the technical literature and a brief summary of the developments in this technology over the last 30 years is presented below.

During the 1970s and 1980s the oil industry made considerable efforts to develop vibration-based damage detection methods for offshore platforms. This damage detection problem is fundamentally different from that of rotating machinery because the damage location is unknown and because the majority of the structure is not readily accessible for measurement. To circumvent these difficulties, a common methodology adopted by this industry was to simulate candidate damage scenarios with numerical models, examine the changes in resonant frequencies that were produced by these simulated changes, and correlate these changes with those measured on a platform. A number of very practical problems were encountered including measurement difficulties caused by platform machine noise,

instrumentation difficulties in hostile environments, changing mass caused by marine growth, varying fluid storage levels, temporal variability of foundation conditions and the inability of wave motion to excite higher vibration modes. These issues prevented adaptation of this technology and efforts at further developing this technology for offshore platforms were largely abandoned in the early 1980s **(Charles R.; Keith Worden, 2006[5])**.

The aerospace community began to study the use of vibration-based damage detection during the late 1970s and early 1980s in conjunction with the development of the space shuttle. This work has continued with current applications being investigated for the National Aeronautics and Space Administration's space station and future reusable launch vehicle designs. **The shuttle modal inspection system (SMIS)** was developed to identify fatigue damage in components such as control surfaces, fuselage panels and lifting surfaces. These areas were covered with a thermal protection system making them inaccessible and, hence, impractical for conventional local non-destructive examination methods. The SMIS has been successful in locating damaged components that are covered by the thermal protection system. All orbiter vehicles have been periodically subjected to SMIS testing since 1987.Changes in stiffness indices as assessed from the two model updates are used to locate and quantify the damage. Since the mid-1990s, studies of damage detection for composite materials have been motivated by the development of a composite fuel tank for a reusable launch vehicle. The failure mechanisms, such as de-lamination caused by debris impacts, and corresponding material response for composite fuel tanks are significantly different to those associated with metallic structures. Moreover, the composite fuel tank problem presents challenges because the sensing systems must not provide a spark source. This challenge has led to the development of SHM based on fibre optic sensing systems.**Boller & Buderath, 2007[6] provid**e a more detailed discussion of SHM applied to aerospace structures in a subsequent article contained in this theme issue.

The civil engineering community has studied vibration-based damage assess-ment of bridge structures and buildings since the early 1980s. Environmental and operating condition variability presents significant challenges to the bridge monitoring application. The physical size of the structure also presents many practical challenges for vibration-based damage assessment. Regulatory requirements in Asian countries, which mandate that the companies that construct the bridges periodically certify their

structural health, are driving current research and commercial development of bridge SHM systems **(Kim, J.-H., H.-S. Jeon, and C.-W. Lee,1992[7]).** These challenges include the development of methods to optimally define the number and location of the sensors; identification of the features sensitive to small damage levels; the ability to discriminate changes in these features caused by damage from those caused by changing environmental and/or test conditions; the development of Statistic methods to discriminate features from undamaged and damaged structures; and performance of comparative studies of different damage identification methods applied to common datasets. These topics are currently the focus of various research efforts by many industries including defence, civil infrastructure, automotive and semiconductor manufacturing where multi-disciplinary approaches are being used to advance the current capabilities of SHM.

3.2 Analytical Studies Focused on Wave's Application for Damage Detection

Abrahams et al. ,1992[8] have examined the scattering of Rayleigh waves by an inclined two-dimensional plane surface breaking crack in an isotropic elastic half-plane. **Biwa et al.,2003[9]** presented a computational procedure for multiple wave scattering in unidirectional fiber-reinforced composite materials. Bruck ,2000[3] proposed a simple, one-dimensional model to develop insight into stress wave management issues. This model is initially applied to FGMs with discrete layering, and then extended to continuously graded architectures. The benefit of the FGM over the sharp interface is to introduce a time delay to the reflected wave propagation when stresses approach peak levels which are highly dependent on the composition gradient and the differences in base material properties. The propagation of the lowest-order, antisymmetric a_0 mode through the joint is examined.

Gilchrist, (1999) showed how horizontal symmetric crack-like defects can be detected rapidly in thin isotropic plates by using longitudinal ultrasonic waves.**Joshi et al., 2003[10]** discussed the characterization of functionally graded materials. **Karagiozova (2004)** obtained the speeds of the stress waves that can propagate in an elastic–plastic medium with isotropic linear strain hardening in a plane stress state, to analyse the influence of the transient deformation process on the initiation of buckling in square tubes under axial impact. It is shown that the plastic wave speeds depend on the stress state and on the direction of wave propagation. The material hardening

properties have a stronger effect on the speed of the slow plastic wave, while the shear stress affects both the speeds of the fast and slow plastic waves.

Krawczuk et al., 2004[11] presented the method of analysis of the wave propagation process in cracked plates. Elastic behaviour of the plate at the crack location was considered as a line spring with a varying stiffness along the crack length.**Lima and Hamilton (2003)** investigated the propagation of finite-amplitude waves in a homogeneous, isotropic, stress-free elastic plate theoretically. Mal (2002) analysed elastic waves generated by localized dynamic sources in structural composites. **Sharma et al. (2004)** studied the thermoelastic interaction in an infinite viscoelastic, thermally conducting plate whose upper and lower surfaces of the plate are subjected to stress-free, thermally insulated or isothermal conditions.**Voyiadjis and Baluch (1981)** developed a technical theory for the flexural motions of isotropic elastic plates, taking into account the influence of transverse normal strain and transverse normal stress, together with rotatory inertia and transverse shear.

Wang (2002) investigated shear horizontal (SH) wave propagation in a semi-infinite solid medium surface bonded by a layer of piezoelectric material abutting the vacuum. The dispersive characteristics and the mode shapes of the deflection, the electric potential, and the electric displacements in the thickness direction of the piezoelectric layer are obtained theoretically.

Yang et al. (1966) deducted a two-dimensional linear theory of motions of heterogeneous plates. Transverse shear deformations and rotatory inertia were also included.

Zak et al. (2006) present certain results of the analysis of wave propagation in an isotropic panel with damage in the form of a fatigue crack.

Mukherjee et al.(2006) used ultrasonic piezoelectric transducers that are employed in various applications to produce a broadband frequency spectrum. However, interference from the sympathetic pulses generated by the transducer limits the duration of the waveform to a very short time. The paper discusses grading of the transducer as a means of alleviating the sympathetic pulses .a simple one dimensional model based on the spectral approach has been presented. The piezoelectric constant e_{33} is graded in various manners and their performances are evaluated .the signal qualities are evaluated by their Euclidean distances from the applied voltage pulse. Linearly graded transducers show the best results.

3.3 **Experimentation**

Francesco et al. (2004) dealt with the propagation of ultrasonic guided waves in adhesively bonded lap–shear joints. **Phillips et al (1978)** studied mechanical stress wave propagation in a long, thin, isotropic, elastic rod containing a single transverse edge crack theoretically and experimentally and found that one-dimensional wave theories, coupled with an effective "compliance" of the cracked region, predict reasonably well the observed dynamic strains induced by a longitudinal impact.**Giurgiutiu (2005)** explored the capability of embedded piezoelectric wafer active sensors (PWAS) to excite and detect tuned Lamb waves for structural health monitoring.

Mukherjee et al propagation through solids to locate the position and extent of crack with single actuator and several surface mounted sensors. **Mukherjee et al ,2006[12]** did the characterization of discretely graded materials using acoustic wave propagation.

3.4 **DPSM technique**:

DPSM technique for ultrasonic field modeling was first developed by Placko and Kundu (2001). They successfully used this technique to model ultrasonic fields in a homogeneous fluid, and in a non-homogeneous fluid with one interface (Lee et al. 2002, Placko et al. 2002) and multiple interfaces (Banerjee, Kundu and Placko, 2005). The interaction between two transducers, for different transducer arrangements and source strengths, placed in a homogeneous fluid has been studied by **Ahmad et al.,2003[13]**. The scattered ultrasonic field generated by a solid scatterer of finite dimension placed in a homogeneous fluid has also been modeled by the DPSM technique (Placko et al. 2003). Recently the method has been extended to model the phased array transducers **(Ahmad et al., 2005[14])**. All these works modeled the ultrasonic field in a fluid medium. The ultrasonic field generated inside the solid half space or the leaky waves in the fluid produced by the guided waves propagating along the fluid –solid interface has been modeled in present work. The modeling of ultrasonic field inside solid has been done using Green functions for displacement and stress (**Banerjee et al, 2007[18])**.Furthetmore ultrasonic field has also been modeled in plates with crack and without crack in both steady state and transient state.

CHAPTER 4

DISTRIBUTED POINT SOURCE METHOD (DPSM)

4.1 Theory of DPSM

As explained, if the front face of a transducer is considered as the main source of an ultrasonic field, then the ultrasonic field generated by that source can be assumed to be the summation of the ultrasonic fields generated by a number of point sources distributed near that finite source. Any interface is responsible for generating reflected and transmitted ultrasonic fields. Therefore, the interface can be replaced by two layers of sources - one layer generating the reflected field and the second layer generating the transmitted field. Two layers of interface sources are distributed on two sides of the interface. Strengths of the point sources distributed near the transducer face and the interface are obtained by satisfying the boundary conditions and interface continuity conditions. For solving this problem we need to calculate the stress and displacement Green's functions in the solid, and pressure and displacement Green's functions in the fluid.

4.2 Computation of Ultrasonic Field in a Homogeneous Fluid.

4.2.1 Computation of Velocity and Pressure Fields in a Fluid Generated by a Set of Point Sources.

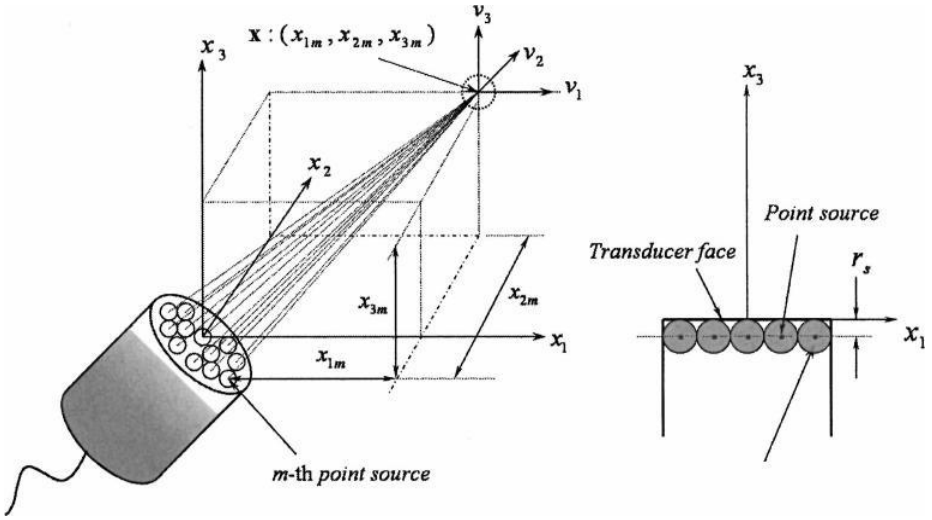

Figure 4.1 Calculation of Velocity and Pressure Field on a Single Point

For a flat surface transducer, where all point sources are excited at the same time, the pressure field generated at a point x (see Fig. 4.1) by the transducer can be obtained by integrating the spherical waves, as done in the conventional surface integral technique. The combined effect of a large number of point sources distributed over a plane surface is the vibration of the surface points in a direction normal to the surface. Following the surface integral technique the pressure field at point x (see Fig. 4.l(b)) in front of the transducer can be obtained by integrating the spherical waves.

$$p(x) = \int B \frac{e^{ik_f r}}{r} ds \tag{4.1}$$

Where '***p'*** is the pressure and '***B'*** represents the source velocity. Therefore '***B'*** is a measure of the strength of the point sources, '***ds'*** represents the elementary area on the surface of the source, '$\boldsymbol{k_f}$' is the wave number in the fluid for a particular frequency of excitation, and '***r***' is the radial distance of the point x from the source. This integral equation can also be written in the summation form.

$$p(x) = \sum_{m=1}^{n} \left(\frac{B}{4} \nabla Sm \right) \frac{e^{ik_f r_m}}{r_m} \tag{4.3}$$

$$\hat{p}_m(r) = A_m \frac{e^{ik_f r_m}}{r_m} \tag{4.4}$$

Let the source strength of the m^{th} point source be '***Am***' and '$\boldsymbol{r_m}$' be the distance of the observation point or target point x from the m^{th} point source. Therefore, pressure at any point at a distance '$\boldsymbol{r_m}$' from the m^{th} point source with source strength '$\boldsymbol{A_m}$' can be written as

$$\hat{p}_m(r) = A_m \frac{e^{ik_f r_m}}{r_m} \tag{4.5}$$

For '*N*' number of point sources distributed on a surface, the pressure at the target point is given by

$$\hat{p}(x) = \sum_{m=1}^{N} P_m(r_m) = \sum_{m=1}^{N} A_m \frac{e^{ik_f r_m}}{r_m} \tag{4.6}$$

From the pressure-velocity relation , the velocity in the radial direction at a distance '***r'*** from the **mth** point source can be written as

$$\hat{v}_m(r) = \frac{A_m}{i\omega\rho}\frac{\partial}{\partial r}\left(\frac{e^{ik_f r_m}}{r_m}\right) \qquad \therefore \hat{v}_m(r) = \frac{A_m}{i\omega\rho}\frac{e^{ik_f r_m}}{r_m}\left(ik_f - \frac{1}{r}\right)$$

(4.7)

The three components of velocity are

$$\hat{v}_{1m}(r) = \frac{A_m}{i\omega\rho}\frac{x_1 e^{ik_f r}}{r^2}\left(ik_f - \frac{1}{r}\right) \tag{4.8}$$

$$\hat{v}_{2m}(r) = \frac{A_m}{i\omega\rho}\frac{x_2 e^{ik_f r}}{r^2}\left(ik_f - \frac{1}{r}\right) \tag{4.9}$$

$$\hat{v}_{3m}(r) = \frac{A_m}{i\omega\rho}\frac{x_3 e^{ik_f r}}{r^2}\left(ik_f - \frac{1}{r}\right) \tag{4.10}$$

When the contributions of all '*N*' sources are added, the total velocity in x_1, x_2, and x_3 directions at point x can be written as

$$v_1(x) = \sum_{m=1}^{N}\frac{A_m}{i\omega\rho}\frac{x_{1m} e^{ik_f r_m}}{r_m^2}\left(ik_f - \frac{1}{r_m}\right) \tag{4.11}$$

$$v_2(x) = \sum_{m=1}^{N}\frac{A_m}{i\omega\rho}\frac{x_{2m} e^{ik_f r_m}}{r_m^2}\left(ik_f - \frac{1}{r_m}\right) \tag{4.12}$$

$$v_3(x) = \sum_{m=1}^{N}\frac{A_m}{i\omega\rho}\frac{x_{3m} e^{ik_f r_m}}{r_m^2}\left(ik_f - \frac{1}{r_m}\right) \tag{4.13}$$

Where $\mathbf{x_{/m}}$ *is* the shortest distance along the *x*, direction between the mth point source and the target point, as shown in Fig. 4.l. If the transducer surface velocity in the x_3 direction is given by v_o, then for all values of x on the transducer surface, the velocity should be equal to v_0. Therefore

$$v_3(x) = \sum_{m=1}^{N}\frac{A_m}{i\omega\rho}\frac{x_{3m} e^{ik_f r_m}}{r_m^2}\left(ik_f - \frac{1}{r_m}\right) = v_0 \tag{4.14}$$

4.2.2 Matrix Formulation.

Velocity of the M target points distributed on the transducer face due to point sources distributed just behind the transducer surface at a distance r_s can be written in the matrix form as

$$v_S = M_{SS} A_S \tag{4.15}$$

where V_S is the (M x 1) vector of the velocity components, perpendicular to the transducer surface. If the velocity of the transducer face is given by v_O, then V_s can be written as

$$\{v_S\}^T = \{v_0^1, v_0^2, v_0^3 \ldots\ldots\ldots v_0^{m-1}, v_0^m\} \tag{4.16 a}$$

where v_O is the velocity of the n[th] target point. If A_s is the *(N x 1)* vector of the source strengths, then

$$\{A_S\}^T = \{A_0^1, A_0^2, A_0^3 \ldots\ldots\ldots A_0^{N-1}, A_0^N\} \tag{4.16 b}$$

From the earlier discussion, we know that each point source is placed inside a sphere; hence, the number of apex points of the spheres will be the same as the number of point sources. When the target points are placed at the apex of the spheres of the point sources, then *M* is equal to *N*. Therefore, when the target points are located at the apex of the spheres of the point sources, the square matrix M_{ss} can be written as

$$Mss = \begin{bmatrix} f(x_{t1}^1, r_1^1) & f(x_{t1}^2, r_1^2) & f(x_{t1}^3, r_1^3) & \ldots\ldots\ldots\ldots & \ldots\ldots\ldots & f(x_{t1}^{N-1}, r_1^{n-1}) & f(x_{t1}^N, r_1^N) \\ f(x_{t2}^1, r_2^1) & f(x_{t2}^2, r_2^2) & f(x_{t2}^3, r_2^3) & \ldots\ldots\ldots & \ldots\ldots & f(x_{t2}^{N-1}, r_2^{n-1}) & f(x_{t2}^N, r_2^N) \\ f(x_{t3}^1, r_3^1) & f(x_{t3}^2, r_3^2) & f(x_{t3}^3, r_3^3) & \ldots\ldots\ldots & \ldots\ldots & f(x_{t3}^{N-1}, r_3^{n-1}) & f(x_{t3}^N, r_3^N) \\ \ldots\ldots & \ldots\ldots & \ldots\ldots & \ldots\ldots\ldots & \ldots\ldots & \ldots\ldots & \ldots\ldots \\ \ldots\ldots & \ldots\ldots & \ldots\ldots & \ldots\ldots\ldots & \ldots\ldots & \ldots\ldots & \ldots\ldots \\ \ldots\ldots & \ldots\ldots & \ldots\ldots & \ldots\ldots\ldots & \ldots\ldots & \ldots\ldots & \ldots\ldots \\ \ldots\ldots & \ldots\ldots & \ldots\ldots & \ldots\ldots\ldots & \ldots\ldots & \ldots\ldots & \ldots\ldots \\ f(x_{tN}^1, r_N^1) & f(x_{tN}^2, r_N^2) & f(x_{tN}^3, r_N^3) & \ldots\ldots\ldots\ldots & \ldots\ldots & f(x_{tN}^{N-1}, r_N^{N-1}) & f(x_{tN}^N, r_N^N) \end{bmatrix} \tag{4.17}$$

Where

$$f(x_{tn}^m, r_n^m) = \frac{x_{tn}^m \exp(ik_f r_n^m)}{i\omega\rho.(r_n^m)^2}\left(ik_f - \frac{1}{r_n^m}\right) = \frac{\exp(ik_f r_n^m)}{i\omega\rho.(r_n^m)^2}\left(ik_f - \frac{1}{r_n^m}\right)\left(x_{3n}^m \cos\theta + x_{1n}^m \sin\theta\right) \tag{4.18}$$

and r_n^m is the distance between the mth point source and the nth target point.

For a general set of target points located on any surface, the velocity due to the transducer sources can be written as

$$v_t = M_{TS}.A_s \tag{4.19}$$

where V_T, the (M x 1) velocity vector, contains the normal velocity components of the target points distributed on the surface. The matrix M_{TS} has elements that are similar to those of M_{ss}, with different x_n^m values and the size of the matrix is (M x N), where M is the number of target points and N is the number of source points. Following the same concept, the pressure at any M number of target points due to N number of source points can be written as

$$PR_T = Q_{TS}.A_s \tag{4.20}$$

where PR_T is the (M x 1) vector of pressure values at M target points, and Q_{TS} is an (M x N) matrix given below

$$Qss = \begin{Vmatrix} \frac{\exp(ik_f r_1^1)}{r_1^1} & \frac{\exp(ik_f r_1^2)}{r_1^2} & \frac{\exp(ik_f r_1^3)}{r_1^3} & .. & .. & .. & \frac{\exp(ik_f r_1^{m-1})}{r_1^{m-1}} & \frac{\exp(ik_f r^m)}{r_1^m} \\ \frac{\exp(ik_f r_2^1)}{r_2^1} & \frac{\exp(ik_f r_2^2)}{r_2^2} & \frac{\exp(ik_f r_2^3)}{r_2^3} & .. & .. & .. & \frac{\exp(ik_f r_2^{m-1})}{r_2^{m-1}} & \frac{\exp(ik_f r_2^m)}{r_2^m} \\ .. & .. & .. & .. & .. & .. & .. & .. \\ .. & .. & .. & .. & .. & .. & .. & .. \\ .. & .. & .. & .. & .. & .. & .. & .. \\ .. & .. & .. & .. & .. & .. & .. & .. \\ \frac{\exp(ik_f r_{n-1}^1)}{r_{n-1}^1} & \frac{\exp(ik_f r_{n-1}^2)}{r_{n-1}^2} & \frac{\exp(ik_f r_{n-1}^3)}{r_{n-1}^3} & .. & .. & .. & \frac{\exp(ik_f r_{n-1}^{m-1})}{r_{n-1}^{m-1}} & \frac{\exp(ik_f r_{n-1}^m)}{r_{n-1}^m} \\ \frac{\exp(ik_f r_n^1)}{r_n^1} & \frac{\exp(ik_f r_n^2)}{r_n^2} & \frac{\exp(ik_f r_n^3)}{r_n^3} & .. & .. & .. & \frac{\exp(ik_f r_1^{m-1})}{r_n^{m-1}} & \frac{\exp(ik_f r_n^m)}{r_n^m} \end{Vmatrix} \tag{4.21}$$

When the target points are located at the apex of the spheres of the point sources, Eq. (4.20) takes the form

$$PR_s = Q_{SS}.A_s \tag{4.22}$$

where $\mathbf{Q_{ss}}$ is an (NxN) matrix.

The definition of r_n^m *is* identical to Eq. (4.18). It is the distance between the m[th] point source and the n[th] target point.

4.2.3 Ultrasonic Field in a Homogenous Fluid-DPSM technique (when transducer is inclined at an angle with vertical):

4.2.3.1 Transducer Face is Inclined at an Angle of θ:

If the transducer face is inclined at an angle of θ, measured from x_3-axis when rotated about the x_2 axis **(Figure 4.2),** the velocity of the transducer face can be expressed as

$$v_3(x) = v_1(\mathbf{x})Sin\theta + v_3(\mathbf{x})Cos\theta$$
$$= \sum_{m=1}^{N} \frac{A_m}{i\omega\rho}\left(ik_f - \frac{1}{r_m}\right)\left(\frac{x_{1m}\exp(ik_f r_m)}{r_m^2}Sin\theta + \frac{x_{3m}\exp(ik_f r_m)}{r_m^2}Cos\theta\right) = v_0 \quad . \tag{4.23}$$

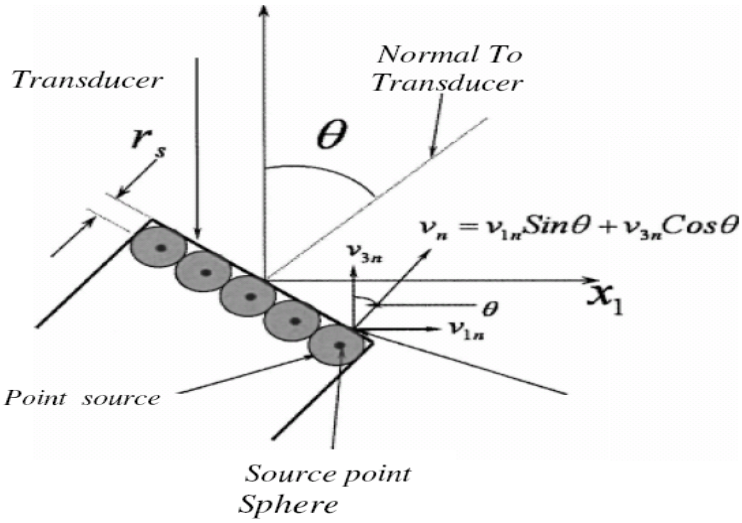

Figure 4.2 Rotation of the Transducer w.r.t. X3-Axis and Velocity of the Nth Observation Point Adjacent to the Transducer Face

4.2.3.2 Matrix Formulation

Velocity of the N target points placed on the transducer face due to point sources distributed just below the transducer surface at a distance r_s, can be written in matrix form as

$$\mathbf{V}_S = \mathbf{M}_{SS}\mathbf{A}_S \qquad \ldots\ldots\ (4.24)$$

where, $\mathbf{V}_S$ is the (Nx1) vector of the velocity components, perpendicular to the transducer surface. If the velocity of the transducer face is given by $v_{0,}$ then $\mathbf{V}_S$ can be written as:

$$\{\mathbf{V}_S\}^T = \begin{bmatrix} v_0^{\,1} & v_0^{\,2} & v_0^{\,3} & \ldots & \ldots & \ldots & \ldots & \ldots & v_0^{\,N-1} & v_0^{\,N} \end{bmatrix}^T_{N\times 1} \quad \ldots. (4.25)$$

where, v_0^n is the velocity of the *n*-th target point. If $\mathbf{A}_S$ is the (Nx1) vector of the source strengths, then

$$\{\mathbf{A}_S\}^T = \begin{bmatrix} A_1 & A_2 & A_3 & A_4 & A_5 & A_6 & \ldots\ldots & A_{N-2} & A_{N-1} & A_N \end{bmatrix}^T \quad (4.26)$$

From the earlier discussion, we know that each point source is placed inside a sphere and hence, the number of apex points of the spheres touching the transducer surface will be the same as the number of point sources. When the target points are placed at the apex of the spheres of the point sources, then M is equal to N. Therefore, for the target points at the apex of the spheres of the point sources, the square matrix $\mathbf{M}_{SS}$ can be written as:

$$\mathbf{M}_{SS} = \begin{bmatrix} f\left(x_{t1}^1, r_1^1\right) & f\left(x_{t2}^1, r_2^1\right) & f\left(x_{t3}^1, r_3^1\right) & f\left(x_{t4}^1, r_4^1\right) & \ldots & \ldots & f\left(x_{tN-1}^1, r_{N-1}^1\right) & f\left(x_{tN}^1, r_N^1\right) \\ f\left(x_{t1}^2, r_1^2\right) & f\left(x_{t2}^2, r_2^2\right) & f\left(x_{t3}^2, r_3^2\right) & f\left(x_{t4}^2, r_4^2\right) & \ldots & \ldots & f\left(x_{tN-1}^2, r_{N-1}^2\right) & f\left(x_{tN}^2, r_N^2\right) \\ f\left(x_{t1}^3, r_1^3\right) & f\left(x_{t2}^3, r_2^3\right) & f\left(x_{t3}^3, r_3^3\right) & f\left(x_{t4}^3, r_4^3\right) & \ldots & \ldots & f\left(x_{tN-1}^3, r_{N-1}^3\right) & f\left(x_{tN}^3, r_N^3\right) \\ f\left(x_{t1}^4, r_1^4\right) & f\left(x_{t2}^4, r_2^4\right) & f\left(x_{t3}^4, r_3^4\right) & f\left(x_{t4}^4, r_4^4\right) & \ldots & \ldots & f\left(x_{tN-1}^4, r_{N-1}^4\right) & f\left(x_{tN}^4, r_N^4\right) \\ \ldots & \ldots & \ldots & \ldots & \ldots & \ldots & \ldots & \ldots \\ \ldots & \ldots & \ldots & \ldots & \ldots & \ldots & \ldots & \ldots \\ \ldots & \ldots & \ldots & \ldots & \ldots & \ldots & \ldots & \ldots \\ f\left(x_{t1}^N, r_1^N\right) & f\left(x_{t2}^N, r_2^N\right) & f\left(x_{t3}^N, r_3^N\right) & f\left(x_{t4}^N, r_4^N\right) & \ldots & \ldots & f\left(x_{tN-1}^N, r_{N-1}^N\right) & f\left(x_{tN}^N, r_N^N\right) \end{bmatrix}_{N\times N}$$

(4.27)

4.3 Computation of Ultrasonic Field in a multi layered fluid

We are interested in computing the ultrasonic field in multilayered fluid systems. In the multilayered problem geometry several interfaces may be present. When fluids with different densities and acoustic properties form a multilayered system, the fluid density should monotonically vary from top to bottom. If we have 'n' number of fluids in the system, we should have (n-1) number of interfaces. Each interface acts as a transmitter as well as a reflector of elastic wave energy generated by the ultrasonic transducers. When the entire system is considered, several continuity conditions across the interfaces and boundary conditions at the transducer surface are to be satisfied. As shown in Fig. 4.3 a number of sources are introduced along the transducer surfaces T as well as along interfaces I1 for two layered fluid geometry. As each interface, two sets of source vectors are introduced. These two sets of source strength vectors are denoted by A (for sources located just above the interface) and A* (for sources located just below the interface). The sources with source strength A generate the ultrasonic field in the fluid below it and the sources with source strength A* generate the ultrasonic field in the fluid above it. The total ultrasonic field in each medium is obtained by superimposing the fields generated by two sets of sources as listed below:

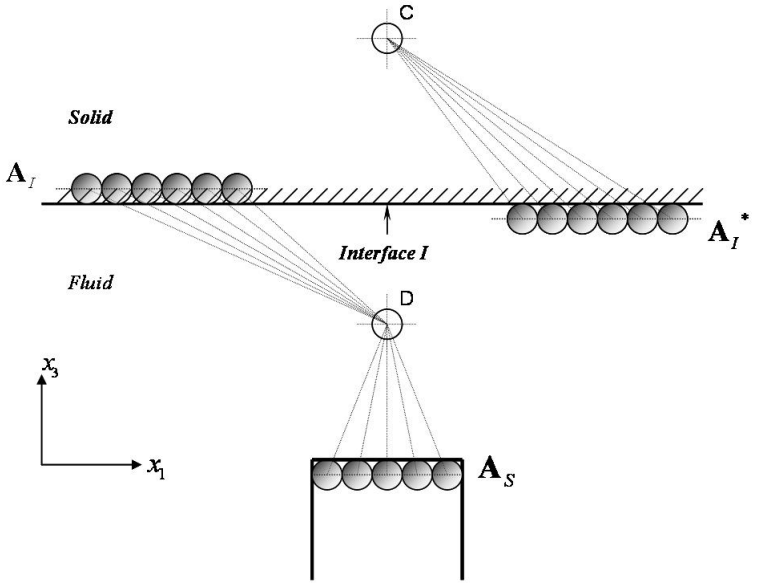

Figure 4.3 Multilayered Fluid Source Distribution

Fluid 1: Summation of fields generated by ***As*** and $\boldsymbol{A_i}$.

Fluid 2: Fields generated by $\boldsymbol{A_i}$*

4.3.1 Strength Determination from Boundary and Interface Conditions.

Certain boundary and interface continuity conditions must be satisfied for this problem geometry. On the transducer surfaces *T*, the velocity fields are specified as V_0. Across the interfaces, the pressure **(P.R)** and the X_3-direction velocity (V) must be continuous.

Since for any set of sources and target points the velocity and pressure fields are given by **V=M.A** and **PR=Q-A** (Refer to Eqs. (4.24) and (4.25)), the boundary and continuity conditions give rise to the following equations:

On the transducer surface

$$\mathbf{M}_{SS}\mathbf{A}_S + \mathbf{M}_{SI}\mathbf{A}_I = \mathbf{V}_{S0} \tag{4.28}$$

On the interface, from the continuity of the normal stress,

$$\mathbf{Q}_{IS}\mathbf{A}_S + \mathbf{Q}_{II}\mathbf{A}_I = -Q_{II^*}\mathbf{A}_I^{\,*} \tag{4.29}$$

Equations (7.23) to (7.24) can be written in matrix form

$$\begin{bmatrix} \mathbf{M_{SS}} & \mathbf{M_{SI}} & \mathbf{0} \\ \mathbf{Q_{IS}} & \mathbf{Q_{II}} & \mathbf{Q_{II^*}} \end{bmatrix} \begin{Bmatrix} \mathbf{A}_S \\ \mathbf{A}_I \\ \mathbf{A}_I^{\,*} \end{Bmatrix} = \begin{Bmatrix} \mathbf{V}_{S0} \\ \mathbf{0} \\ \mathbf{0} \end{Bmatrix} \tag{4.30}$$

or, $$[\mathbf{MAT}]\{\mathbf{\Lambda}\} = \{\mathbf{V}\} \tag{4.31}$$

Solution

The vector of source strengths of the total system can be calculated by taking inverse of $[\mathbf{MAT}]$ and multiplying it with the vector $\{\mathbf{V}\}$,

4.4 Ultrasonic Field Modeling Near Fluid Solid Interface

For solving this problem we need to calculate the stress and displacement Green's functions in the solid, and pressure and displacement Green's functions in the fluid.

4.4.1 Calculation of displacement and stress Green's functions in the Solid

Navier's equation of motion can be written as

$$(\lambda + 2\mu)u_{j,ij} + \mu \in_{ijk} \in_{kmn} u_{n,mj} + F_i = \rho \ddot{u}_i \tag{4.32}$$

where u_i is the displacement at a point in the solid. F_i represents the body force per unit volume. Subscripts i, j etc. take values 1,2,3 . Equation (4.32) can also be written in the vector form

$$(\lambda + 2\mu)\nabla(\nabla.\mathbf{u}) - \mu\nabla \times (\nabla \times \mathbf{u}) + \mathbf{F} = \rho \ddot{\mathbf{u}} \tag{4.33}$$

Using Helmholtz decomposition, the displacement vector field can be expressed in terms of two vector potentials.

$$\mathbf{u} = \nabla(\nabla.\mathbf{\Phi}) - \nabla \times (\nabla \times \mathbf{\Psi}) \tag{4.34}$$

We know that longitudinal-wave or P-wave speed in isotropic homogeneous solid is $c_p = \sqrt{\frac{\lambda + 2\mu}{\rho}}$ and transverse-wave or S-wave speed is $c_s = \sqrt{\frac{\mu}{\rho}}$. Dividing both sides of Navier's equation by ρ , we get.

$$c_p{}^2(\nabla(\nabla.\mathbf{u})) - c_s{}^2(\nabla \times (\nabla \times \mathbf{u})) + \frac{\mathbf{F}}{\rho} = \ddot{\mathbf{u}} \tag{4.35}$$

Substituting equation (4.29) in to equation (4.35) we get

$$\nabla\nabla.(c_p{}^2\nabla^2\mathbf{\Phi} - \ddot{\mathbf{\Phi}}) - \nabla \times \nabla \times (c_s{}^2\nabla^2\mathbf{\Psi} - \ddot{\mathbf{\Psi}}) + \frac{\mathbf{F}}{\rho} = 0 \tag{4.36}$$

Here $\mathbf{\Phi}$ and $\mathbf{\Psi}$ are both vector potentials and functions of space and time.

4.4.1.1 Point source excitation in solid

Our objective is to obtain the displacements and stresses in a solid due to a point source excitation, or in other words, the Green's functions for the solid. When a point source is acting in a solid, the body force will change to a concentrated time dependent impulsive force. This force can be represented by dirac delta function in space. So, decoupling the independent parameters, the body force can be written as

$$\mathbf{F}(\mathbf{x}, t) = \mathbf{P}.f(t)\delta(\mathbf{x}) \quad \text{or} \quad F_i = P_i f(t)\delta(x_j) \tag{4.37}$$

Where, $\mathbf{P}$ is the force vector without the time and space dependence. Looking in to the spatial derivative of the potentials, the general solution of the Poisson's equation [$\nabla^2\eta = q(\mathbf{x})$] can be written as

$$\eta = -\frac{1}{4\pi}\int_V \frac{q(\mathbf{y})}{|\mathbf{x}-\mathbf{y}|}dV \tag{4.38}$$

Observing $q(\mathbf{x}) = \delta(\mathbf{x})$, and using the properties of the dirac delta function $\int_V \delta(\mathbf{x})g(x)dV = g(0)$ we can write $\eta = -\frac{1}{4\pi|\mathbf{x}|}$ and $\nabla^2\left(-\frac{1}{4\pi r}\right) = \delta(\mathbf{x})$, (where $r = |\mathbf{x}|$ when the source is at the origin).

Substituting the expression of $\delta(\mathbf{x})$ in Equation (4.37) we get

$$\mathbf{F} = -\mathbf{P}\nabla^2\left(\frac{f(t)}{4\pi r}\right) = \mathbf{P}\left[\nabla\left(\nabla.\left(\frac{f(t)}{4\pi r}\right)\right) - \nabla\times\left(\nabla\times\left(\frac{f(t)}{4\pi r}\right)\right)\right] \tag{4.39}$$

Without any loss of generality the vector potentials can be expressed in terms of two scalar potentials in the form $\mathbf{\Phi} = \mathbf{P}\phi$ and $\mathbf{\Psi} = \mathbf{P}\psi$.

Substituting Equation (4.39) in to Equation (4.35) we get

$$\nabla\nabla.\mathbf{P}\left(c_p{}^2\nabla^2\phi - \ddot{\phi} - \frac{f(t)}{4\pi r\rho}\right) - \nabla\times\nabla\times\mathbf{P}\left(c_s{}^2\nabla^2\psi - \ddot{\psi} - \frac{f(t)}{4\pi r\rho}\right) = 0 \tag{4.40}$$

It is now assumed that the time dependency of the concentrated force in all three directions is purely harmonic, $e^{-i\omega t}$ with frequency equal to $\omega/2\pi$. By decoupling the variables it is possible to resolve all primary unknown parameters in two different space and time dependent parameters. Inevitably the time dependency of all primary unknown parameters should be harmonic, $e^{-i\omega t}$.

Therefore, $\phi(x_j,t) = \phi(x_j)e^{-i\omega t}$, $\psi(x_j,t) = \psi(x_j)e^{-i\omega t}$ and

$u_i(x_j,t) = U_i(x_j)e^{-i\omega t}$. Substituting these expressions in Equation (4.40) we get

$$\nabla\nabla.\mathbf{P}\left(c_p{}^2\nabla^2\phi + \omega^2\phi - \frac{1}{4\pi r\rho}\right)e^{-i\omega t} - \nabla\times\nabla\times\mathbf{P}\left(c_s{}^2\nabla^2\psi + \omega^2\psi - \frac{1}{4\pi r\rho}\right)e^{-i\omega t} = 0 \tag{4.41}$$

Thus,

$$\nabla^2\phi + \frac{\omega^2}{{c_p}^2}\phi = \frac{1}{4\pi\rho {c_p}^2 r} \tag{4.42}$$

$$\nabla^2\psi + \frac{\omega^2}{{c_s}^2}\psi = \frac{1}{4\pi\rho {c_s}^2 r} \tag{4.43}$$

The particular solutions of Equations (4.42) and (4.43) can be expressed as

$\phi = \frac{1-e^{ik_p r}}{4\pi\rho\omega^2 r}$ and $\psi = \frac{1-e^{ik_s r}}{4\pi\rho\omega^2 r}$ respectively, where $k_p = \frac{\omega}{c_p}$ and $k_s = \frac{\omega}{c_s}$.

(4.44)

4.4.1.2 Calculation of displacement Green's function

Substituting Equation (4.46) in to Equation (4.34) we get

$$\mathbf{u} = \mathbf{U}e^{-i\omega t} = \nabla\left(\nabla.\mathbf{P}\left(\frac{1-e^{1k_p r}}{4\pi\rho\omega^2 r}\right)\right) - \nabla\times\left(\nabla\times\mathbf{P}\left(\frac{1-e^{ik_s r}}{4\pi\rho\omega^2 r}\right)\right) \tag{4.45}$$

Using orthogonal operators, the displacement vector can be written as

$$\mathbf{u} = \mathbf{U}e^{-i\omega t} = \nabla\left(\nabla.\mathbf{P}\left(\frac{1-e^{1k_p r}}{4\pi\rho\omega^2 r}\right)\right) + \nabla^2\mathbf{P}\left(\frac{1-e^{ik_s r}}{4\pi\rho\omega^2 r}\right) - \nabla\left(\nabla.\mathbf{P}\left(\frac{1-e^{ik_s r}}{4\pi\rho\omega^2 r}\right)\right) \tag{4.46}$$

Applying Laplace operator on $\mathbf{P}\left(\frac{1-e^{ik_s r}}{4\pi\rho\omega^2 r}\right)$ we get

$$\mathbf{u} = \mathbf{U}e^{-i\omega t} = \nabla\nabla.\left(\mathbf{P}\frac{e^{ik_p r}-e^{ik_s r}}{4\pi\rho\omega^2 r}\right)e^{-i\omega t} + \frac{\mathbf{P}e^{ik_s r}}{4\pi\rho\omega^2 r}{k_s}^2 e^{-i\omega t} = \underline{\mathbf{G}}(\mathbf{x};\mathbf{0}).\mathbf{P}.e^{-i\omega t} \tag{4.47}$$

In index notation

$$U_i = \frac{1}{4\pi\rho\omega^2}\left({k_s}^2\frac{e^{ik_s r}}{r}\delta_{ij} - \frac{\partial^2}{\partial x_i \partial x_j}\left(\frac{e^{ik_p r}-e^{ik_s r}}{r}\right)\right)P_j = G_{ij}(\mathbf{x};\mathbf{0})P_j \tag{4.48}$$

When the point source is at **y** and the response at **x** is to be determined then we can write

$$u_i = U_i e^{-i\omega t} = G_{ij}(\mathbf{x};\mathbf{y})P_j e^{-i\omega t} \tag{4.49}$$

Here $G_{ij}(\mathbf{x};\mathbf{y})$ is called the space dependent Green's function of displacement for the isotropic homogeneous solid. Substituting $r = |\mathbf{x} - \mathbf{y}|$, the displacement Green's function can be written as **(Mal and Singh 1991)**

$$G_{ij}(\mathbf{x};\mathbf{y}) = \frac{1}{4\pi\rho\omega^2}\left[\begin{array}{l} \dfrac{e^{ik_p r}}{r}\left(k_p{}^2 R_i R_j + \left(3R_i R_j - \delta_{ij}\right)\left(\dfrac{ik_p}{r} - \dfrac{1}{r^2}\right)\right) + \\ \dfrac{e^{ik_s r}}{r}\left(k_s{}^2\left(\delta_{ij} - R_i R_j\right) - \left(3R_i R_j - \delta_{ij}\right)\left(\dfrac{ik_s}{r} - \dfrac{1}{r}\right)\right) \end{array}\right] \quad \text{where,}$$

$$R_i = \frac{x_i - y_i}{r}$$

(4.50)

In the matrix form

$$\underline{\mathbf{G}}(\mathbf{x};\mathbf{y}) = \left[\underline{\mathbf{G}_1}(\mathbf{x};\mathbf{y}) \quad \underline{\mathbf{G}_2}(\mathbf{x};\mathbf{y}) \quad \underline{\mathbf{G}_3}(\mathbf{x};\mathbf{y})\right]^T \quad \text{and}\, \mathbf{u} = \underline{\mathbf{G}}(\mathbf{x};\mathbf{y})\mathbf{P} \tag{4.51}$$

If the unit excitation force at **y** acts in the j-th direction, then the displacement at **x** in i th direction is given by $G_{ij}(\mathbf{x};\mathbf{y})$.

4.4.1.3 Calculation of Stress Green's function

For isotropic homogeneous solids the expression for stresses can be written as

$$\sigma_{ij} = 2\mu\varepsilon_{ij} + \lambda\delta_{ij}\varepsilon_{kk} \tag{4.52}$$

Where, λ, μ are the two Lamé constants and δ_{ij} is the Kronecker Delta.

We know that strain can be expressed as a function of displacement, $\varepsilon_{ij} = \frac{1}{2}(u_{i,j} + u_{j,i})$. Substituting the expression for displacement (Equation (4.49)) in the expression for strains,

$$\varepsilon_{ij} = \frac{1}{2}\left(G_{ik,j} + G_{jk,i}\right)P_k \tag{4.53}$$

In the following the harmonic time dependence is implied and is not explicitly written for convenience. Substituting the expression for strains in equation (4.52), the stress Green's function at **x** due to a concentrated time harmonic force at **y** can be obtained.

For isotropic homogeneous linearly elastic material, we can write the expression for the stress Green's function at **x** due to a concentrated harmonic force at **y** as

$$S_{ij}(\mathbf{x};\mathbf{y}) = \mu\left(G_{ik,j} + G_{jk,i}\right)P_k + \lambda\delta_{ij}G_{kq,k}P_q \tag{4.54}$$

$$\text{or } S_{ij}(\mathbf{x};\mathbf{y}) = \left(\mu\left(G_{ik,j} + G_{jk,i}\right)\delta_{kq} + \lambda\delta_{ij}G_{kq,k}\right)P_q \tag{4.55}$$

By rigorous differentiation, expressions for all stresses from Equation (4.55) have been found and presented in Appendix.

4.4.1.4 Computation of Displacements and Stresses in the Solid due to a group of point sources

When a group of point sources distributed over a finite dimension in a solid are excited, the response at any point in the solid can be computed by superimposing the contribution of each point source. Let there be a solid half space and M number of point sources at the free boundary. Our objective is to compute the response at point A due to M number of point sources at the free boundary. Response at A will be the superposition of the contribution of each point source. So, the total displacement at A can be written as

$$u_1 = \sum_{m=1}^{M}\left(G_{11}^m P_1^m + G_{12}^m P_2^m + G_{13}^m P_3^m\right) = \sum_{m=1}^{M}\underline{\mathbf{G}_1}^m\mathbf{P}^m \tag{4.56.1}$$

$$u_2 = \sum_{m=1}^{M}\left(G_{21}^m P_1^m + G_{22}^m P_2^m + G_{23}^m P_3^m\right) = \sum_{m=1}^{M}\underline{\mathbf{G}_2}^m\mathbf{P}^m \tag{4.56.2}$$

$$u_3 = \sum_{m=1}^{M}\left(G_{31}^m P_1^m + G_{32}^m P_2^m + G_{33}^m P_3^m\right) = \sum_{m=1}^{M}\underline{\mathbf{G}_3}^m\mathbf{P}^m \tag{4.56.3}$$

Similarly the stresses at A may be written as:

$$S_{33} = \sum_{m=1}^{M}\left[\left(\sigma_{33}^1\right)^m P_1^m + \left(\sigma_{33}^2\right)^m P_2^m + \left(\sigma_{33}^3\right)^m P_3^m\right] = \sum_{m=1}^{M}\underline{\mathbf{s}_{33}}^m\left(\frac{\mathbf{P}}{4\pi}\right)^m \tag{4.57.1}$$

$$S_{11} = \sum_{m=1}^{M}\left[\left(\sigma_{11}^1\right)^m P_1^m + \left(\sigma_{11}^2\right)^m P_2^m + \left(\sigma_{11}^3\right)^m P_3^m\right] = \sum_{m=1}^{M}\underline{\mathbf{s}_{11}}^m\left(\frac{\mathbf{P}}{4\pi}\right)^m \tag{4.57.2}$$

$$S_{22} = \sum_{m=1}^{M}\left[\left(\sigma_{22}^1\right)^m P_1^m + \left(\sigma_{22}^2\right)^m P_2^m + \left(\sigma_{22}^3\right)^m P_3^m\right] = \sum_{m=1}^{M}\underline{\mathbf{s}_{22}}^m\left(\frac{\mathbf{P}}{4\pi}\right)^m \tag{4.57.3}$$

$$S_{31} = \sum_{m=1}^{M}\left[\left(\sigma_{31}^1\right)^m P_1^m + \left(\sigma_{31}^2\right)^m P_2^m + \left(\sigma_{31}^3\right)^m P_3^m\right] = \sum_{m=1}^{M}\underline{\mathbf{s}_{31}}^m\left(\frac{\mathbf{P}}{4\pi}\right)^m \tag{4.57.4}$$

$$S_{32} = \sum_{m=1}^{M} \left[\left(\sigma_{32}^{1}\right)^m P_1^m + \left(\sigma_{32}^{2}\right)^m P_2^m + \left(\sigma_{32}^{3}\right)^m P_3^m \right] = \sum_{m=1}^{M} \underline{\mathbf{s}_{32}}^m \left(\frac{\mathbf{P}}{4\pi} \right)^m \quad (4.57.5)$$

$$S_{12} = \sum_{m=1}^{M} \left[\left(\sigma_{12}^{1}\right)^m P_1^m + \left(\sigma_{12}^{2}\right)^m P_2^m + \left(\sigma_{12}^{3}\right)^m P_3^m \right] = \sum_{m=1}^{M} \underline{\mathbf{s}_{12}}^m \left(\frac{\mathbf{P}}{4\pi} \right)^m \quad (4.57.6)$$

4.4.1.5 Matrix representation

In our earlier discussion the displacements and stresses at a point have been presented. The equations can be presented in the matrix form. Let us now compute the displacement and stress fields at a group of observation points (we will call them target points). We assume that there are *N* number of target points and that each displacement and stress expression at N target points due to M source points are to be computed. N target points and M source pointes are shown in Figure 4.3.

One can write,

$$\mathbf{u1}_T = \mathbf{DS1}_{TS}.\mathbf{A}_S \quad (4.58.1)$$

$$\mathbf{u2}_T = \mathbf{DS2}_{TS}.\mathbf{A}_S \quad (4.58.2)$$

$$\mathbf{u3}_T = \mathbf{DS3}_{TS}.\mathbf{A}_S \quad (4.58.3)$$

$$\mathbf{s33}_T = \mathbf{S33}_{TS}.\mathbf{A}_S \quad (4.59.1)$$

$$\mathbf{s11}_T = \mathbf{S11}_{TS}.\mathbf{A}_S \quad (4.59.2)$$

$$\mathbf{s22}_T = \mathbf{S22}_{TS}.\mathbf{A}_S \quad (4.59.3)$$

$$\mathbf{s31}_T = \mathbf{S31}_{TS}.\mathbf{A}_S \quad (4.59.4)$$

$$\mathbf{s32}_T = \mathbf{S32}_{TS}.\mathbf{A}_S \quad (4.59.5)$$

$$\mathbf{s12}_T = \mathbf{S12}_{TS}.\mathbf{A}_S \quad (4.59.6)$$

Where, $\{\mathbf{A}_S\}^T = \frac{1}{4\pi}\left[\mathbf{P}^1 \quad \mathbf{P}^2 \quad \mathbf{P}^3 \quad \mathbf{P}^4 \quad \mathbf{P}^5 \quad \ldots \quad \ldots \quad \mathbf{P}^{M-2} \quad \mathbf{P}^{M-1} \quad \mathbf{P}^M\right]^T_{(3Mx1)}$ (4.60)

$\mathbf{P}^i$ is a (1x3) vector, defined in the Appendix (Equation (A40)). Stress and displacement matrices of Equation (4.57.1) to (4.59.6) have the following form. Only $\mathbf{S33}_{TS}$ and $\mathbf{DS3}_{TS}$ matrices are given below.

$$\mathbf{S33}_{TS} = \begin{bmatrix} \mathbf{s}_{33}{}^{1}{}_{1} & \mathbf{s}_{33}{}^{2}{}_{1} & \mathbf{s}_{33}{}^{3}{}_{1} & \mathbf{s}_{33}{}^{4}{}_{1} & \mathbf{s}_{33}{}^{5}{}_{1} & \dots & \dots & \mathbf{s}_{33}{}^{M-2}{}_{1} & \mathbf{s}_{33}{}^{M-1}{}_{1} & \mathbf{s}_{33}{}^{M}{}_{1} \\ \mathbf{s}_{33}{}^{1}{}_{2} & \mathbf{s}_{33}{}^{2}{}_{2} & \mathbf{s}_{33}{}^{3}{}_{2} & \mathbf{s}_{33}{}^{4}{}_{2} & \mathbf{s}_{33}{}^{5}{}_{2} & \dots & \dots & \mathbf{s}_{33}{}^{M-2}{}_{2} & \mathbf{s}_{33}{}^{M-1}{}_{2} & \mathbf{s}_{33}{}^{M}{}_{2} \\ \mathbf{s}_{33}{}^{1}{}_{3} & \mathbf{s}_{33}{}^{2}{}_{3} & \mathbf{s}_{33}{}^{3}{}_{3} & \mathbf{s}_{33}{}^{4}{}_{3} & \mathbf{s}_{33}{}^{5}{}_{3} & \dots & \dots & \mathbf{s}_{33}{}^{M-2}{}_{3} & \mathbf{s}_{33}{}^{M-1}{}_{3} & \mathbf{s}_{33}{}^{M}{}_{3} \\ \dots & \dots & \dots & \dots & \dots & \dots & \dots & \dots & \dots & \dots \\ \dots & \dots & \dots & \dots & \dots & \dots & \dots & \dots & \dots & \dots \\ \mathbf{s}_{33}{}^{1}{}_{N-2} & \mathbf{s}_{33}{}^{2}{}_{N-2} & \mathbf{s}_{33}{}^{3}{}_{N-2} & \mathbf{s}_{33}{}^{4}{}_{N-2} & \mathbf{s}_{33}{}^{5}{}_{N-2} & \dots & \dots & \mathbf{s}_{33}{}^{M-2}{}_{N-2} & \mathbf{s}_{33}{}^{M-1}{}_{N-2} & \mathbf{s}_{33}{}^{M}{}_{N-2} \\ \mathbf{s}_{33}{}^{1}{}_{N-1} & \mathbf{s}_{33}{}^{2}{}_{N-1} & \mathbf{s}_{33}{}^{3}{}_{N-1} & \mathbf{s}_{33}{}^{4}{}_{N-1} & \mathbf{s}_{33}{}^{5}{}_{N-1} & \dots & \dots & \mathbf{s}_{33}{}^{M-2}{}_{N-1} & \mathbf{s}_{33}{}^{M-1}{}_{N-1} & \mathbf{s}_{33}{}^{M}{}_{N-1} \\ \mathbf{s}_{33}{}^{1}{}_{N} & \mathbf{s}_{33}{}^{2}{}_{N} & \mathbf{s}_{33}{}^{3}{}_{N} & \mathbf{s}_{33}{}^{4}{}_{N} & \mathbf{s}_{33}{}^{5}{}_{N} & \dots & \dots & \mathbf{s}_{33}{}^{M-2}{}_{N} & \mathbf{s}_{33}{}^{M-1}{}_{N} & \mathbf{s}_{33}{}^{M}{}_{N} \end{bmatrix}_{(Nx3M)} . \quad (4.61.1)$$

and

$$\mathbf{DS3}_{TS} = \begin{bmatrix} \mathbf{G}_{3}{}^{1}{}_{1} & \mathbf{G}_{3}{}^{2}{}_{1} & \mathbf{G}_{3}{}^{3}{}_{1} & .. & \mathbf{G}_{3}{}^{M-1}{}_{1} & \mathbf{G}_{3}{}^{M}{}_{1} \\ \mathbf{G}_{3}{}^{1}{}_{2} & \mathbf{G}_{3}{}^{2}{}_{2} & \mathbf{G}_{3}{}^{3}{}_{2} & \dots & \mathbf{G}_{3}{}^{M-1}{}_{2} & \mathbf{G}_{3}{}^{M}{}_{2} \\ \mathbf{G}_{3}{}^{1}{}_{3} & \mathbf{G}_{3}{}^{2}{}_{3} & \mathbf{G}_{3}{}^{3}{}_{3} & \dots & \mathbf{G}_{3}{}^{M-1}{}_{3} & \mathbf{G}_{3}{}^{M}{}_{3} \\ \dots & \dots & .. & \dots & .. & \dots \\ \mathbf{G}_{3}{}^{1}{}_{N-1} & \mathbf{G}_{3}{}^{2}{}_{N-1} & \mathbf{G}_{3}{}^{3}{}_{N-1} & \dots & \mathbf{G}_{3}{}^{M-1}{}_{N-1} & \mathbf{G}_{3}{}^{M}{}_{N-1} \\ \mathbf{G}_{3}{}^{1}{}_{N} & \mathbf{G}_{3}{}^{2}{}_{N} & \mathbf{G}_{3}{}^{3}{}_{N} & \dots & \mathbf{G}_{3}{}^{M-1}{}_{N} & \mathbf{G}_{3}{}^{M}{}_{N} \end{bmatrix}_{(Nx3M)} \quad (4.61.2)$$

$\mathbf{s}_{33}{}^{m}{}_{n}$ and $\mathbf{G}_{3}{}^{m}{}_{n}$ at the n-th target point due to m-th point source have the following form

$$\mathbf{s}_{33}{}^{m}{}_{n} = \left[\left(\sigma_{33}^{1}\right)^{m} \quad \left(\sigma_{33}^{2}\right)^{m} \quad \left(\sigma_{33}^{3}\right)^{m} \right]_{n} \text{and} \, \mathbf{G}_{3}{}^{m}{}_{n} = \left[G_{31}{}^{m} \quad G_{32}{}^{m} \quad G_{33}{}^{m} \right]_{n} \quad (4.62)$$

Similarly, other stress and displacement matrices can also be written in this form.

4.5 Application 2: Ultrasonic Field Modeling In a Solid Plate Banerjee and Kundu, 2007)

In this section our objective is to model the ultrasonic field generated by ultrasonic transducers of finite dimension in the vicinity of a solid plate when both the plate and the transducers are immersed in a fluid. Thus, it numerically simulates the ultrasonic experiments for plate inspection.

For modeling this problem by the DPSM technique, it is necessary to calculate stress and displacement Green's functions for fluid and solid media explicitly. Calculation of Green's functions for the solid medium has been discussed in Section 4.4.2. The ultrasonic fields in the solid plate are calculated for critical angles corresponding to the symmetric and antisymmetric guided wave modes in the plate.

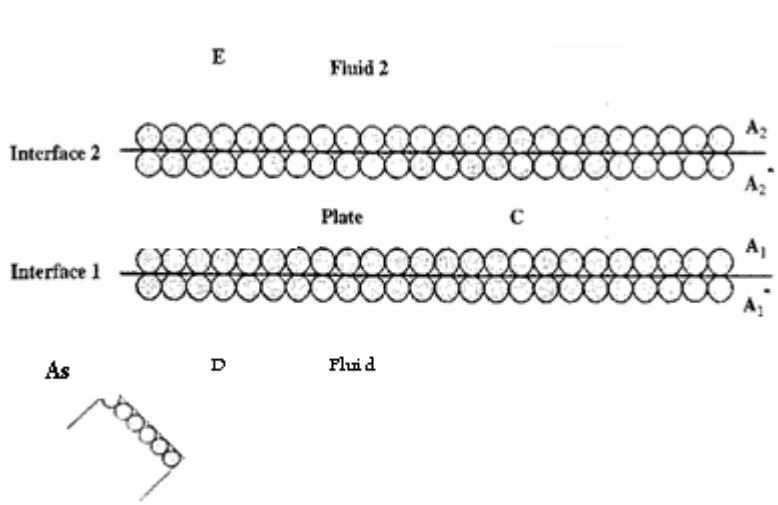

Figure 4.4 Source And Target Definition for Plate Submerged In Water

4.5.1 for mathematical modeling of plate the following boundary conditions has been used:

Across the fluid-solid interfaces, the displacement normal to the interface should be continuous. Also, across the interfaces, the normal stress (s33) in solid and fluid media should be continuous and the shear stresses at the interfaces must vanish. If the normal velocities of the two transducer faces are assumed to be $\mathbf{V}_S$o and $\mathbf{V}_{R_0}$, then the velocity of the surface of the transducer (designated as S) can be expressed as

$$MssAs+MsiAi = V_{S0} \qquad (4.63)$$

and on the surface of the transducer designated as R.

$$M_{R2}.A^*+M_{RR}AR = V_{RO} \qquad (4.64)$$

At the interfaces, from the continuity of the normal stress,

$$QisAs + \mathbf{Q_{11}\ A_1} = -S33_{11}.A_1^* - S33_{12}A_2 \qquad (4.65)$$

$$Q_{22}.A^* + Q_{2R}A_R = -S33_{21}.A^* - S33_{22}A_2 \qquad (4.66)$$

Continuity of the normal displacement across the two interfaces gives

$$DF3_{1s}As + DF3_{11}A_1 = DS3_{11}-A_1^* + DS3_{12}A_2 \qquad (4.67)$$

$$DF3_{22}.\ A_2^{*} + DF3_{2R}\ A_R = DS3_{21}.A_1^{*} + DS3_{22}A_2 \qquad (4.68)$$

and from the vanishing shear stress condition at the fluid-solid interface

$$S31_{11}.A_1{*}+S31_{I2}A_2=0 \qquad (4.69)$$

$$S32_{11}.A_1^{*}+S32_{12}A_2=0 \qquad (4.70)$$

4.5.2 Solution

Using the above mentioned boundary condition a matrix can be found that matrix is MATV which contains the geometric parametric relations of source and target in relation to stress, displacement, pressure, velocity whichever is intended to find out.

The source strength vector {A} of the total system can be calculated from Eq. (4.71)

$$\{A\} = [MAT]\text{-}'\{V\} \qquad (4.71)$$

After calculating the source strengths, the pressure, velocity, stress, and displacement values at any point can be calculated. For example, the pressure field in the fluid can be written as

$$\mathbf{P_R(Fi) = Q(Fi)}sA_s + \mathbf{Q(FI)IAI} \qquad (4.72)$$

$$\mathbf{PS(F2) = Q(F2)RAR + Q(F2)2}.A_2^{*} \qquad (4.73)$$

where, Fl is a set of target points inside the fluid medium below the plate and F2 is a set of target points inside the fluid medium above the plate. Similarly, in the solid plate, the stress and displacement fields can be obtained from the following set of equations:

$$s33_{(s)} = S33_{(S)1}.A_1^{*} + S33_{(S)2}A_2$$

$$s1l_{(s)} = Sll_{(s)1}.A_1^{*} + Sll_{(s)2}A_2$$

..... (4.74)

$$u3_{(s)}=DS3_{(s)1}.A_1{*}+DS3_{(s)2}A_2$$

$$ul_{(S)} = DSl_{(s)}\mathbf{i}.A_1^{*} + DS1_{(S)2}A_2 \qquad (4.75)$$

Where S is a set of target points inside the solid plate.

4.6 Application 3: Ultrasonic Field Modeling In A Solid Plate With Internal Defect (Banerjee And Kundu, 2007)

Let us consider a half-space and a plate containing an internal anomaly as shown in Fig. 4.5. One can see from this figure that the half-space has a fluid-solid interface and the plate is bounded by two solid-fluid interfaces. A cavity or an inclusion is entrapped inside the solid medium. Along the cavity boundary the stress free boundary condition and at the inclusion boundary continuity of the displacement and stress components must be enforced. Along the fluid-solid interfaces one layer of point sources are distributed as shown by the small circles in Fig. 4.5. Point sources are also distributed along the cavity boundary as shown in the figure.

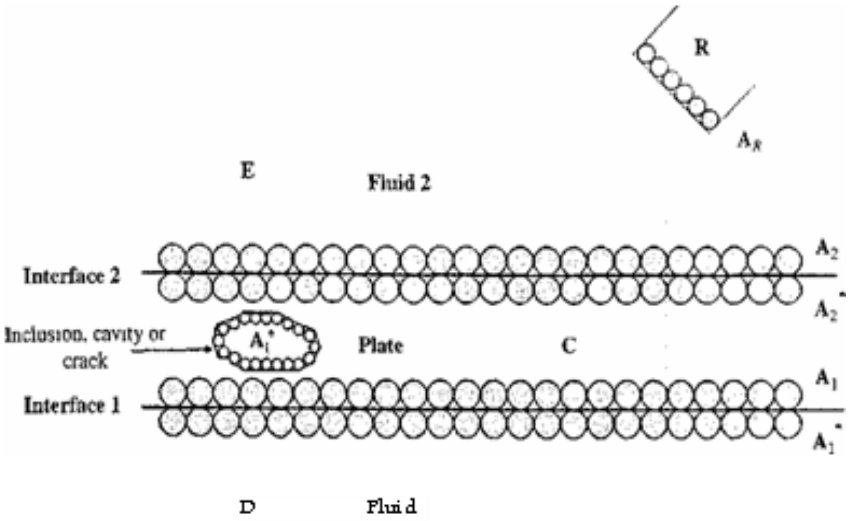

Figure 4.5 Plate with Internal Defect

4.6.1 for mathematical modeling of plate the following boundary conditions has been used:

If the normal velocities of the two transducer faces are assumed to be $\mathbf{V}_S$o and $\mathbf{V}_{R_0}$, then the velocity of the surface of the transducer (designated as S) can be expressed as

$$MssAs+MsiAi = V_{S0} \qquad (4.75)$$

and on the surface of the transducer designated as R.

$$M_{R2}.A^{*}+M_{RR}AR = V_{RO} \quad (4.76)$$

At the interfaces, from the continuity of the normal stress,

$$QisAs + \mathbf{Q_{11}\ A_1} = -S33_{1c}A_c^{*}\text{-}33_{11}.A_1^{*} - S33_{12}A_2 \quad (4.77)$$

$$Q_{22}.A^{*} + Q_{2R}A_R = -S33_{2c}.A_c^{*}\text{-}S33_{21}.A^{*} - S33_{22}A_2 \quad (4.78)$$

Continuity of the normal displacement across the two interfaces gives

$$DF3_{1s}As + DF3_{11}A_1 = DS3_{1c}\text{-}A_c^{*} + DS3_{11}\text{-}A_1^{*} + DS3_{12}A_2 \quad (4.79)$$

$$DF3_{22}.\ A_2^{*} + DF3_{2R}\ A_R = DS3_{2c}\text{-}A_c^{*} + DS3_{21}.A_1^{*} + DS3_{22}A_2 \quad (4.80)$$

and from the vanishing shear stress condition at the fluid-solid interface

$$S31_{1c}.A_c^{*}+S31_{11}.A_1^{*}+S31_{I2}A_2=0 \quad (4.81)$$

$$S31_{2c}.A_c^{*}+S32_{11}.A_1^{*}+S32_{12}A_2=0 \quad (4.82)$$

Vanishing normal and shear stress near boundaries of defect in plate:

$$S33_{CIC}.A_c^{*}+S33_{CI1}.A_1^{*}+S33_{CI2}A_2=0 \quad (4.83)$$

$$S31_{CIC}.A_c^{*}+S31_{CI1}.A_1^{*}+S31_{CI2}A_2=0 \quad (4.84)$$

$$S32_{CIC}.A_c^{*}+S32_{CI1}.A_1^{*}+S32_{CI2}A_2=0 \quad (4.85)$$

4.6.2 Solution

Using the above mentioned boundary condition a matrix can be found that matrix is MATV which contains the geometric parametric relations of source and target in relation to stress, displacement, pressure, velocity whichever is intended to find out.

The source strength vector {A} of the total system can be calculated from Eq. (4.86)

$$\{A\} = [MAT]\text{-}'\{V\} \quad (4.86$$

After calculating the source strengths, the pressure, velocity, stress, and displacement values at any point can be calculated. For example, the pressure field in the fluid can be written as

$$\mathbf{P_R(Fi) = Q(Fi)}sA_s + \mathbf{Q(FI)IAI} \qquad (4.87)$$

$$\mathbf{PS(F2) = Q(F2)RAR + Q(F2)2}.A_2^* \qquad (4.88)$$

for finding out stress and displacements in solid the same set of equations are used as discussed for plates without anomalities the only thing which needs to be added is the effect of defect stress and displacement on that of the plate

CHAPTER 5

Results and Discussions

MATHCAD programs have been developed to model the ultrasonic field in fluid as well as solid media based on the DPSM formulation presented. Modeling of ultrasonic field in homogeneous and non homogeneous fluid is already being done in both steady and transient states where transducer was considered to be at normal incidence to the interface. Present work is extended to model ultrasonic field in homogeneous fluid and non homogeneous fluid when transducer is placed at non-normal incidence. Ultrasonic field have also been modeled in infinite solid and then at fluid-solid interface. In later case plate submerged completely in water with existing crack and without crack has been considered. The numerical results clearly shows that the pressure/stress decays both in liquids/solids as the distance from the transducer increases and the field becomes more collimated as the frequency of the transducer increases. In case of solid the penetration of ultrasonic beam increases as the frequency increases and it becomes surface wave when the transducer inclination angle approaches critical angle of Rayleigh waves. For MATHCAD programming the above mentioned work has been subdivided into different cases. For each case separate codes are developed for both steady state and transient state. Before getting at results directly assumptions for both steady state and transient states needs to be studied. In all cases diameter of transducer is assumed to be 0.1 inches. The axis nomenclature for transducer is shown in figure5.1.For accurate modeling of field while using DPSM, discritization of transducer surface is of utmost importance. Discritization routines have been developed in MATHCAD for both source and target points as shown in figure 5.2.This chapter contains detailed discussions on results for each case considered.

5.1 Basic Assumptions and conventions used for MATHCAD Programs

The most basic element of ultrasonic testing is a finite dimension transducer. In all following cases discussed in this chapter the transducer size is assumed to be 0.1 inches. Following figure 5.1 shows the axis pattern that is considered while modeling field using MATHCAD routines.

- Transducer Axes Definition

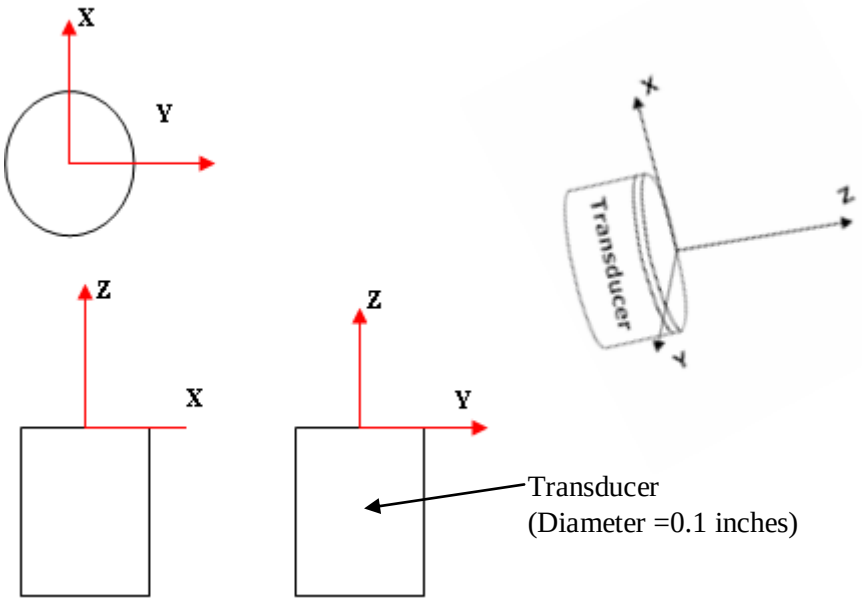

Figure 5.1 Circular Transducer-Axis Definition

The three axes that are shown in above figure are used in all cases for modeling field using DPSM technique.

- Discretization of transducer surface (source points)

To model the field accurately the discritization of source surface is of utmost importance. MATHCAD program has been developed to discritize the surface of circular transducer to find out the coordinates of source point. This has been done by making a library function **Trans** (with Diameter of transducer and radius of source point as its arguments).For source point's grid the following check has been placed in every routine for MATHCAD programming:

$$rs <<< \lambda/2\pi$$

Where,

rs, is radius of single source point

λ, wavelength of propagating wave

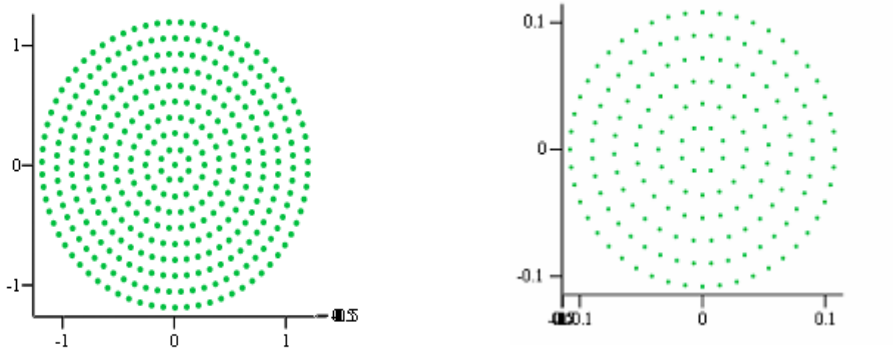

a) Trans (0.254, $6*10^{-3}$),N=225,Freq=2 MHz b) Trans (0.254, $9*10^{-3}$),N=80,Freq=1MHz

Where, N=number of source points

Figure 5.2 Source Points grid

From the above figure it can be concluded that when the radius of source increases the number of source point decreases to larger extent. Hence the check mentioned above needs to be put in all of routines because it varies the number of source points and also connects the frequency of transducer with source point grid

- Discretization for developing target grid source point

For target points grid generation the area of interest is divide into number of target points using developed MATHCAD routines .If the grid mesh is coarse the number of target points will be lesser which leads to reduction in calculations and time but accuracy suffers. In other case when target grid is finer the number of points will increase and on expense of computational and accuracy. Following plots shows the target grid at different planes, which are used while developing MATHCAD programs.

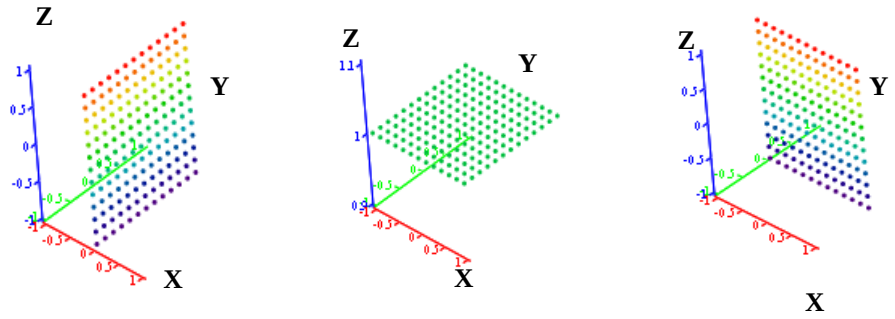

a) YZ plane **b) XY plane** **c) XZ plane**

Figure 5.3 Target Point Discretization in Different Planes

- Transient Analysis (Input and Flow Chart)

Fast Fourier transform (FFT) is used to convert time domain impulse into frequency domain pulse. Then for each frequency, DPSM method is applied and obtained response is again transformed to time domain using inverse Fourier transforms (IFFT). Frequencies up to Nyquist frequencies are used for analysis and effect of remaining frequencies are taken care by superimposing anti-symmetry behavior of imaginary part about Nyquist frequency. **Figure 5.4** shows the flowchart for reconstruction of transient wave program in homogenous fluid using DPSM techniques.

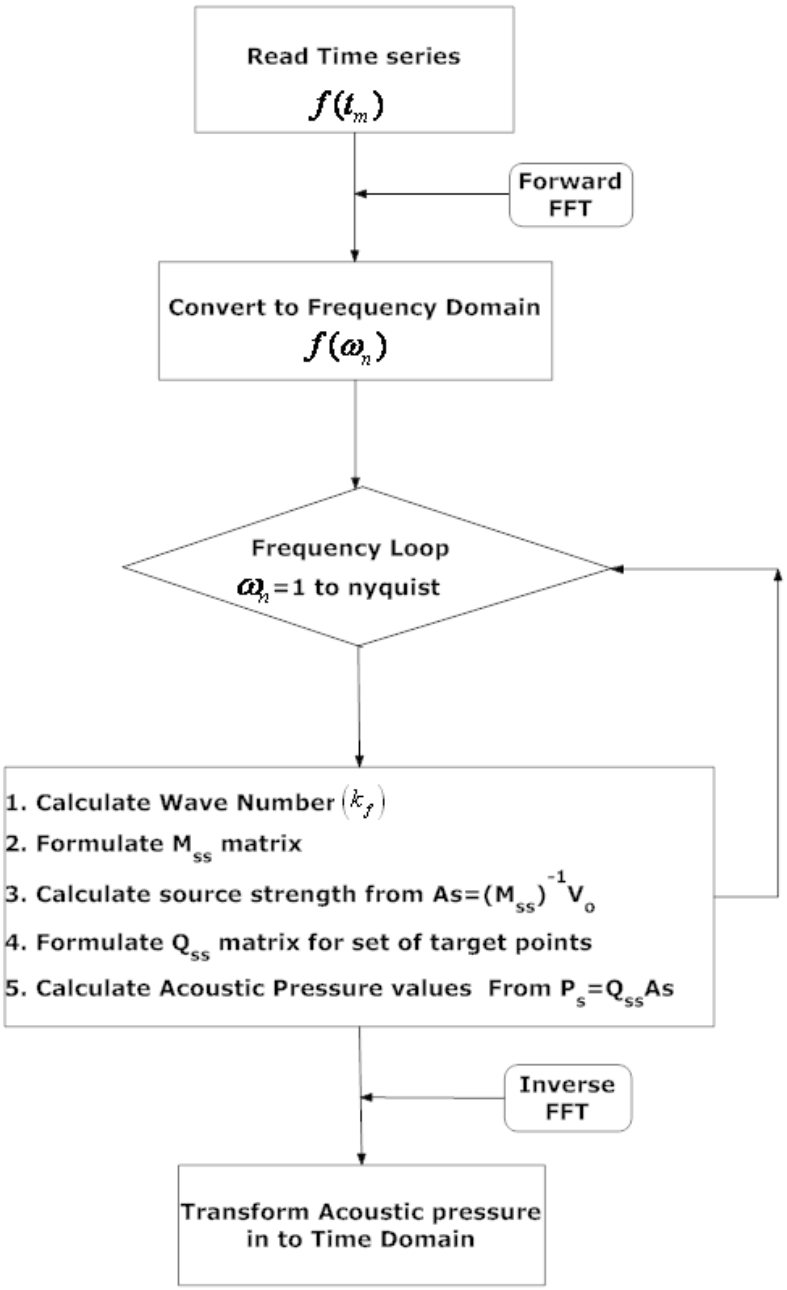

Figure 5.4 Flow Chart for Transient Analysis

- Input signal used for transient analysis

Input signal that has been used throughout the transient analysis is a five cycle tone burst. Following figure shows the time distribution of the harmonic function and its FFT in frequency domain.

Tone Burst Velocity Impulse:

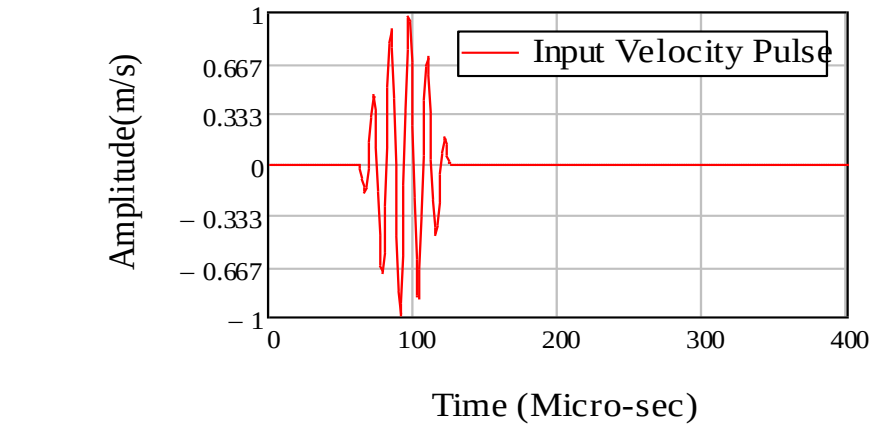

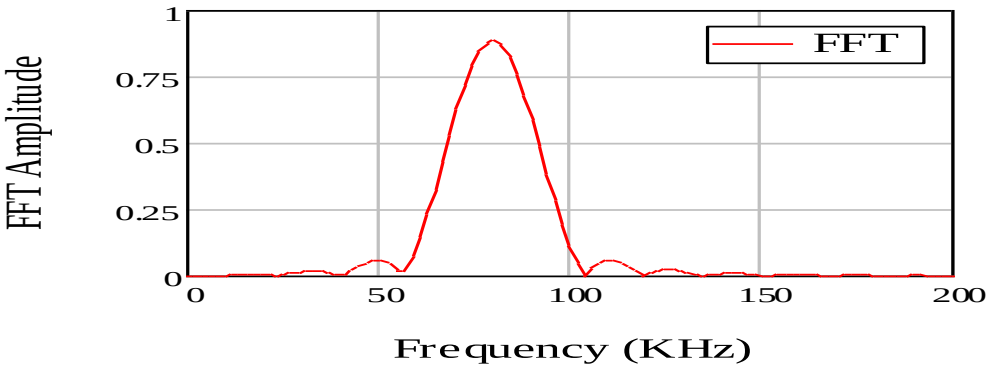

Figure 5.5 Tone Burst Signal as Input and Its FFT

Now as all the basic assumptions have been discussed which are used extensively in all the developed MATHCAD programs. In next sections the modeling results have been discussed for each separate cases of fluids and solids

5.2 Case 1: Wave Propagation in Homogenous Fluid (Transducer at Non normal Incidence):

5.2.1 Steady state analysis

In this case only one fluid is present and the ultrasonic field is modeled .Here both steady and Transient Wave propagation is studied. The discretization of transducer is already being discussed. In this case the transducer is inclined with respect to normal as shown in figure 5.6

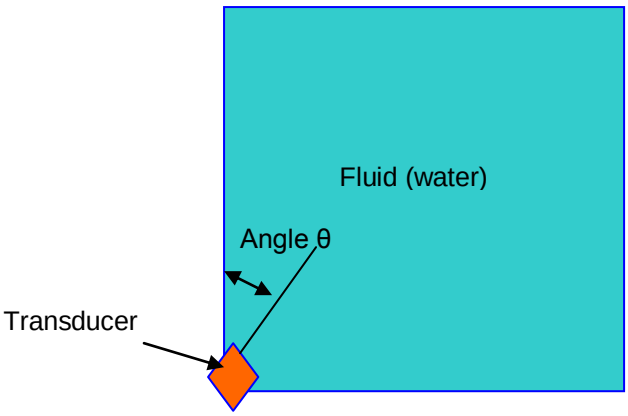

Figure 5.6 Homogeneous Fluid Non Normal Incidence of Transducer

Name of Fluid	Density (gm/cc)	P-Wave Speed (C_p)(km/sec)
Water ($20°C$)	1	1.49

Table 5.1 Properties of Fluid

While modeling field of an inclined transducer in homogeneous fluid the point of strike and the initial velocity of transducer changes. As discussed in chapter 4 (equation 4.23) it is clear that for considering inclination the MSS matrix is modified figure 5.7 shows the results for the same in steady state. These results are evaluated at different angles of incidences and frequencies. It can be clearly seen that when frequency increases the scattering of wave decreases and wave behaves as if the whole energy is concentrated in middle core.

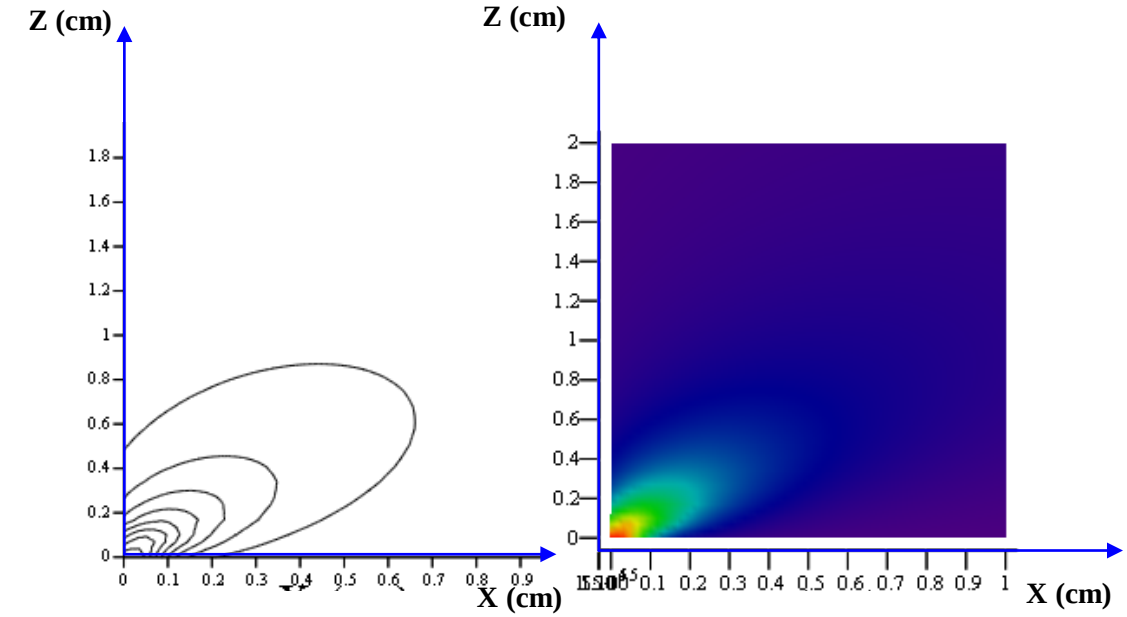

a) Freq= 1MHz (80 source points)

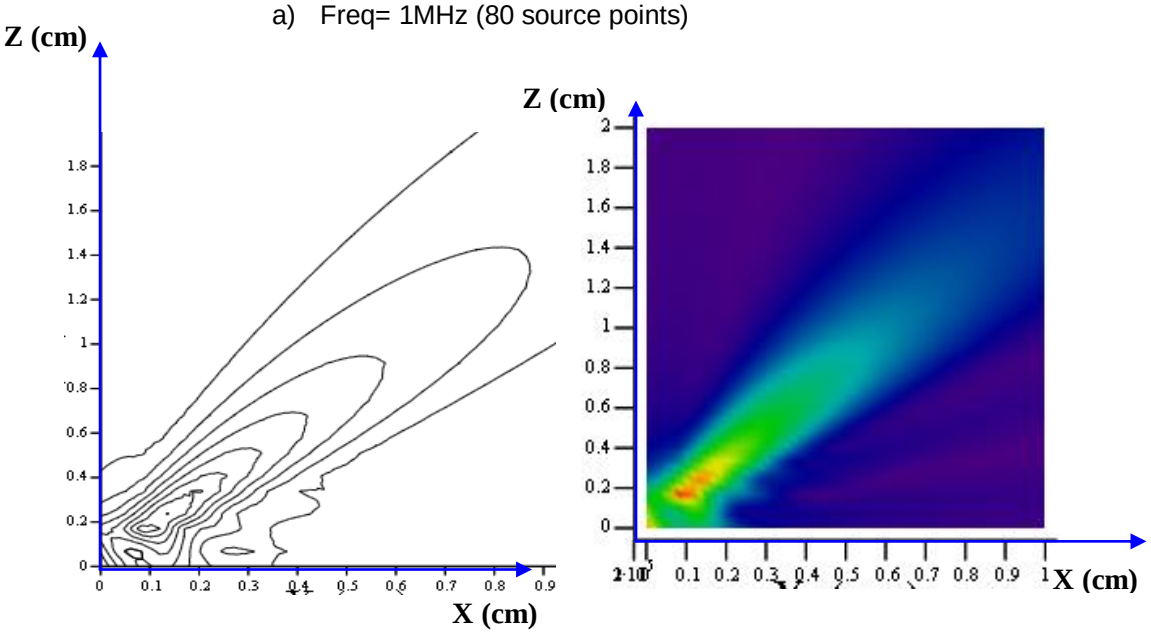

b.) Freq= 2.2 MHz (490 source points)

Figure 5.7 Pressure Plot of Homogeneous Fluid ($\theta = 35^0$)

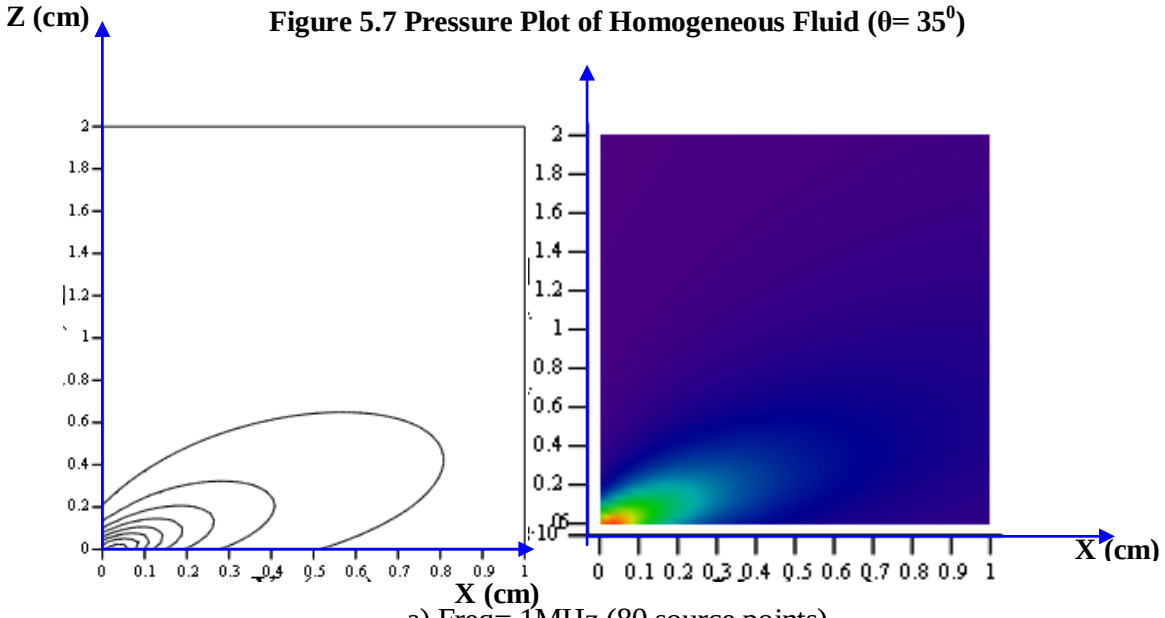

a) Freq= 1MHz (80 source points)

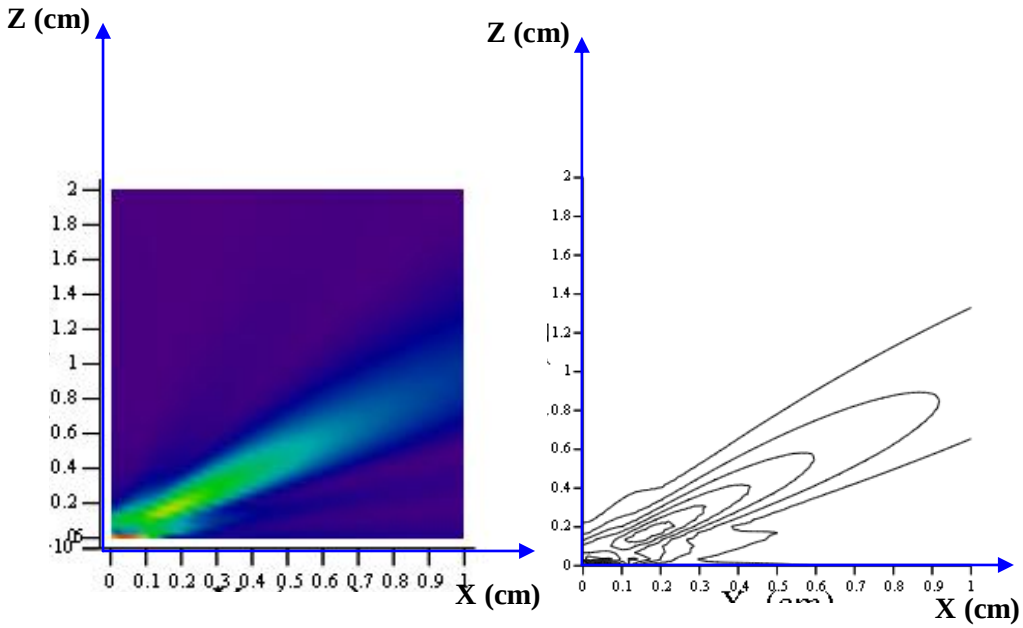

b) Freq= 2.2 MHz (490 source points)

Figure 5.8 Pressure Plot of Homogeneous Fluid For ($\theta=50^0$

5.2.2 Transient Analysis For Homogeneous Fluid

Figure 5.4 shows the flowchart for reconstruction of transient wave program in homogenous fluid using DPSM techniques. The same principal is used for non normal incidence of transducer beam in fluid.

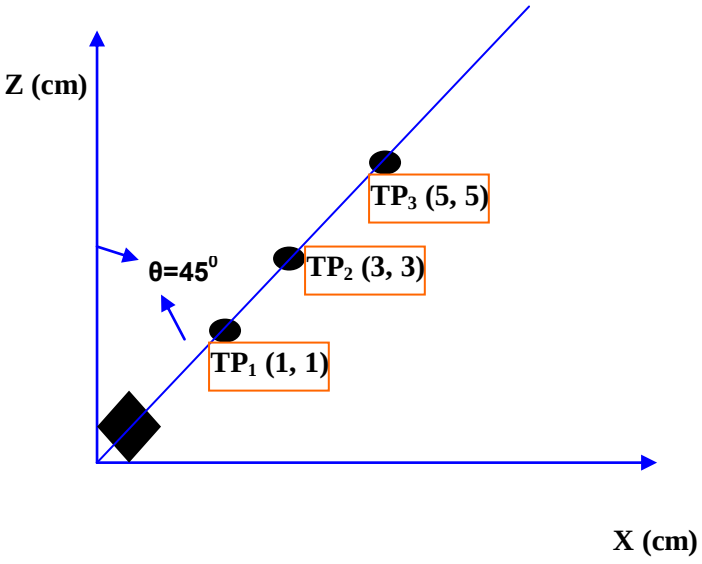

Figure 5.9 Target points in Homogeneous Fluid

Three target points are considered and transient wave propagation is studies through time validations of DPSM results with analytical results.

At target point 1, TP_1 (1, 1)

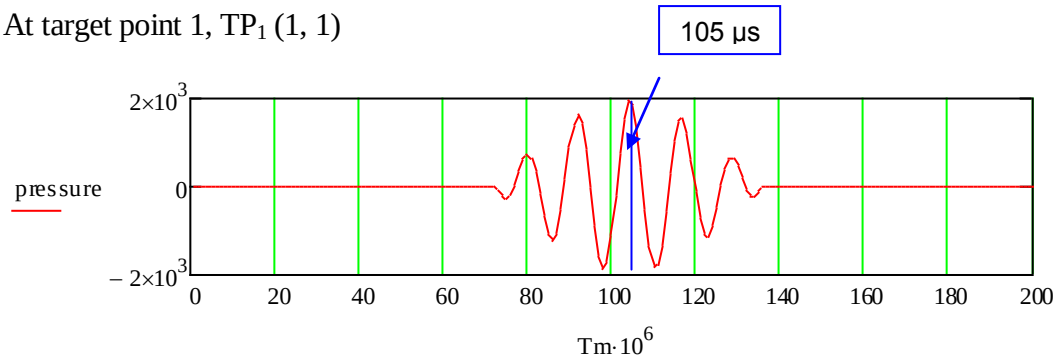

Target point 2, TP2 (3, 3)

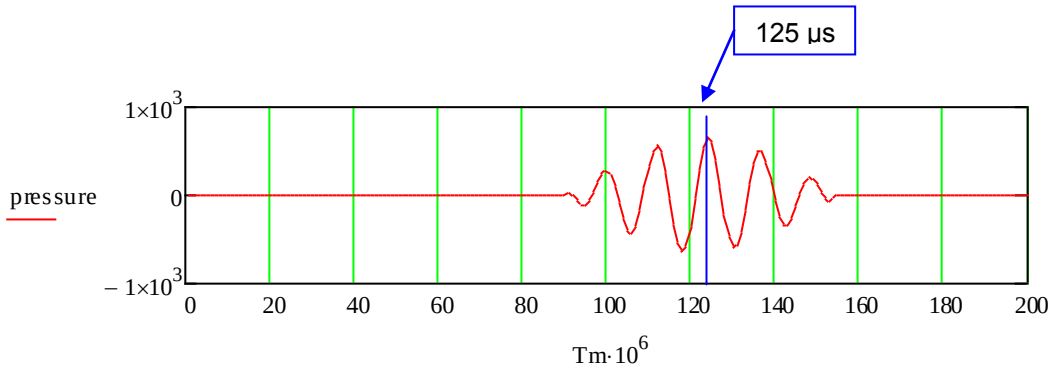

Target point 3, TP3 (5, 5)

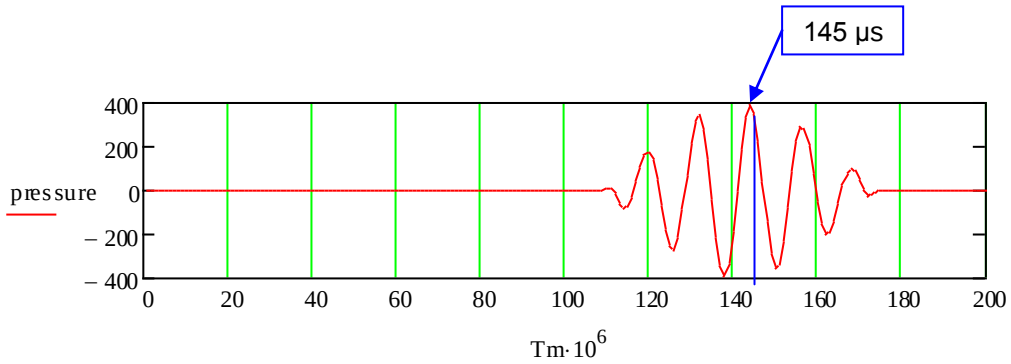

Figure 5.10 Transient Results for Homogeneous Fluid

Target point Location	Analytical results (Time=Distance/Speed)	DPSM
TP_1(1,1)	(14.14/1.49)+98 = 106.5 μs	105 μs
TP_1(3,3)	(42.43/1.49)+98 =126 μs	125 μs
TP_1(5,5)	(70.71/1.49)+98 =147 μs	145 μs

Table 5.2 Time validation Homogeneous fluid

5.3 Case 2: Wave Propagation in Non-Homogenous Fluid (Transducer Inclined With Vertical):

In this case two layers of fluids are arranged such that their density monotonically increases from bottom to top and Transient wave propagation is studied in this.

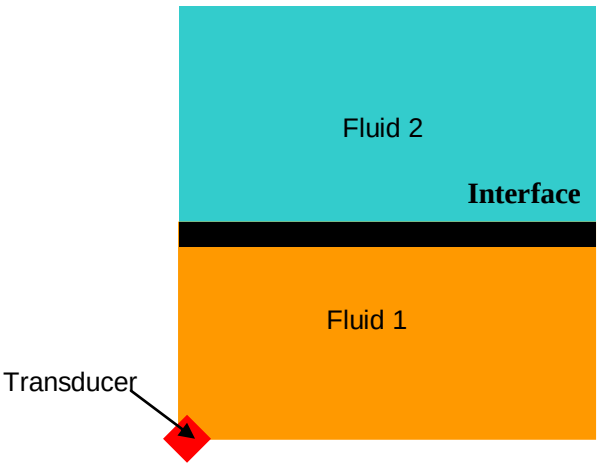

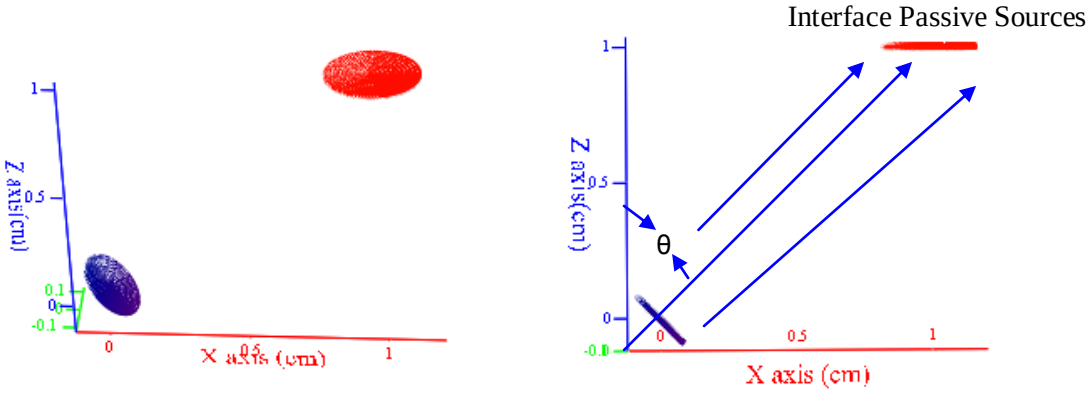

Figure 5.11 Non Homogeneous Fluid at Non Normal Incidence of Transducer

Name of Fluid	Density (gm/cc)	P-Wave Speed (C_p) (Km/sec)
Fluid 1	1	1.49
Fluid 2	1.5	2.00

Table 5.3 Fluid Properties for Fluid1/Fluid 2 Interface

We are interested in computing the ultrasonic field in multilayered fluid systems. In the multilayered problem geometry several interfaces may be present as discussed in chapter4. When fluids with different densities and acoustic properties form a multilayered system, the fluid density should monotonically vary from top to bottom. For a system with n number of fluids there will be (n-1) number of interfaces. Each interface acts as a transmitter as well as a reflector of elastic wave energy generated by the ultrasonic transducers.

5.3.1 Results for Steady State in Non Homogeneous Fluid:

Routine has been developed for modeling ultrasonic field when transducer emitting energy at a certain angle. The mentioned approach (as discussed in chapter 4 section 4.3) is used to find the source strength for a given velocity of source points, then pressure and velocity at any point within the two fluids can be calculated using equations 4.28 and 4.29 (chapter 4).To generate the ultrasonic field in two fluids a rectangular grid has been created for target points.

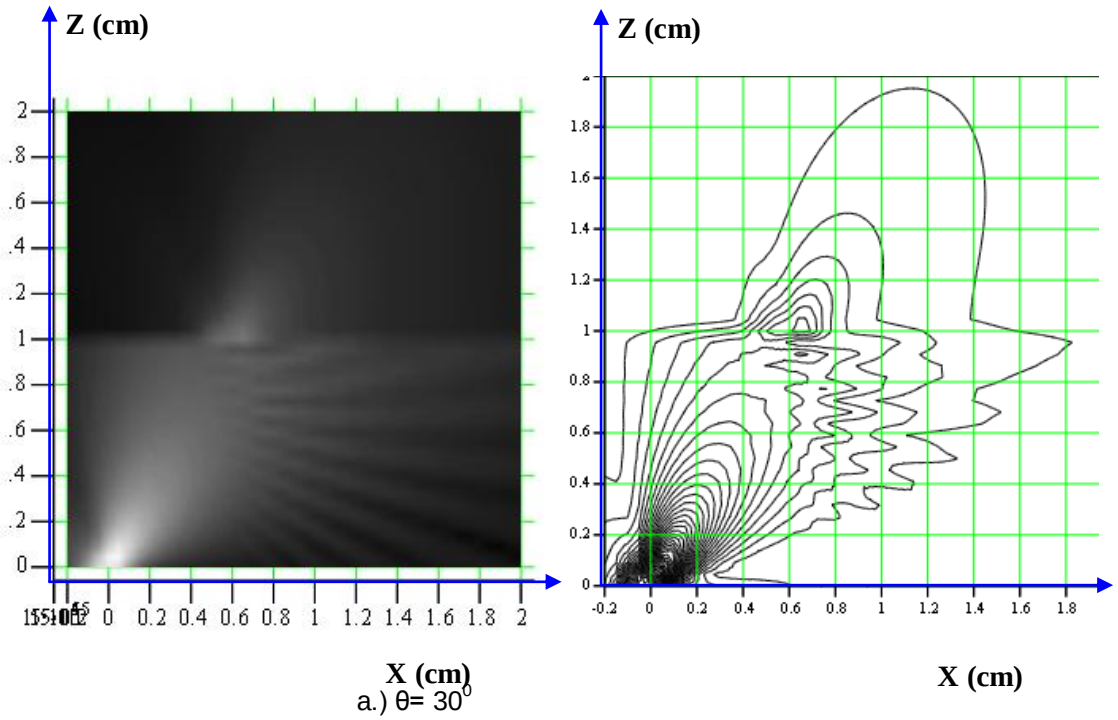

a.) $\theta = 30^0$

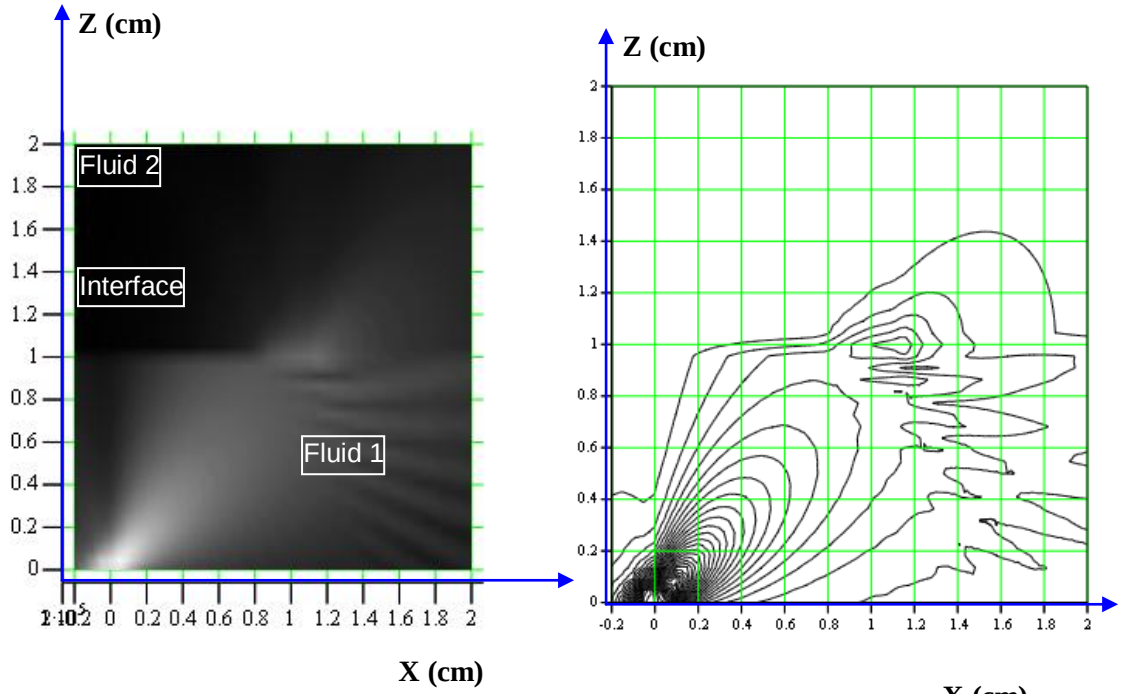

b)θ=45^0

Figure 5.12 Pressure Plots at Different Angle (Freq=1 MHz)

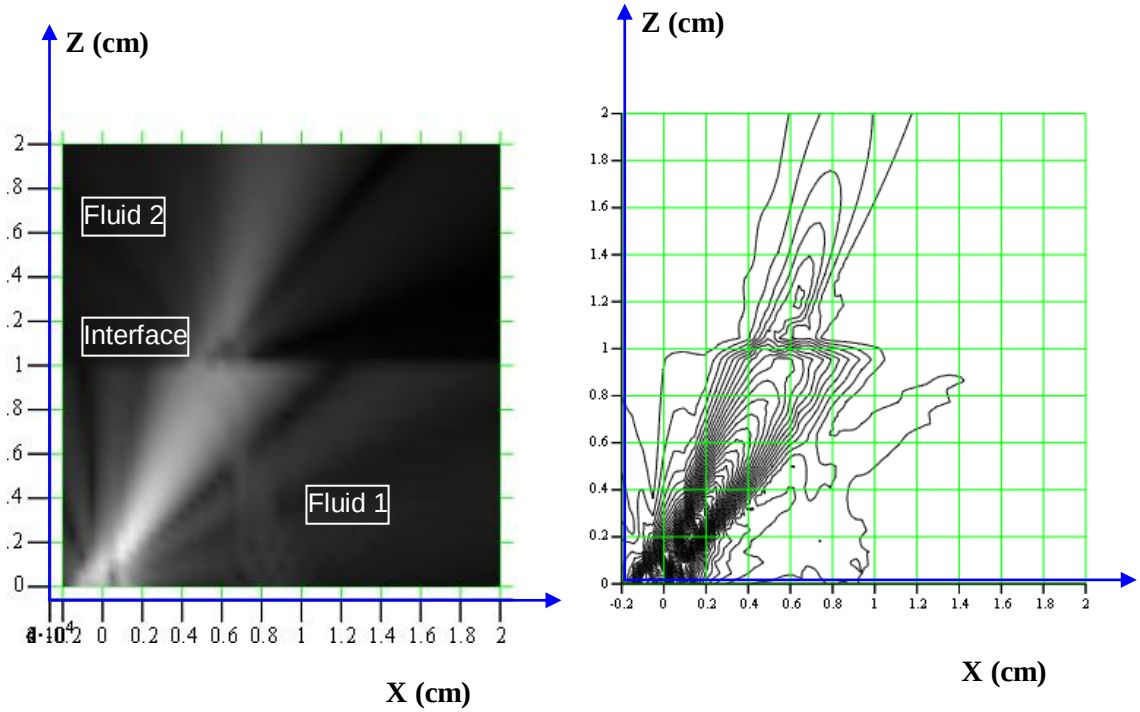

a.) θ=30^0

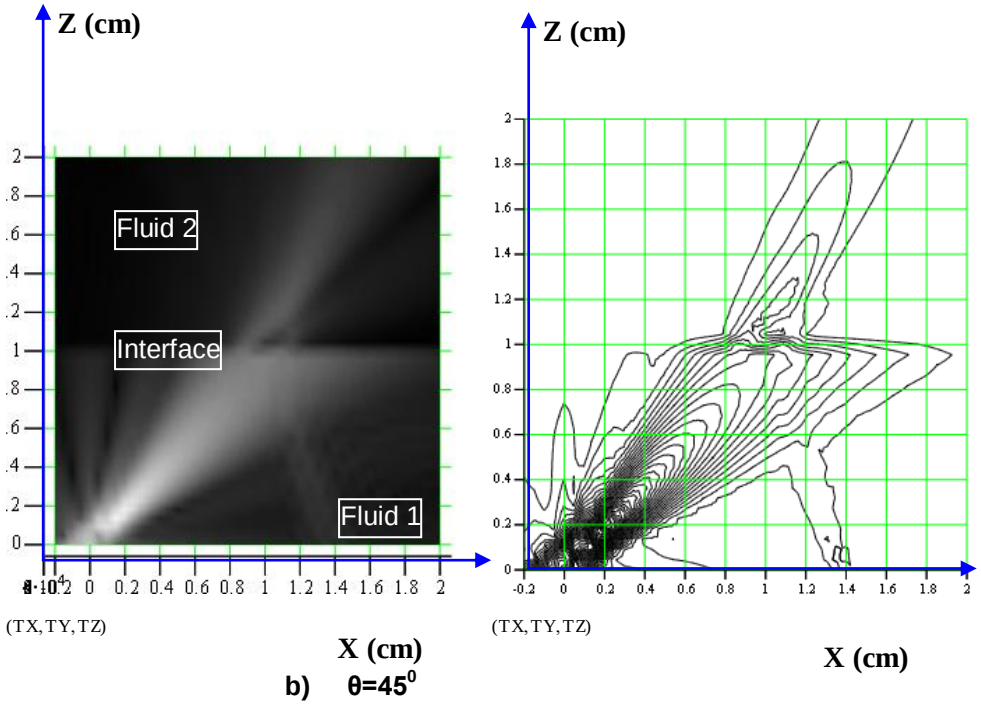

Figure 5.Pressure Plots at Different Angle (Freq= 2.2 MHz)

5.3.2 Transient Analysis fro Non Homogeneous Fluid

The formulation for transient program for non homogeneous fluid is same as that of homogeneous fluid. Following discussion validates the MATHCAD results with analytical results.

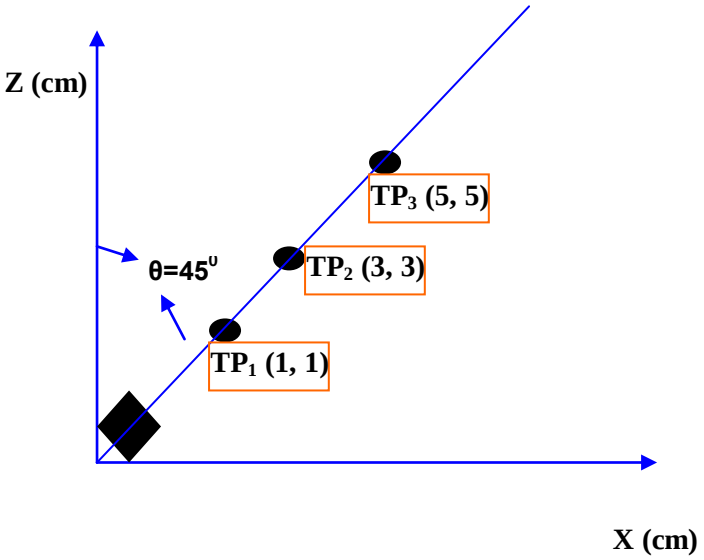

Figure 5.13 Target points in Non Homogeneous Fluid

Three target points are considered and transient wave propagation is studies through time validations of DPSM results with analytical results.

At target point 1, TP_1 (1, 1)

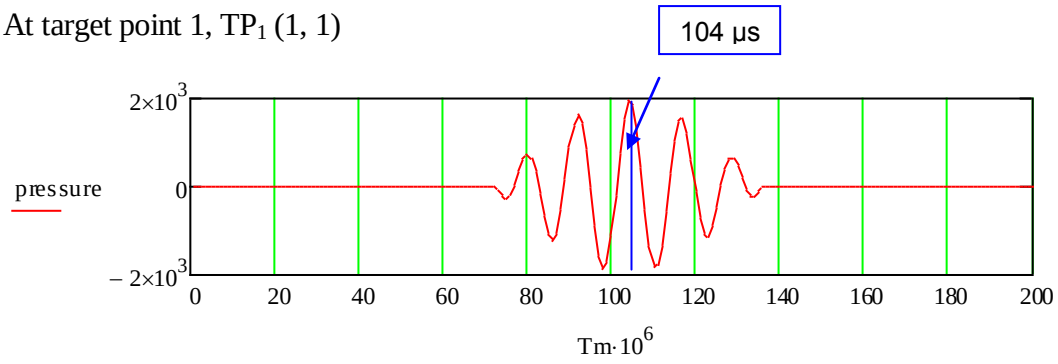

Target point 2, TP2 (3, 3)

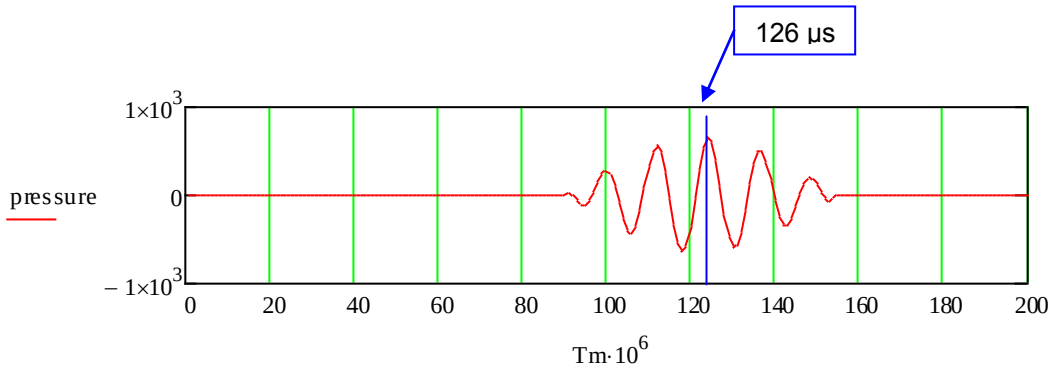

Target point 3, TP3 (5, 5)

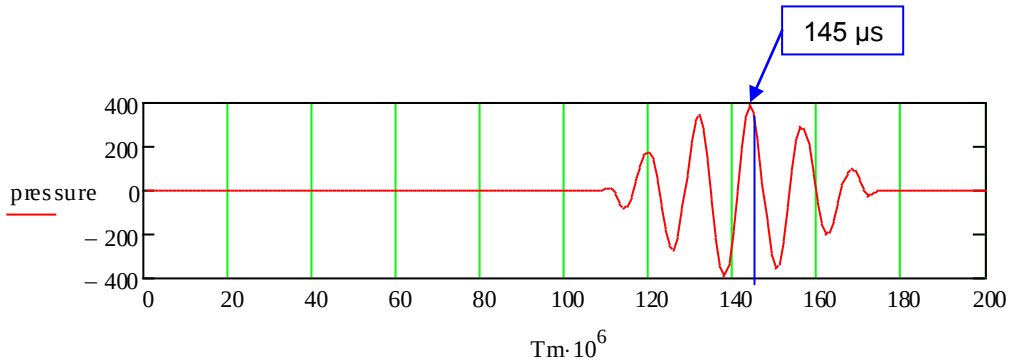

Figure 5.14 Transient Results for Homogeneous Fluid

Target point Location	Analytical results (Time=Distance/Speed)	DPSM
TP_1(1,1)	(14.14/1.49)+98 = 106.5 µs	104 µs
TP_1(3,3)	(42.43/1.49)+98 =126 µs	126 µs
TP_1(5,5)	(70.71/1.49)+98 =147 µs	145 µs

Table 5.4 Time validation for Non Homogeneous Fluid

5.4 Case 3: Wave Propagation in homogeneous solid

Field modeling inside a solid is a tedious task because of presence of shear waves which cannot exist in liquids. So for modeling the effect of both P wave and S-wave propagations needs to be considered.

MathCAD routines have been developed to model the ultrasonic field inside a homogeneous solid and at fluid solid interface. The modeling is further extended to model field inside a plate immersed in water. Plate with a rectangular defect has also been modeled. Following are MathCAD routines outputs in each case considered:

5.4.1 Ultrasonic field inside homogeneous solid with circular transducer

MATHCAD routines have been developed to model the ultrasonic field inside an infinite solid. The simplest case considered is shown below:

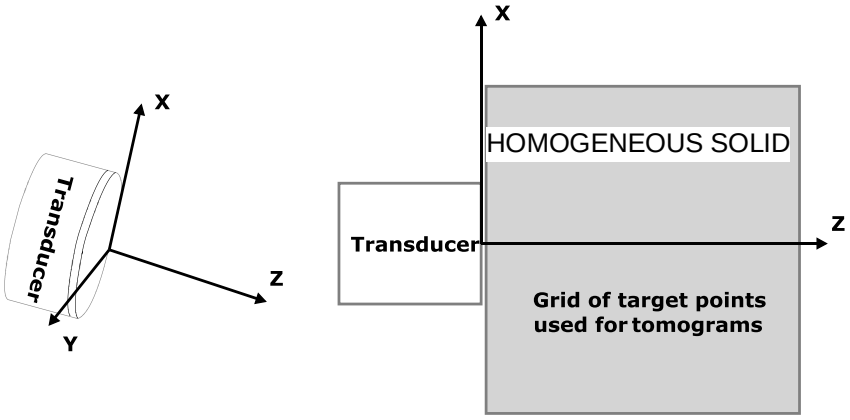

Figure 5.15 Source and Target Point for an Infinite Homogeneous Solid

in this case a discritized transducer is placed directly on the grid and it assumed to deliver an arbitary forcing function. Two different solids (Steel, Aluminum) have been considered while modeling field in homogeneous solid. The properties of solid are mentioned below.

Materials	Steel	Aluminum
P-wave speed (c_p)	5.66 km/sec	6.5 km/sec
S-wave speed (c_s)	3.05 km/sec	3.13 km/sec

Density (ρ_s)	7.8 gn/cc	2.7 gm/c.c.
First Lamé constant (λ)	104.1 GPa	61.17 GPa
Second Lamé constant (μ)	72 GPa	26.45 GPa

Table 5.5 Solid Properties

Following figure shows the variation of stress and displacement in solid near the transducer surface when different frequencies has been considered.

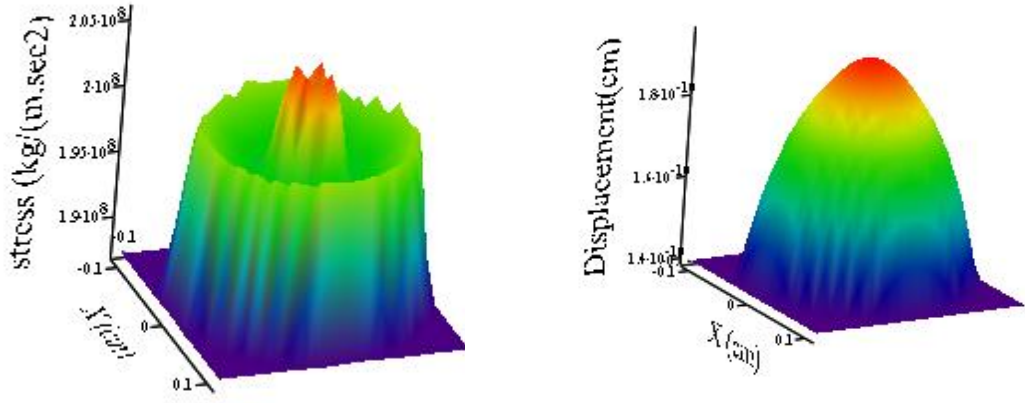

Number of points (both source and target) =68

a) Stress at transducer surface b) Displacement at transducer surface

Figure 5.16 Displacement U33 And Stress S33 Surface Plots (Freq= 0.1 MHz)

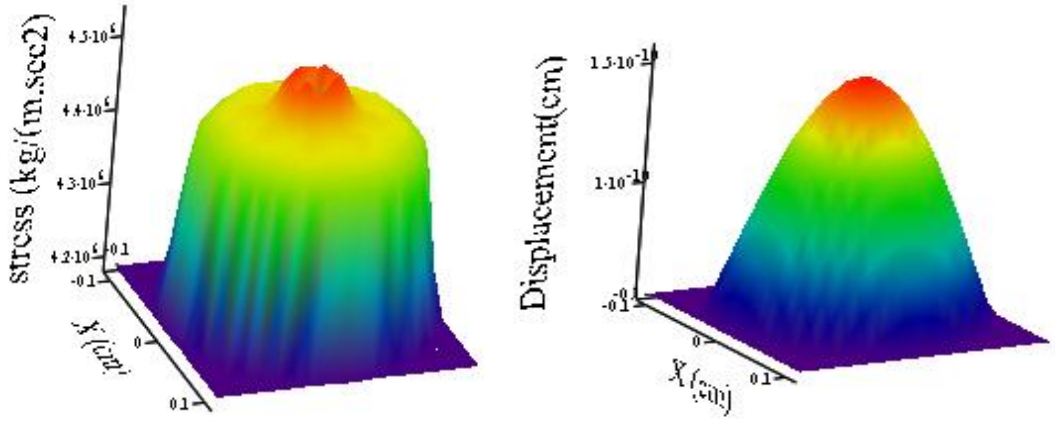

Number of points (both source and target) =118

a) Stress at Transducer Surface b) Displacement at Transducer Surface

Figure 5.17 Displacement U33 And Stress S33 (Freq= 1 MHz)

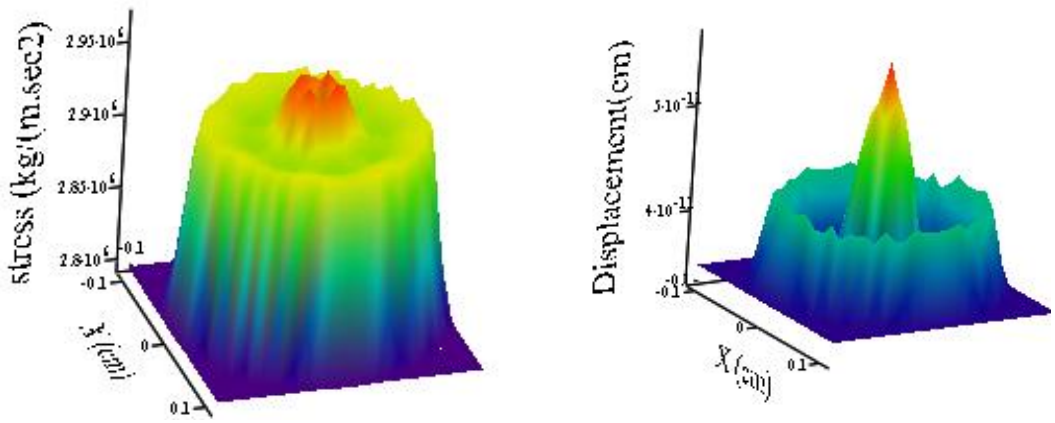

Number of points (both source and target) =358

a) Stress at transducer surface b) Displacement at transducer surface

Figure 5.18 Stress And Displacement Plot (Freq=2 MHz)

It can be clearly seen from above figures that when frequency is increased the energy emitted by transducer accumulates on core. At 0.1 MHz the spread of surface plot is more as compared to 1 and 2 MHz. As frequency increased from 0.1 to 1 MHz and then 1 MHz to 2MHz the surface plot of displacement changes. The above results have been calculated with circular transducer. In the next section rectangular transducer is considered and the stress and displacement.

5.4.2 Ultrasonic field inside homogeneous solid with rectangular transducer

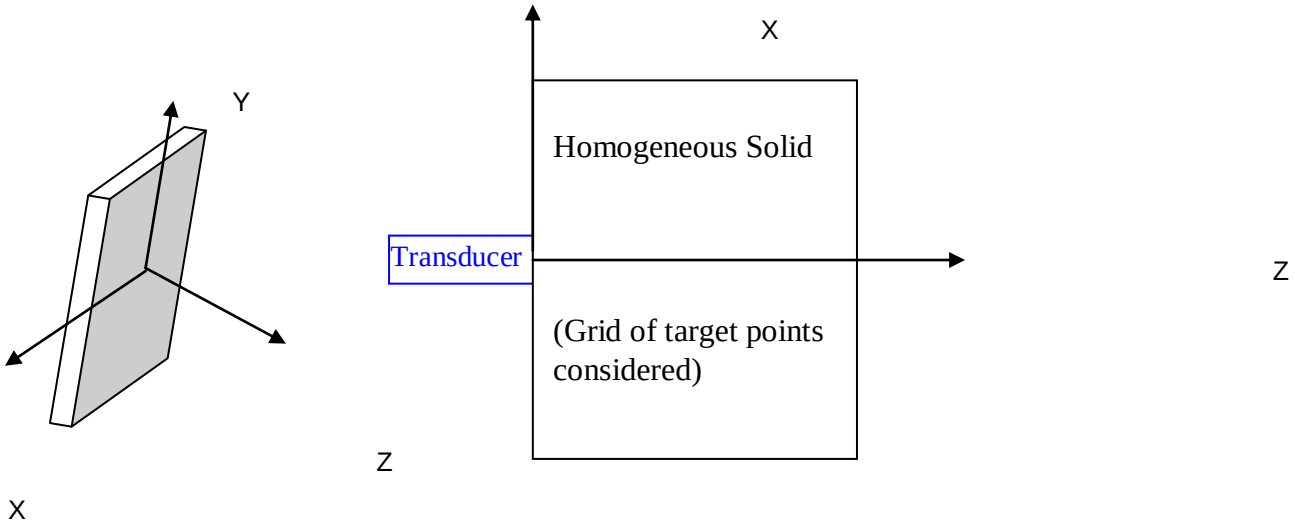

Figure 5.19 Source and Target Definition for Rectangular Transducer

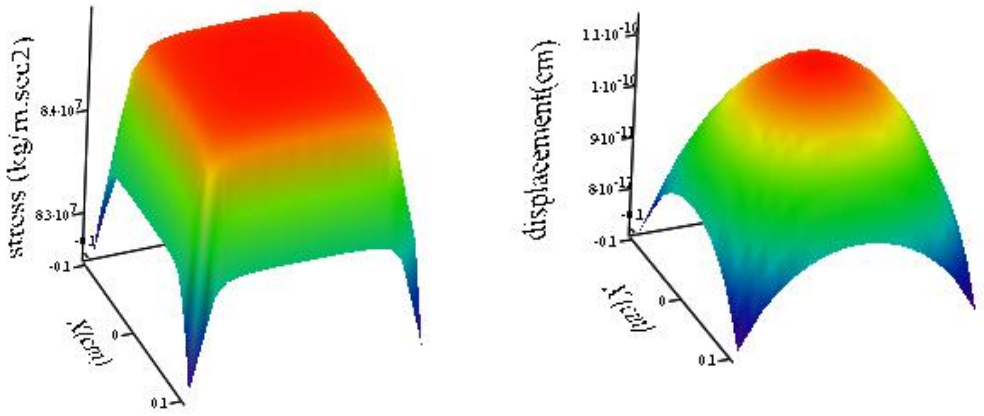

a) Stress at transducer surface b) Displacement at transducer surface

Figure 5.20 Stress And Displacement at Transducer Surface (Freq= 0.1 MHz)

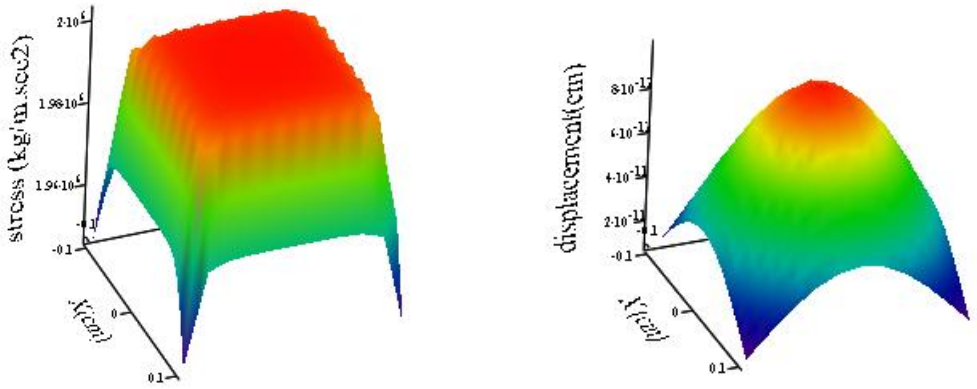

a) Stress at transducer surface b) Displacement at transducer surface

Figure 5.21 Stress And Displacement (Freq= 1MHz)

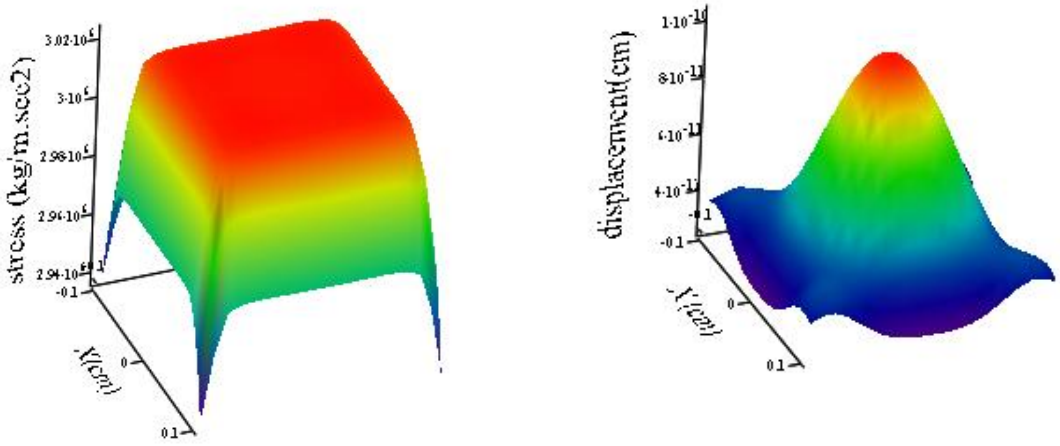

a.) Stress at transducer surface b.) Displacement at transducer surface

Figure 5.22 Surface Plot for Stress and Displacement (Freq= 1.5 MHz)

The above two cases discussed in section 5.4.1 and 5.4.2 are for steady states. In next section transient wave propagation is discussed for both circular and rectangular transducer.

5.4.3 Transient wave propagation in steel for circular transducer

For calculating stress and displacement for a duration of time(transient effect),the target points considered are taken at different distances from transducer and the effect of transducer is calculated and shown in following figures.

5.4.3.1 Time Validation:

Time validation refers to the validation of MATHCAD results with the analytical results. In following figures the maximum amplitude peak of input tone burst signal is considered. The noted time has been compared with the analytically calculated time.

Parameter	Units
Pressure/Stress	Kg/cm.sec^2
Displacement	cm
Velocity	Cm/sec

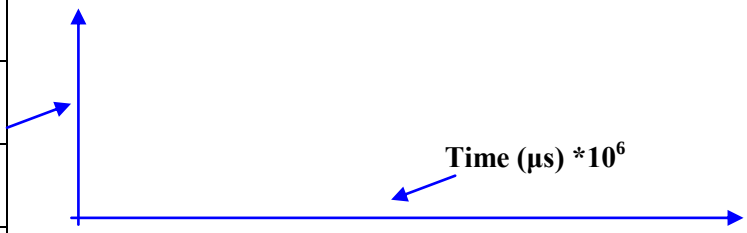

Figure 5.23 Axes Definition for Transient analysis

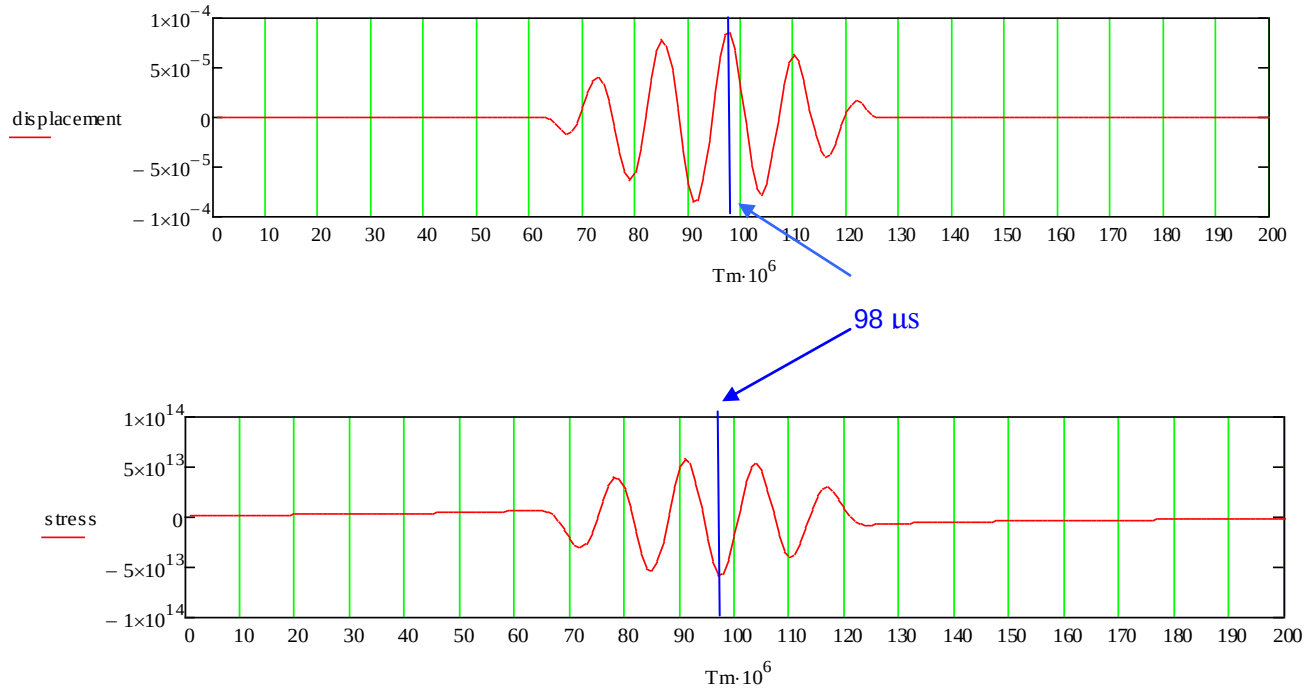

Figure 5.24 Output Signal for steel Z=0 cm

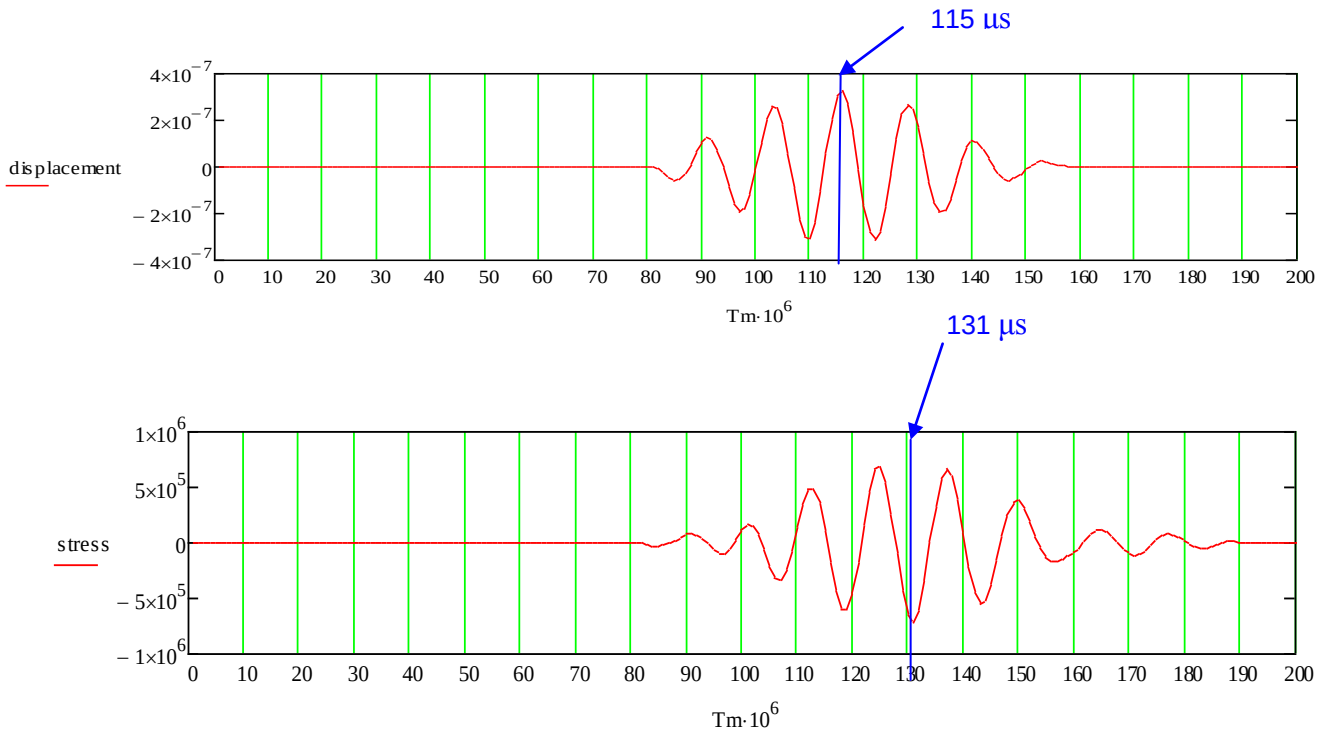

Figure 5.25 Output Signal for steel Z=10 cm

Method	Cp=5.66 km/sec	Cs =3.05 km/sec(STRESS)
Analytical (Z=10 cm)	100/5.66+98 = 115.6 μs	100/3.05+98=129.98 μs
DPSM	115 μs	132 μs

Table 5.6 Time Validation at Z=10cm

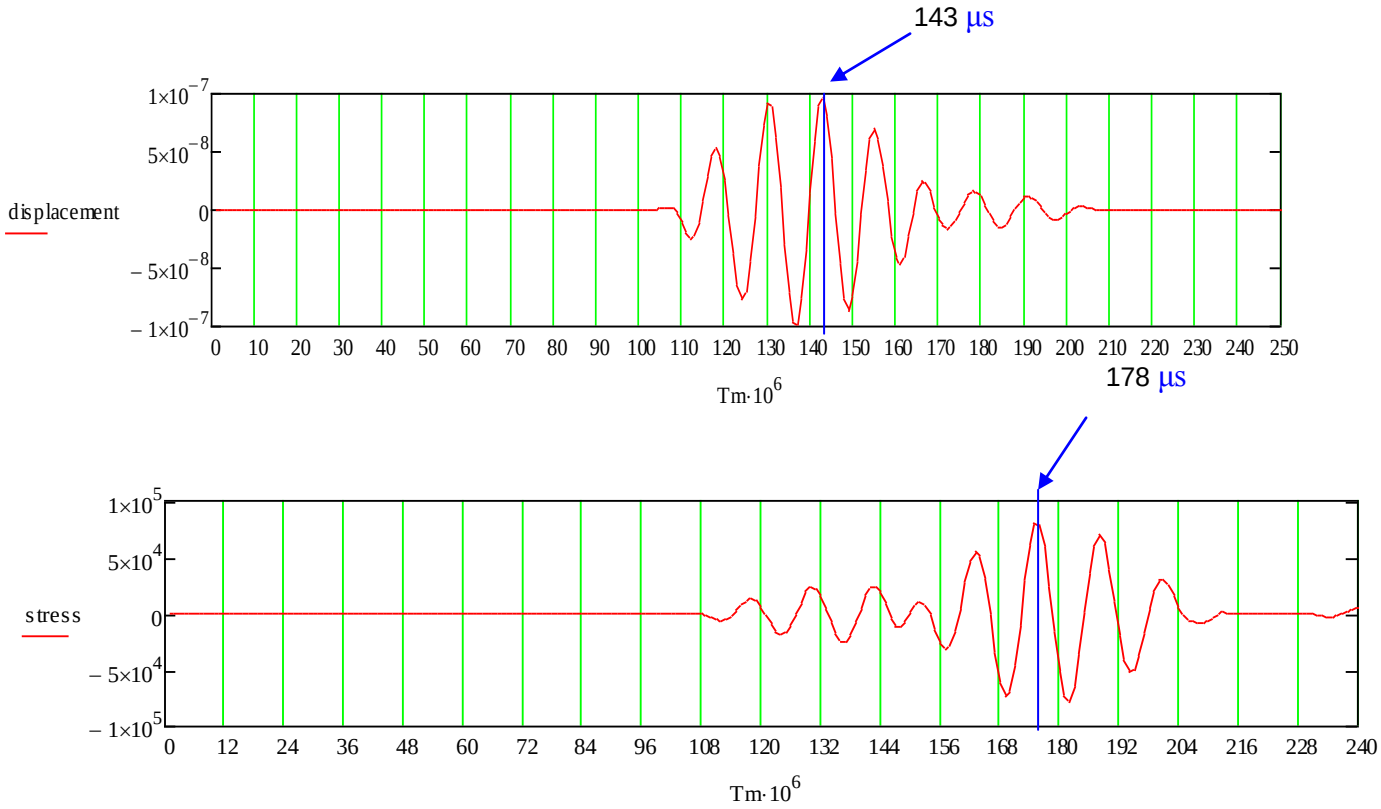

Figure 5.26 Output Signal for steel Z=25 cm

Method	Cp=5.66 km/sec	Cs =3.05 km/sec(STRESS)
Analytical (Z=25 cm)	250/5.66+98 = 142.6 μs	250/3.05+98=179.66 μs
DPSM	143 μs	178 μs

Table 5.7 Time Validation at Z=25cm

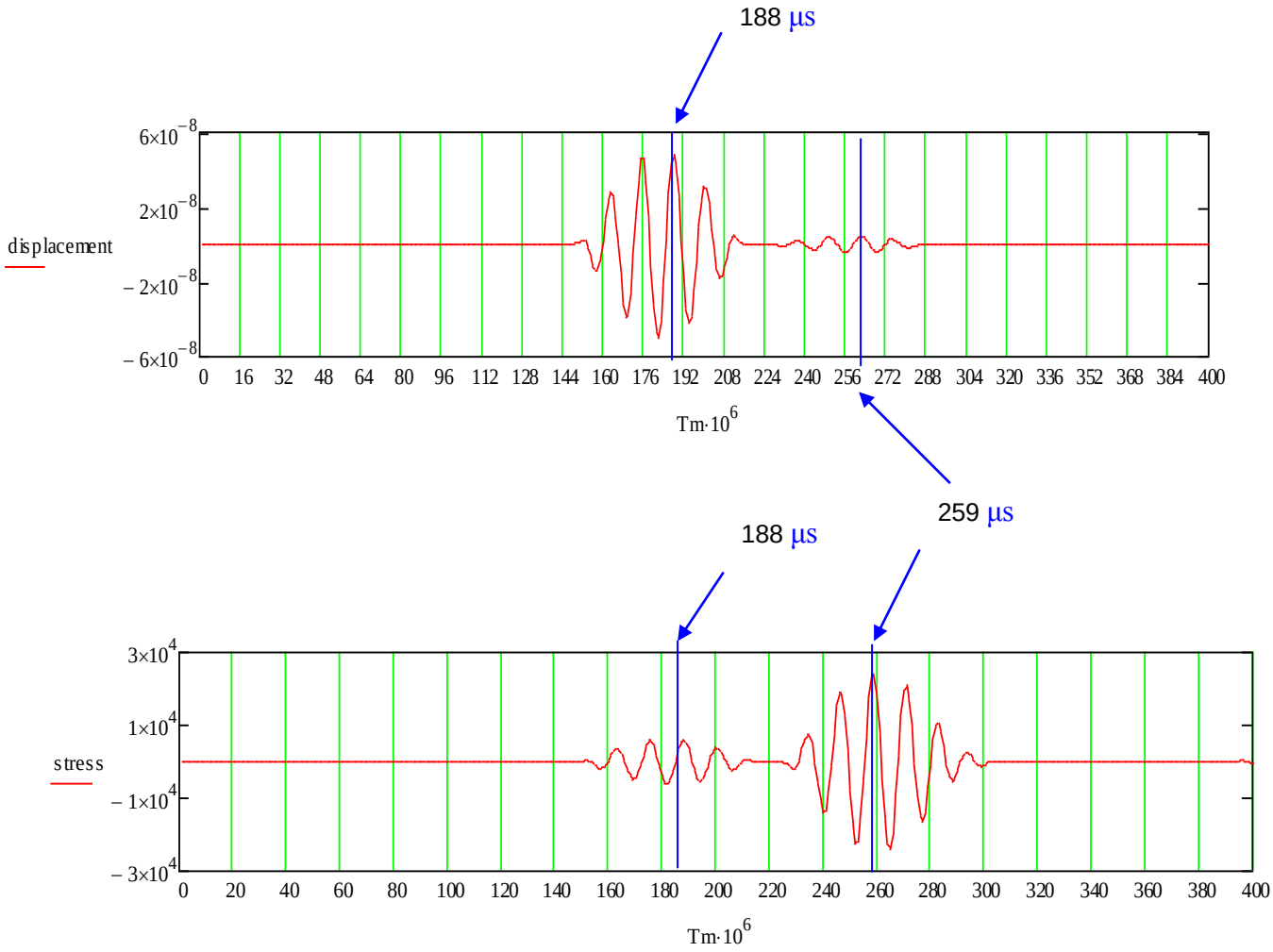

Figure 5.27 Output Signal for steel Z=50 cm

Method	Cp=5.66 km/sec	Cs =3.05 km/sec(STRESS)
Analytical (Z=50 cm)	500/5.66+98 = 188.8 μs	500/3.05+98=260 μs
DPSM	188 μs	259 μs

Table 5.8 Time Validation at Z=50cm

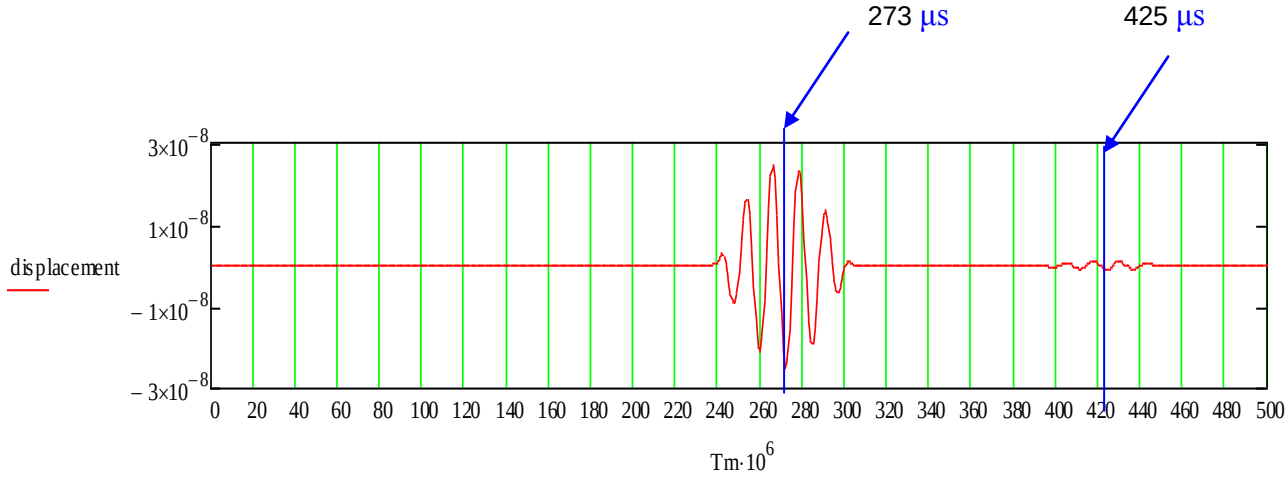

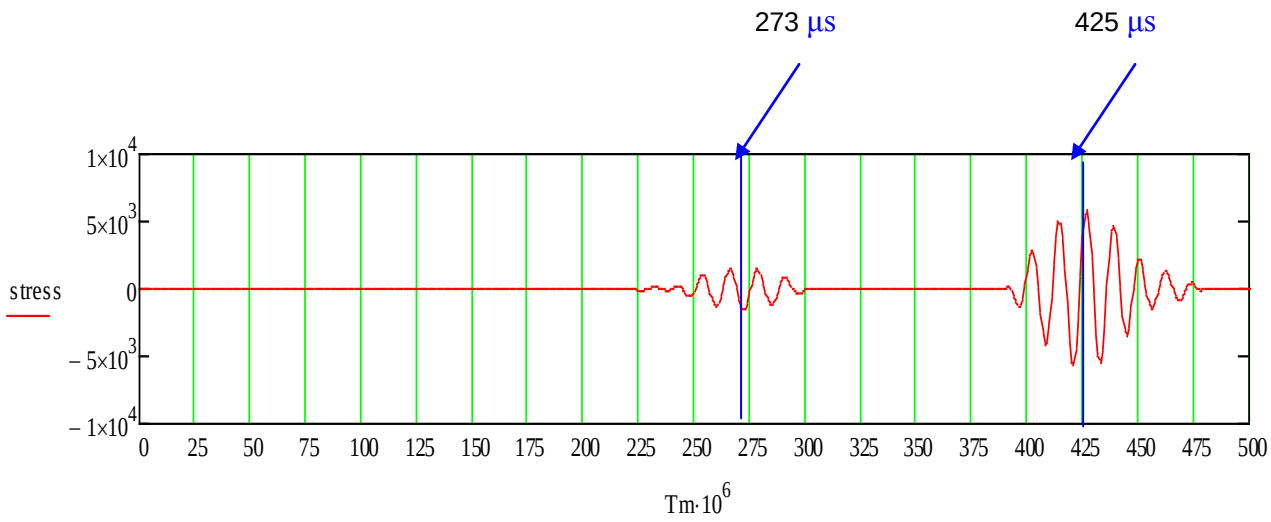

Figure 5.28 Output Signal for steel Z=100 cm

Method	Cp=5.66 km/sec	Cs =3.05 km/sec(STRESS)
Analytical (Z=100 cm)	1000/5.66+98 = 274.6 µs	1000/3.05+98=425.3 µs
DPSM	274 µs	425 µs

Table 5.9 Time validation =100 cm

For ***Aluminum*** the values of P-wave velocity and Shear wave velocity differs following results shows the transient wave propagating inside aluminum.

At transducers surface,

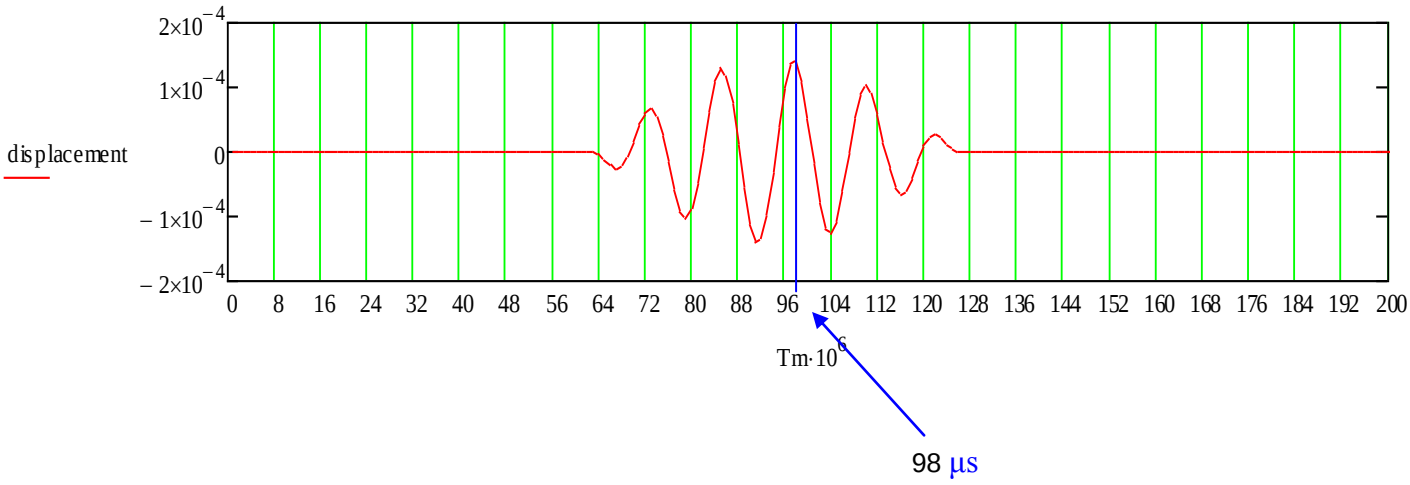

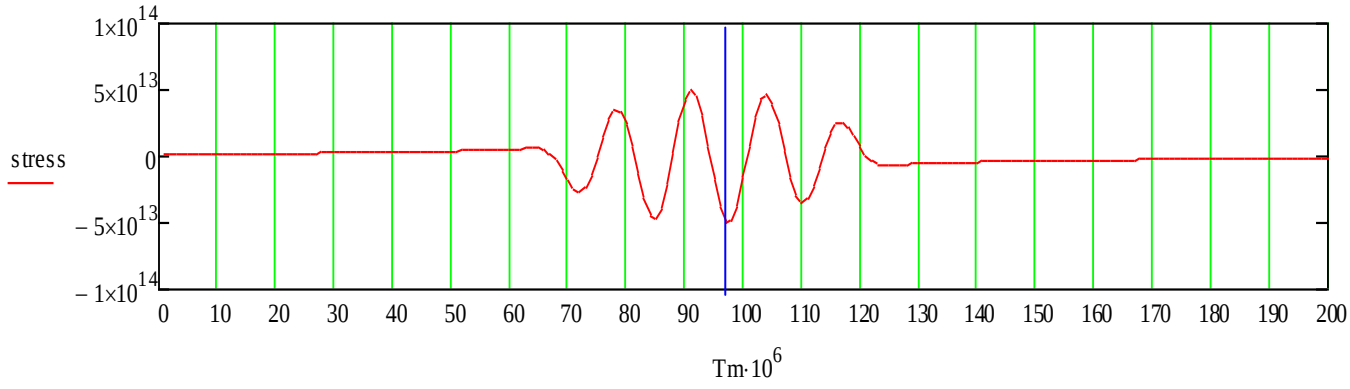

Figure 5.29 Output Signal for Aluminum at Transducer Surface

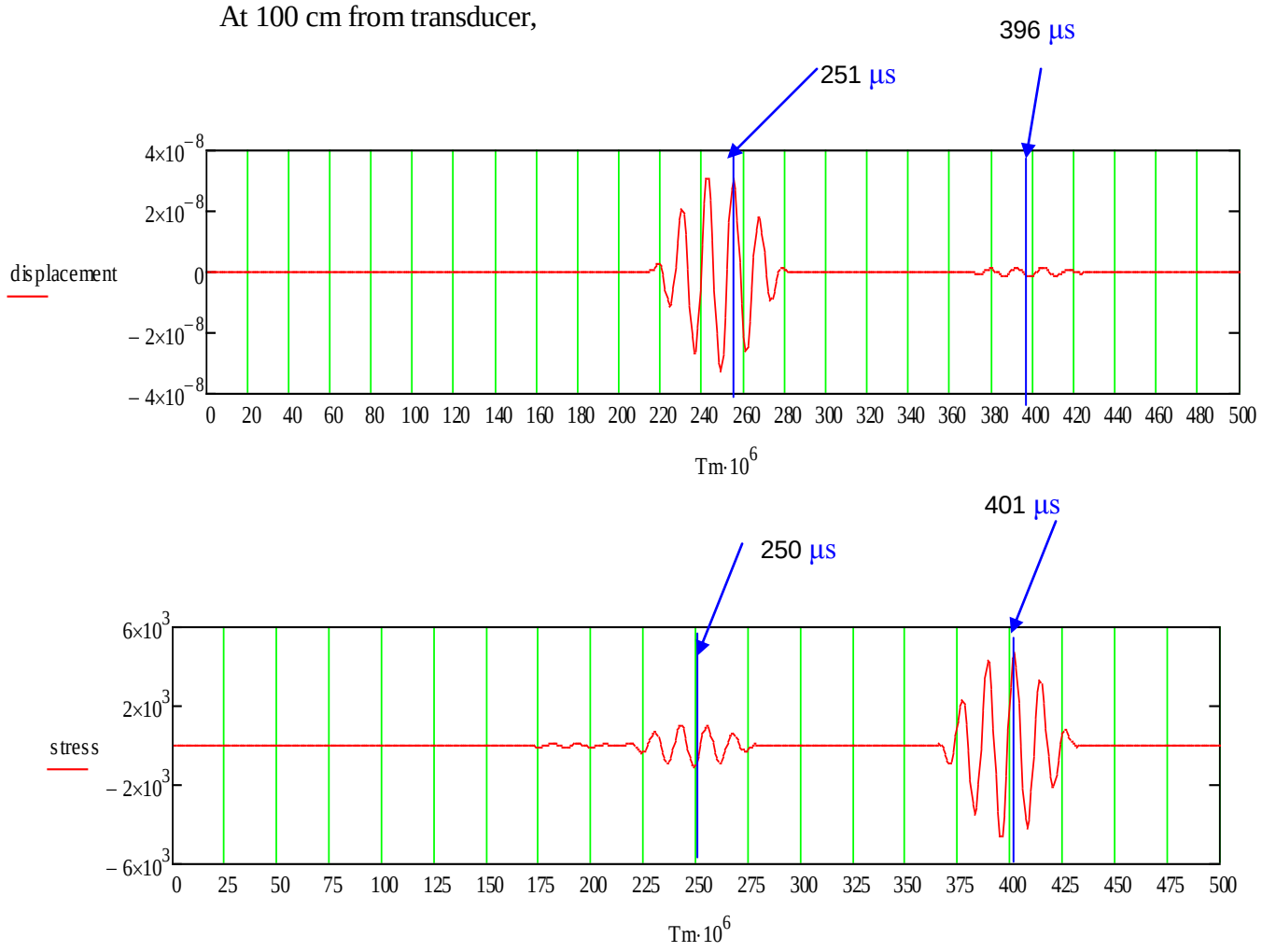

Figure 5.30 Output Signal for Aluminum Z=100 Cm

Method	Cp=6.5 km/sec	Cs=3.3 km/sec(STRESS)
Analytical (Z=100 cm)	1000/6.5+98 = 250.1 μs	1000/3.3+98=395.6 μs
DPSM	250 μs	401 μs

Table 5.10 Time Validation at Z=100cm for Aluminum

From the above validations it can be established that when source and target point distance increases there is significant decreases in displacement and stress values. Furthermore the maximum amplitude peak shifted to right side thereby validating the time taken by wave to travel a particular distance within the medium. For above validations circular transducer is used in next case the shape of transducer is changed to rectangular and its effect on time and amplitude variation has been studied.

5.4.4 Transient wave propagation in homogeneous solid (steel) for rectangular transducer

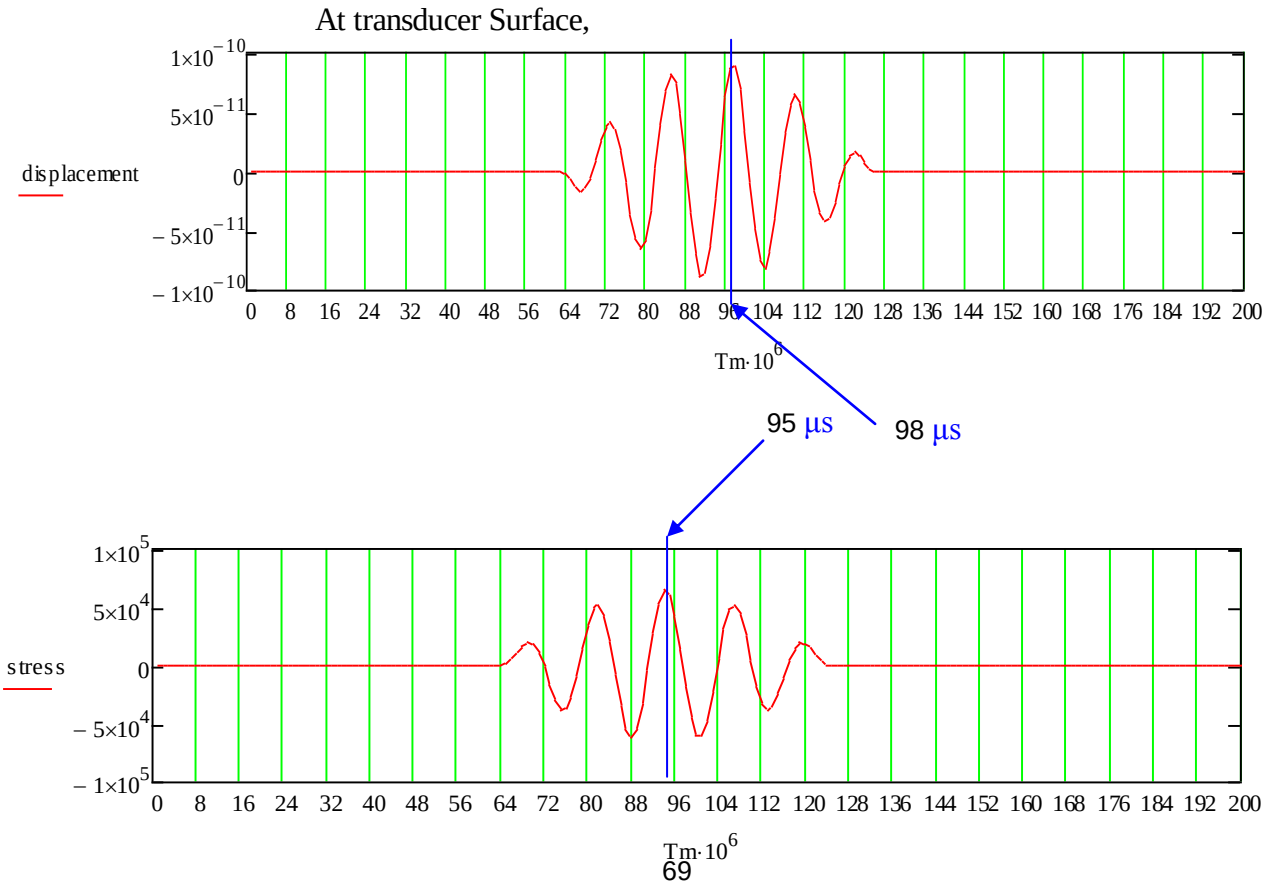

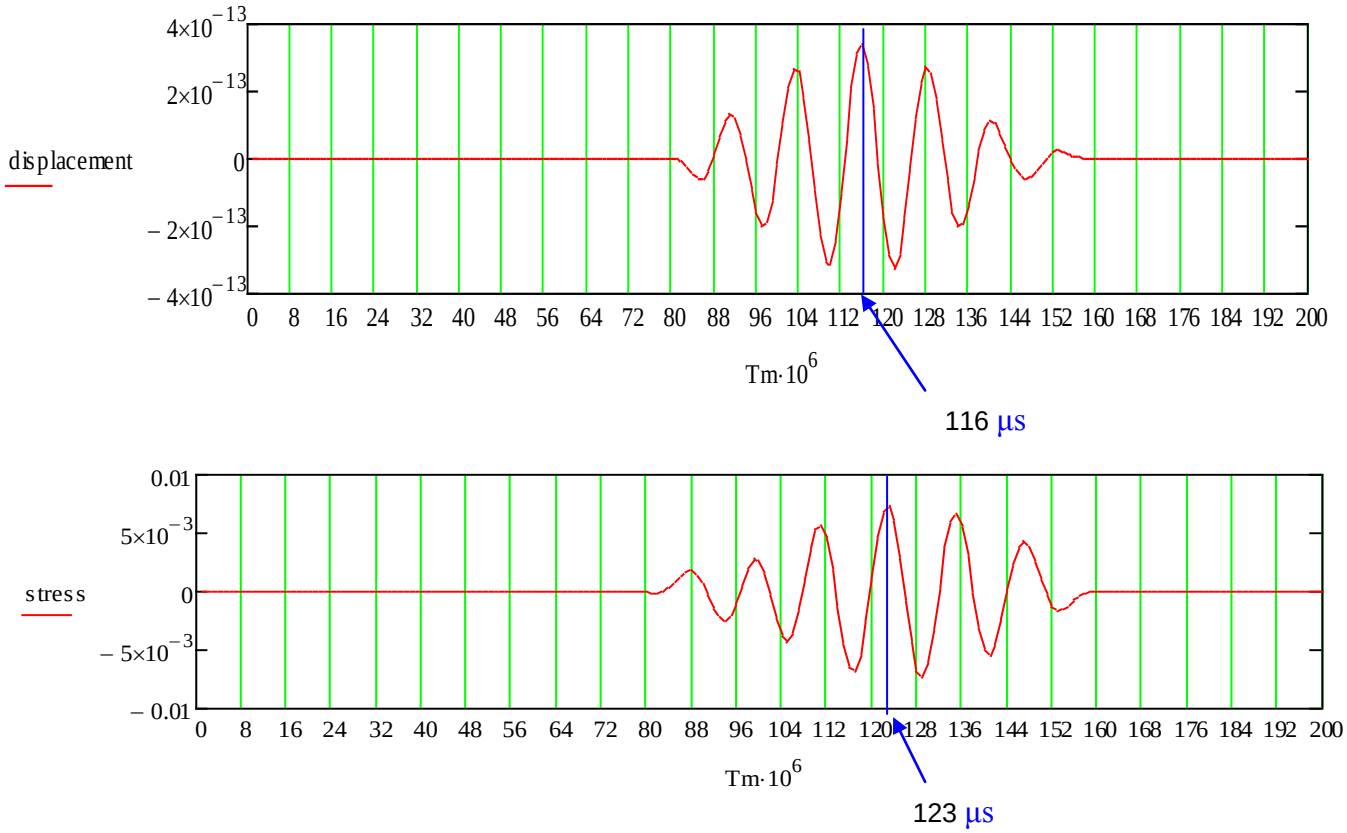

Figure 5.31 Output Signal for Steel Z=10 Cm

Method	Cp=5.66 km/sec	Cs =3.05 km/sec(STRESS)
Analytical (Z=10 cm)	100/5.66+98 = 115.6 μs	100/3.05+96=126.98 μs
DPSM	115 μs	132 μs

Table 5.11 Time Validation at Z=10cm

At 50 cm from transducer,

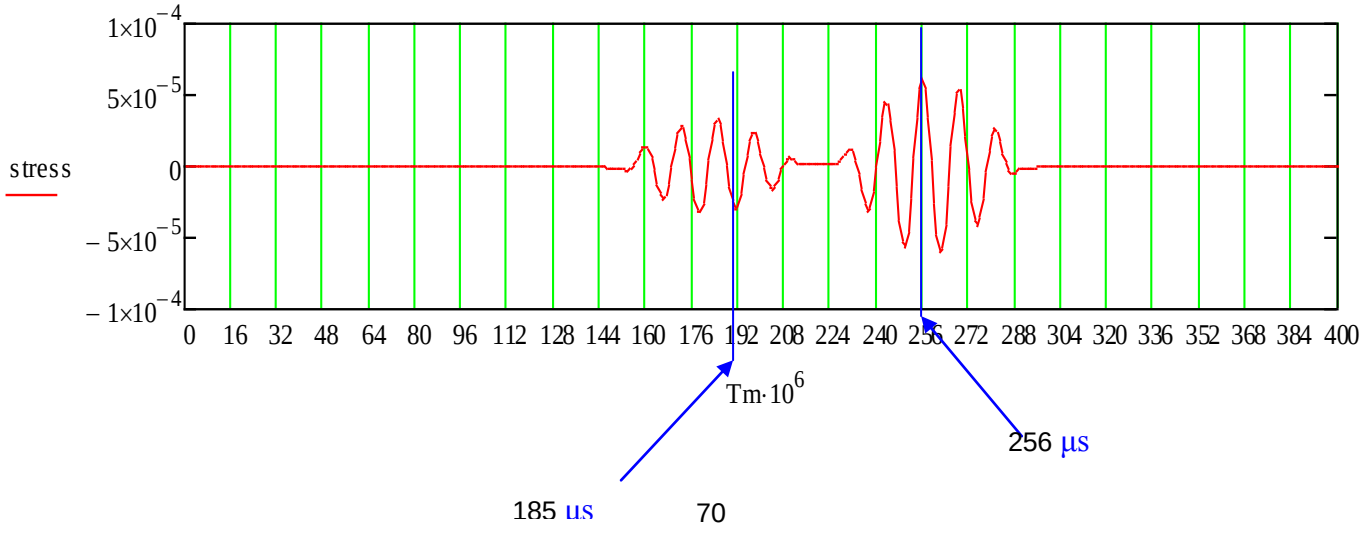

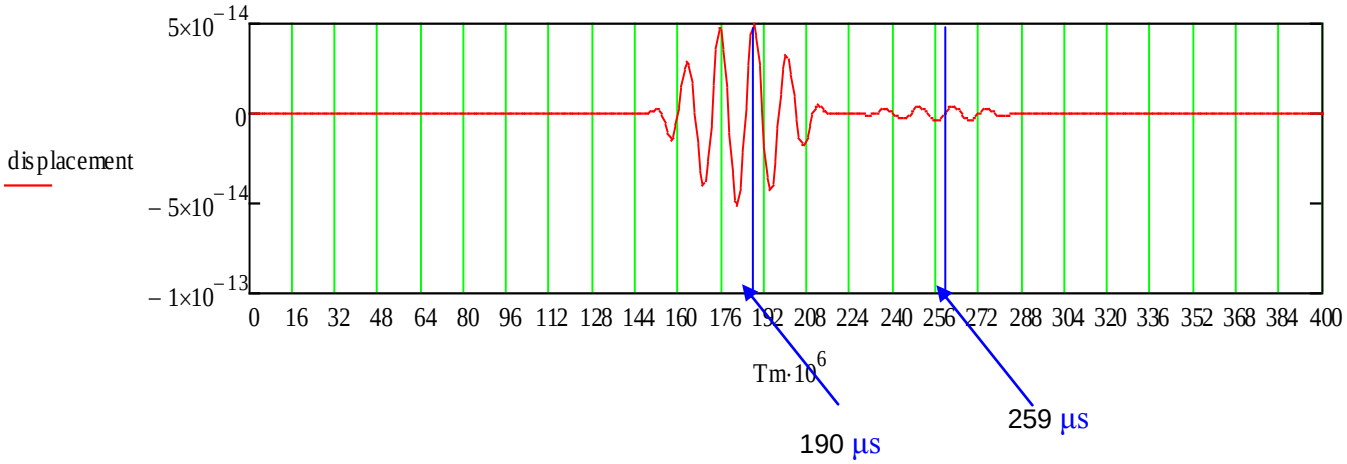

Figure 5.32 output signal for steel Z=50 cm

Method	Cp=5.66 Km/sec	Cs =3.05 Km/sec(STRESS)
Analytical (Z=50 cm)	500/5.66+98 = 188.8 μs	500/3.05+96=260 μs
DPSM	188 μs	259 μs

Table 5.12 Time Validation at Z=50 cm

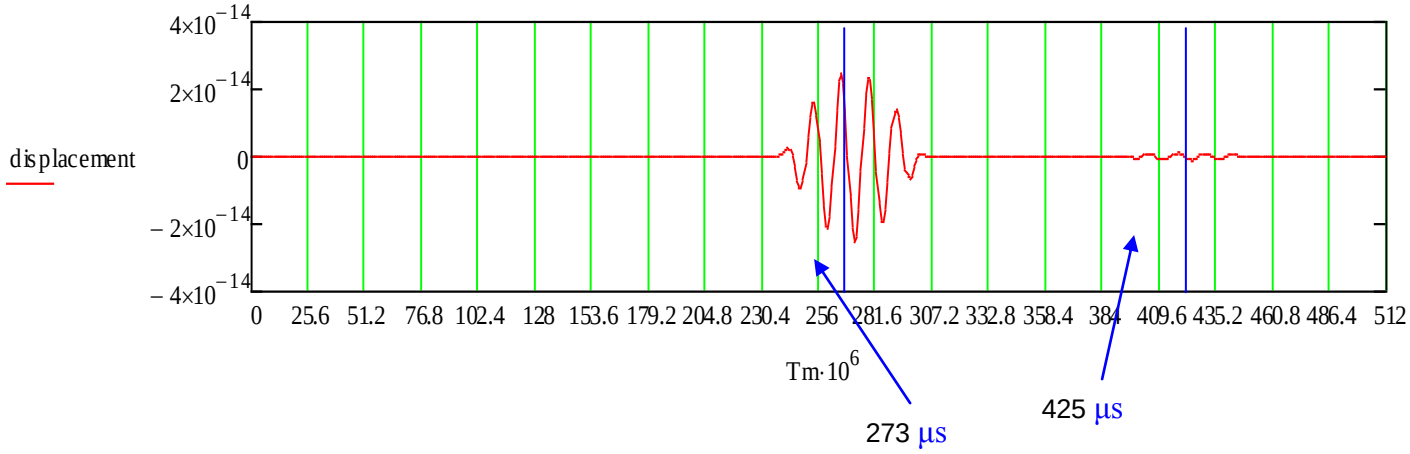

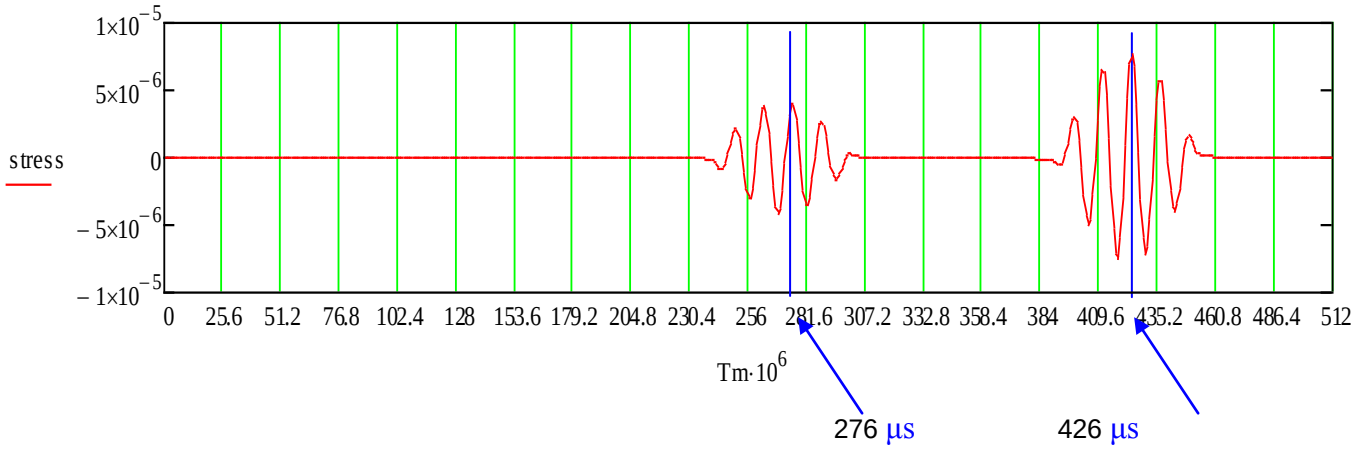

Figure 5.33 Output Signal for steel Z=100cm

Method	Cp=5.66 km/sec	Cs =3.05 km/sec(STRESS)
Analytical (Z=100 cm)	1000/5.66+98 = 274.6 µs	1000/3.05+96=424.3 µs
DPSM	274 µs	425 µs

Table 5.13 Time Validation at Z=100

For ***Aluminum*** the values of P-wave velocity and Shear wave velocity differs. The same approach which is used for steel has been employed for aluminum also.

At surface

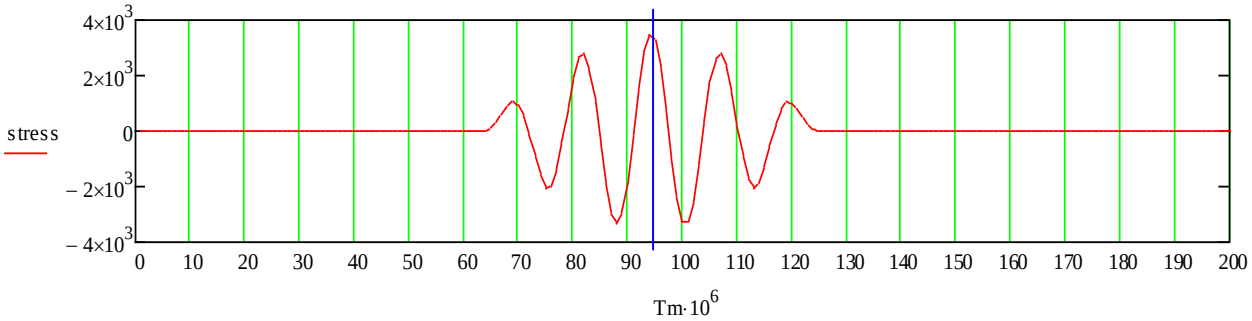

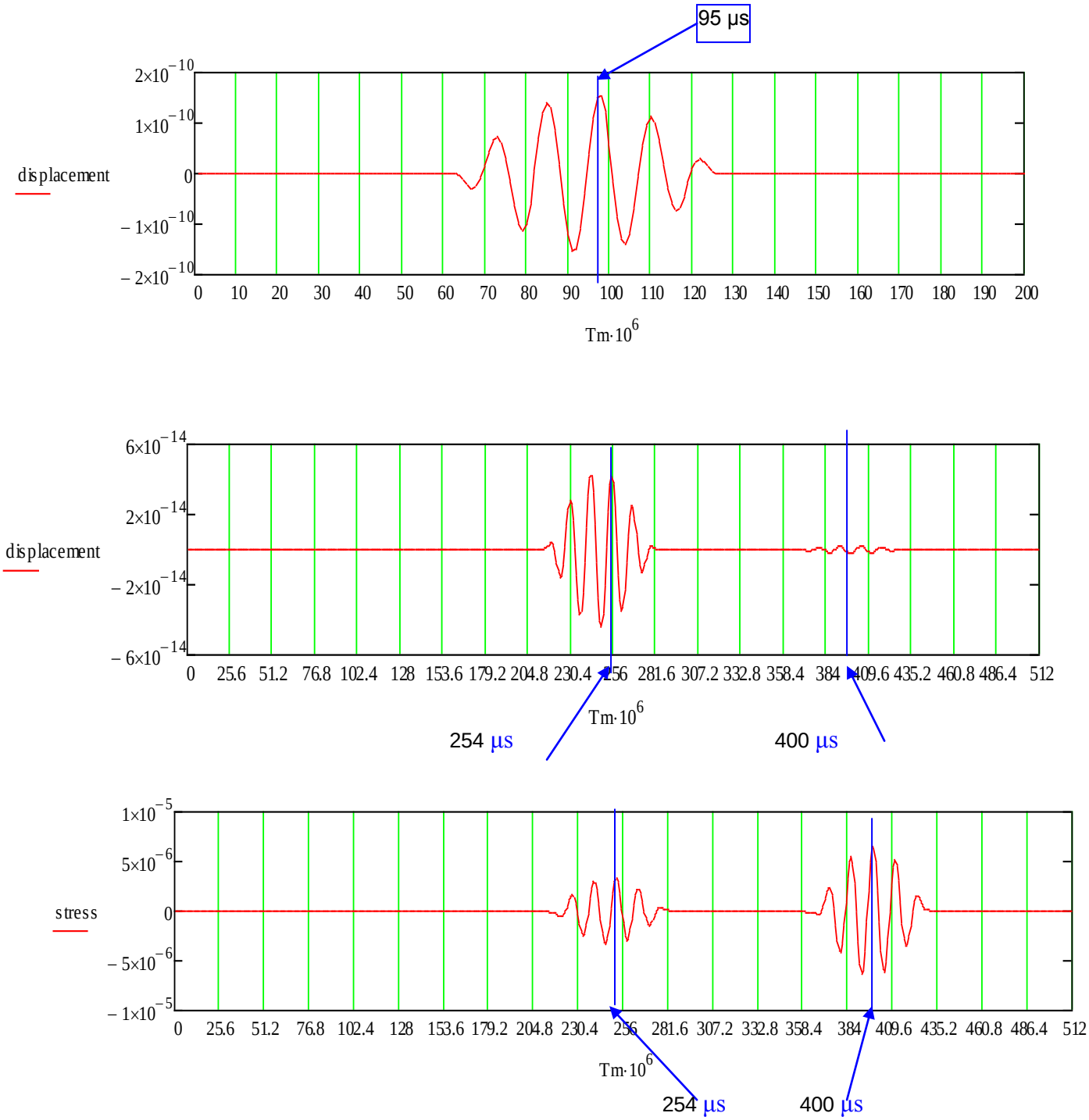

Figure 5.34 Output Signal for Aluminum at Z=100cm

Method	Cp=6.5 km/sec	Cs=3.3 km/sec(STRESS)
Analytical (Z=100 cm)	1000/6.5+98 = 250.1 µs	1000/3.3+98=395.6 µs
DPSM	250 µs	401 µs

Table 5.14 Time Validation at Z=100 Aluminum

5.5 Ultrasonic Field Modeling At Fluid Solid Interface

Following are the results of MATHCAD routines which have been developed for modeling the ultrasonic field near fluid –solid interface mathematical modeling and equation are already been discussed in chapter 4 sec 4.4. .

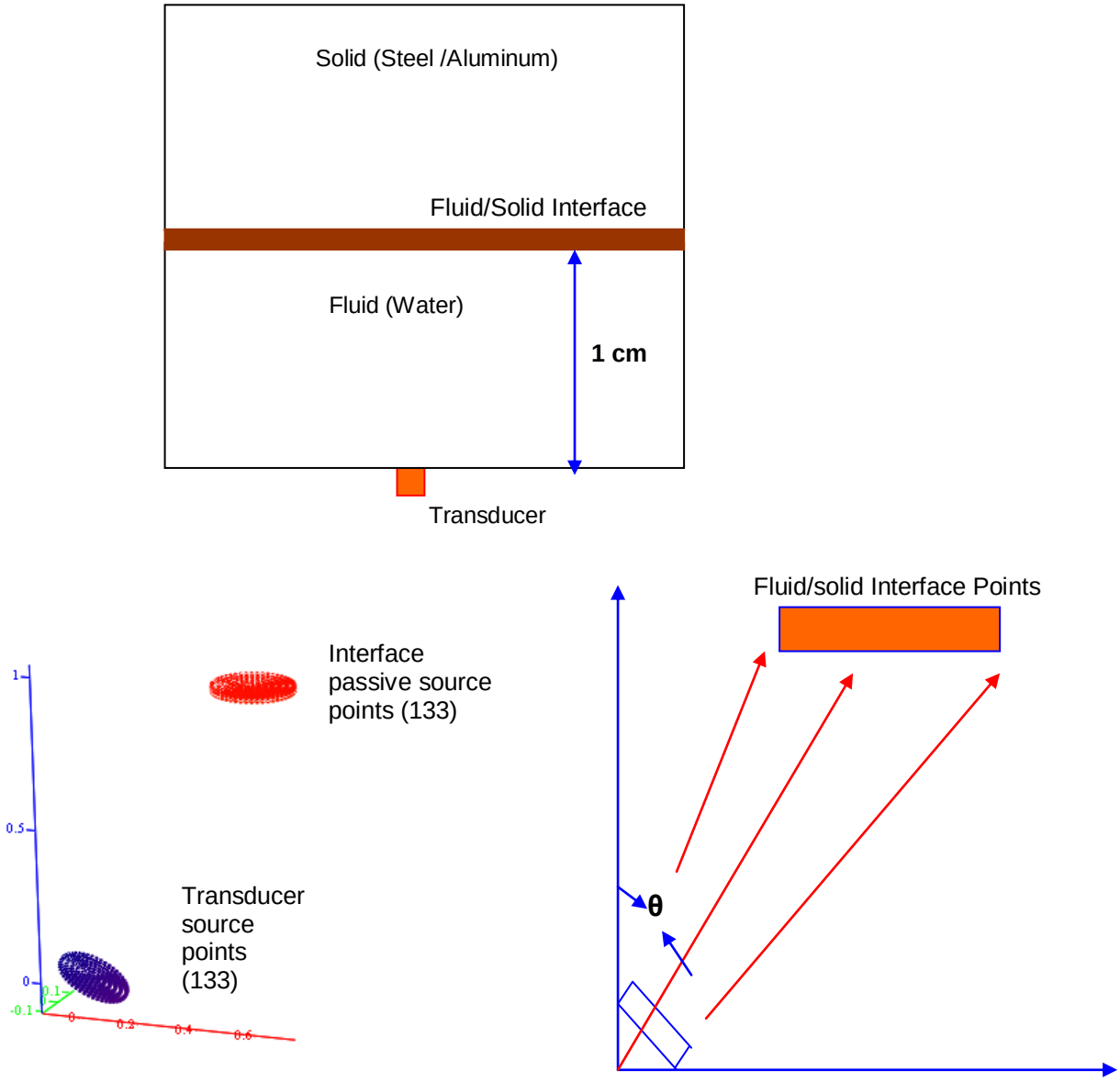

Figure 5.35 Source and Target Point Definition near Fluid-Solid Interface

5.5.1 Pressure distribution inside fluid:

The following plot shows the pressure variation in fluid space when interface is present at 1 cm above the transducer surface. The angle of transducer is varied and its effect on energy transferred has been studied.

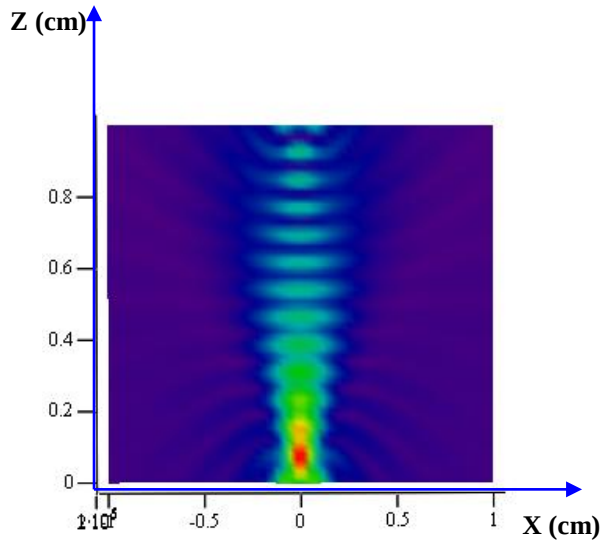

a) Freq= 1 MHz (θ=0^0)

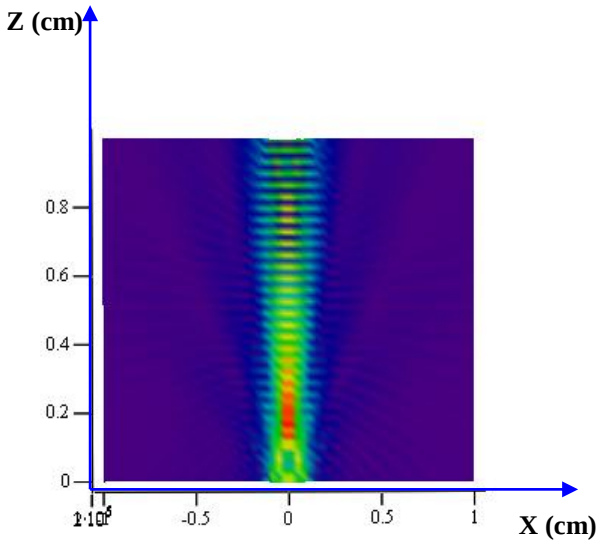

b) Freq=2.2 MHz (θ =0^0)

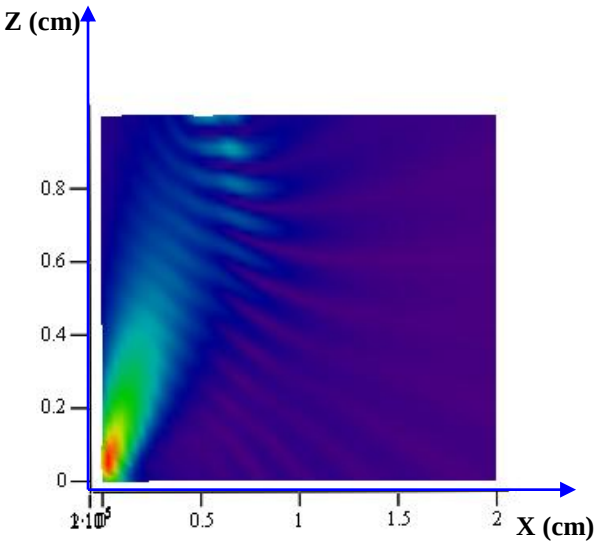

c)Freq= 1 MHz (θ =30^0)

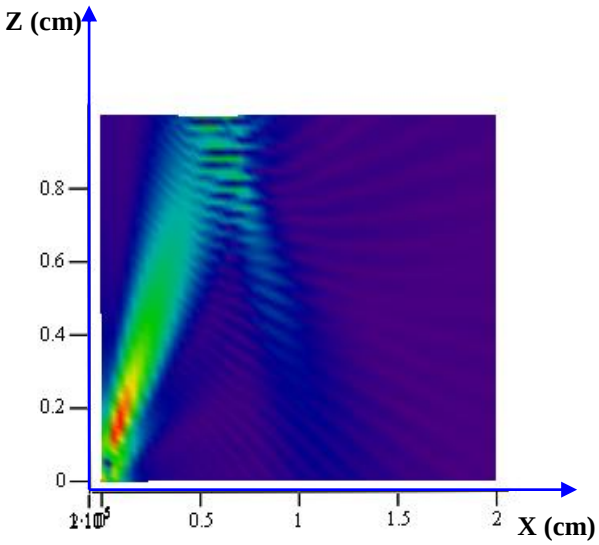

d) Freq=2.2 MHz (θ =30^0)

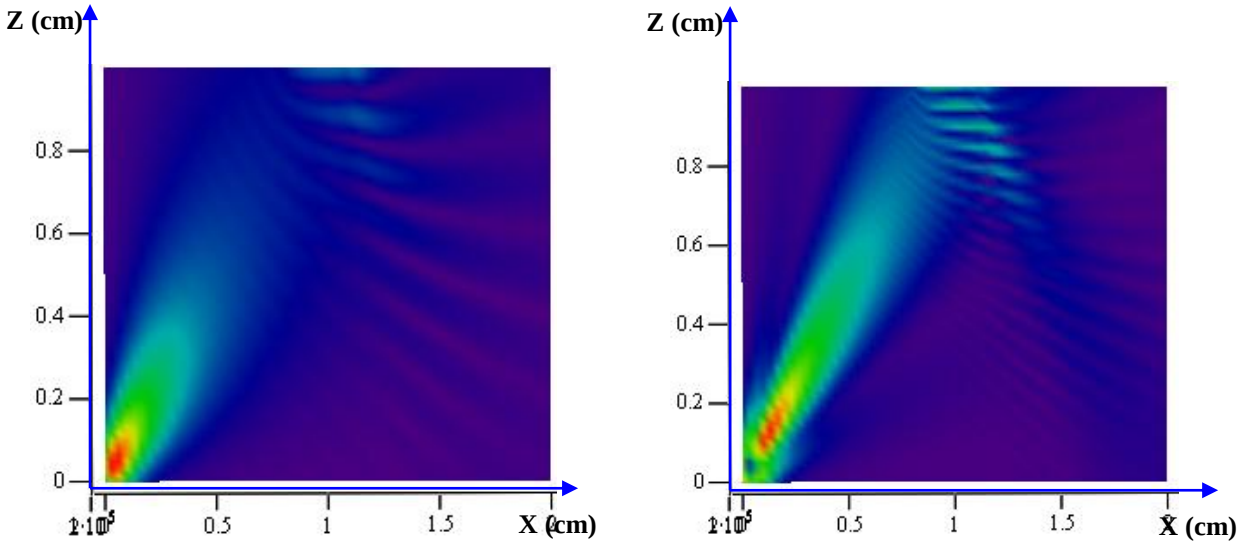

e) Freq=1 MHz (θ =45^0) **f) Freq=2.2 MHz (θ =45^0)**

Figure 5.36 Pressure Distribution in Fluid (When Fluid Solid Interface is considered)

5.5.2 Displacement plots in solid (U33)

Unlike liquid in case of solid shear waves are generated .Effect of shear wave propagation is as crucial as longitudinal waves in solid. Following displacement plot shows the variation of displacement throughout the control volume considered. Although the displacement magnitude is less but relative plotting can be done easily using MATHCAD view options.

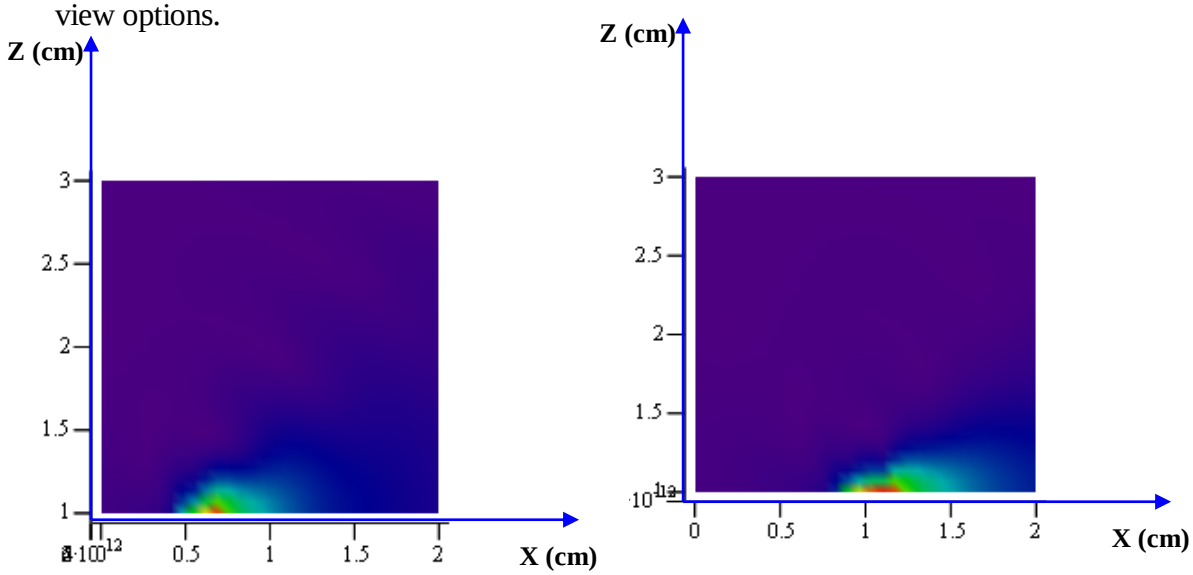

a) Freq=1 MHz (θ =30^0) **b) Freq=2.2 MHz (θ =30^0)**

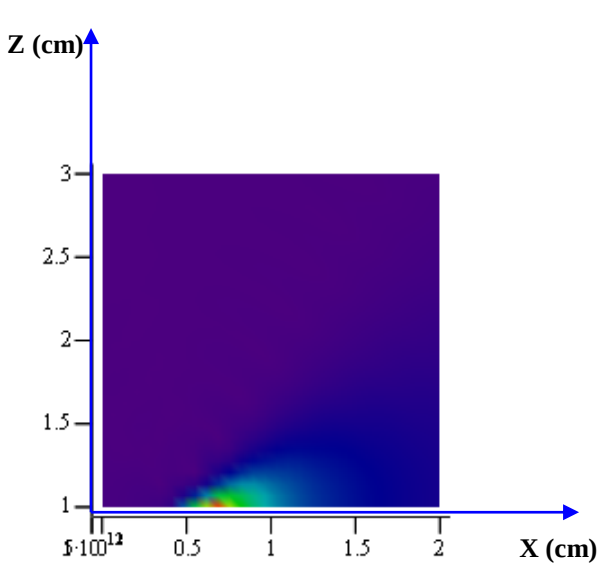

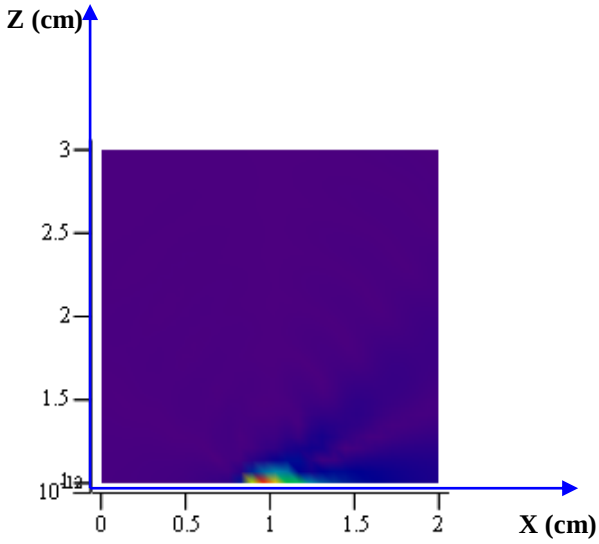

c)Freq= 1 MHz (θ =45^0) **d)Freq=2.2 MHz (θ =45^0)**

Figure 5.37 Displacement Variation in Solid above Interface

5.5.3 Stress distribution in solid (S33)

For calculating stresses at each point in target space green function is used as discussed in chapter 4. Following graphs shows stress variations in solid in normal Z directions generally called as S33.

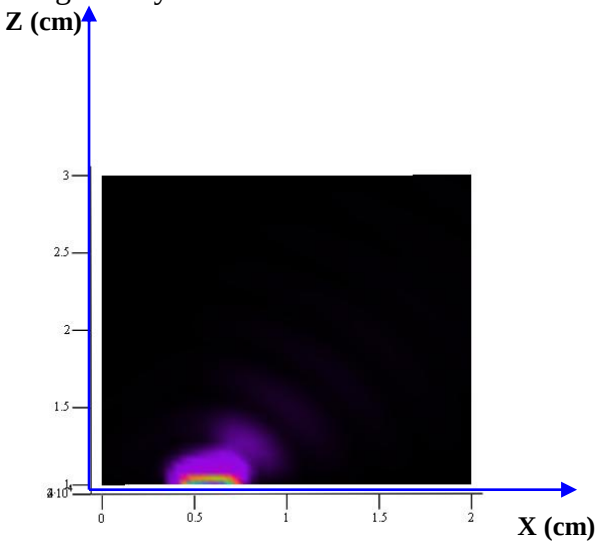

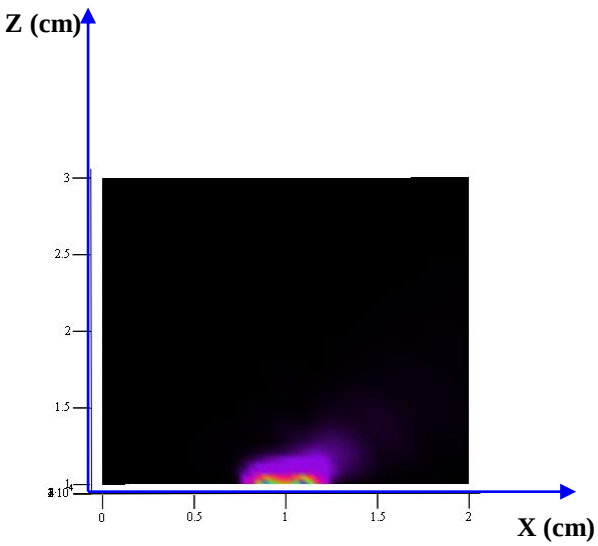

a)Freq= 1 MHz (θ =30^0) **b)Freq= 2.2 MHz (θ =30^0)**

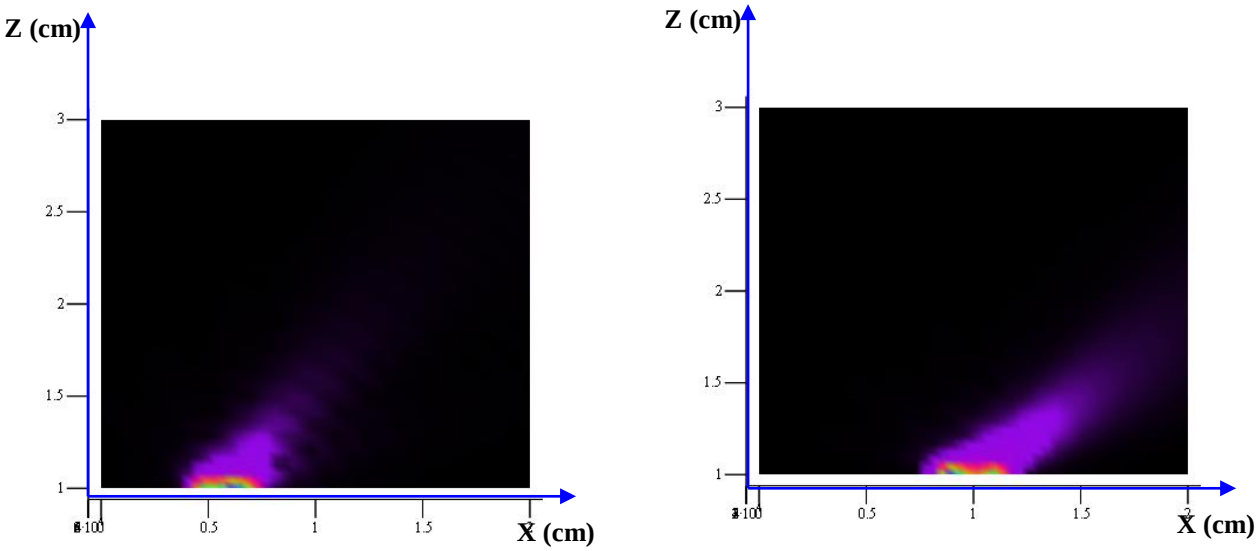

c)Freq=1 MHz (θ =45^0) **d)Freq= 2.2 MHz (θ =45^0)**

Figure 5.38 Stress (S33) Distribution in Solid

5.5.4 Stress and Pressure combined plots.

Following figures shows the total field generated in both fluid and solid half space when the transducer lies in fluid medium. Both pressure and stress values are shown in mentioned graphs. The inclination of transducer and its frequency has been varied to get different graphs.

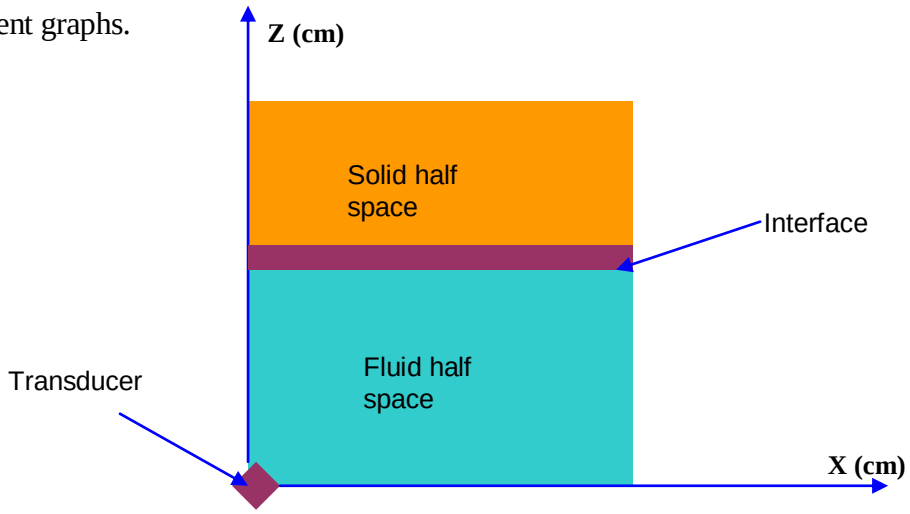

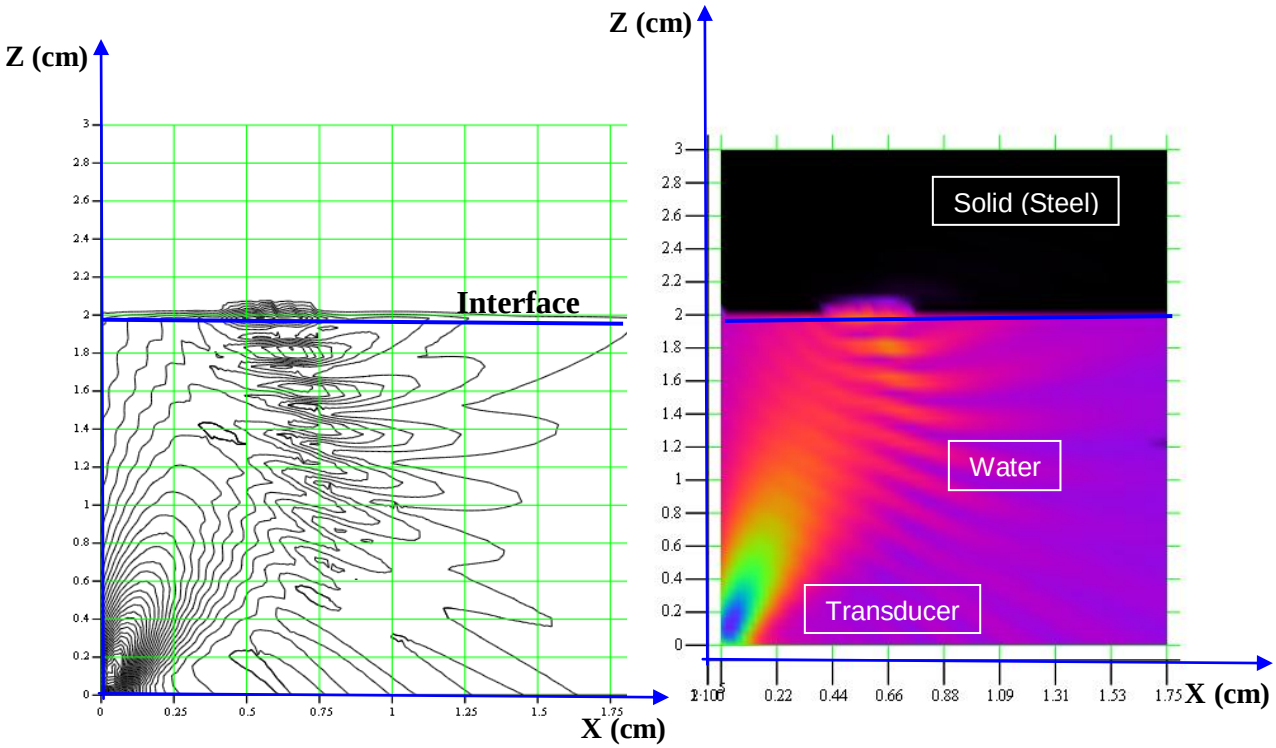

a) Freq= 1MHz(θ=30^0)

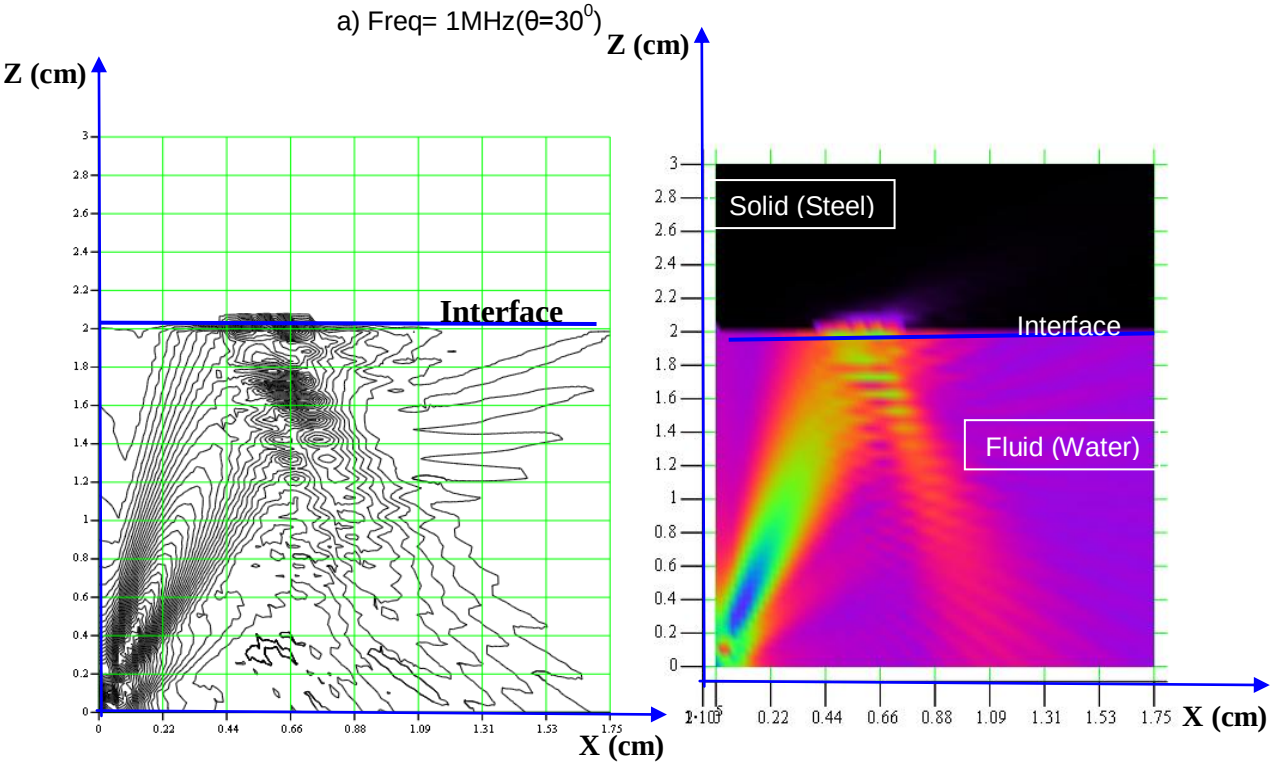

b)Freq= 2.2MHz(θ=30^0)

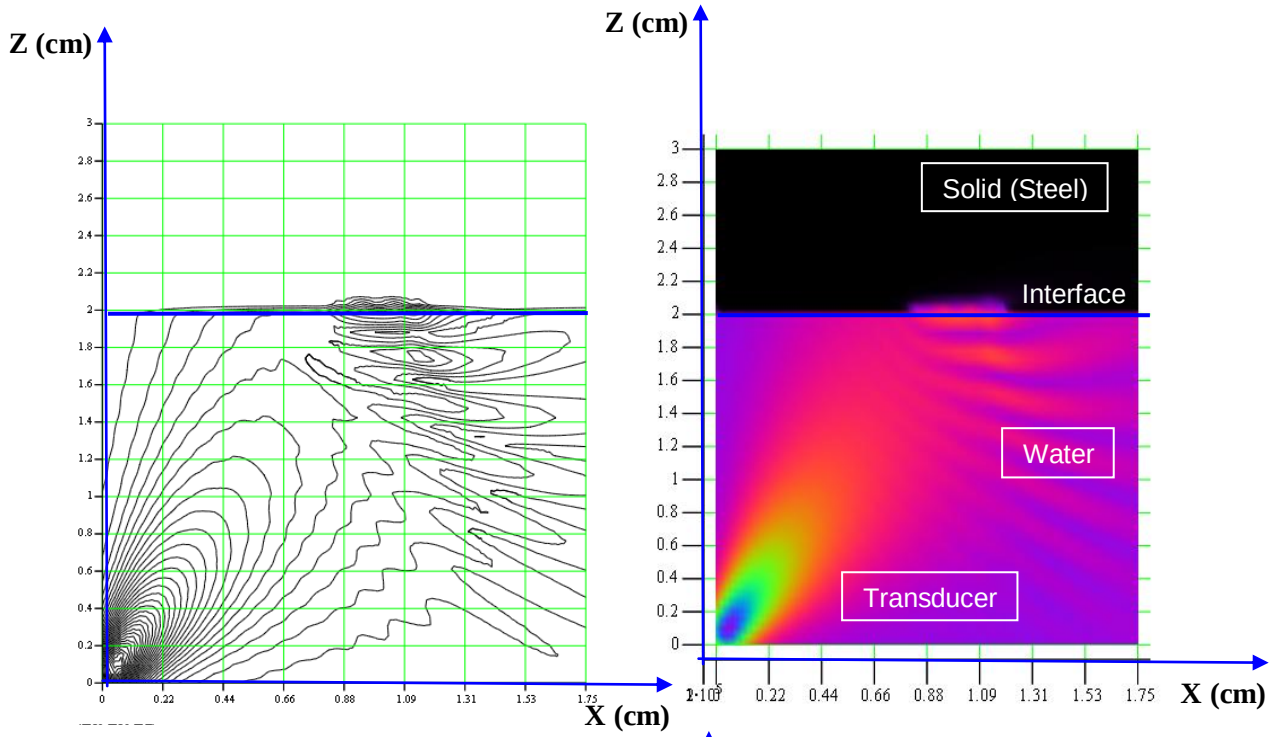

c) Freq= 1MHz (θ=45^0)

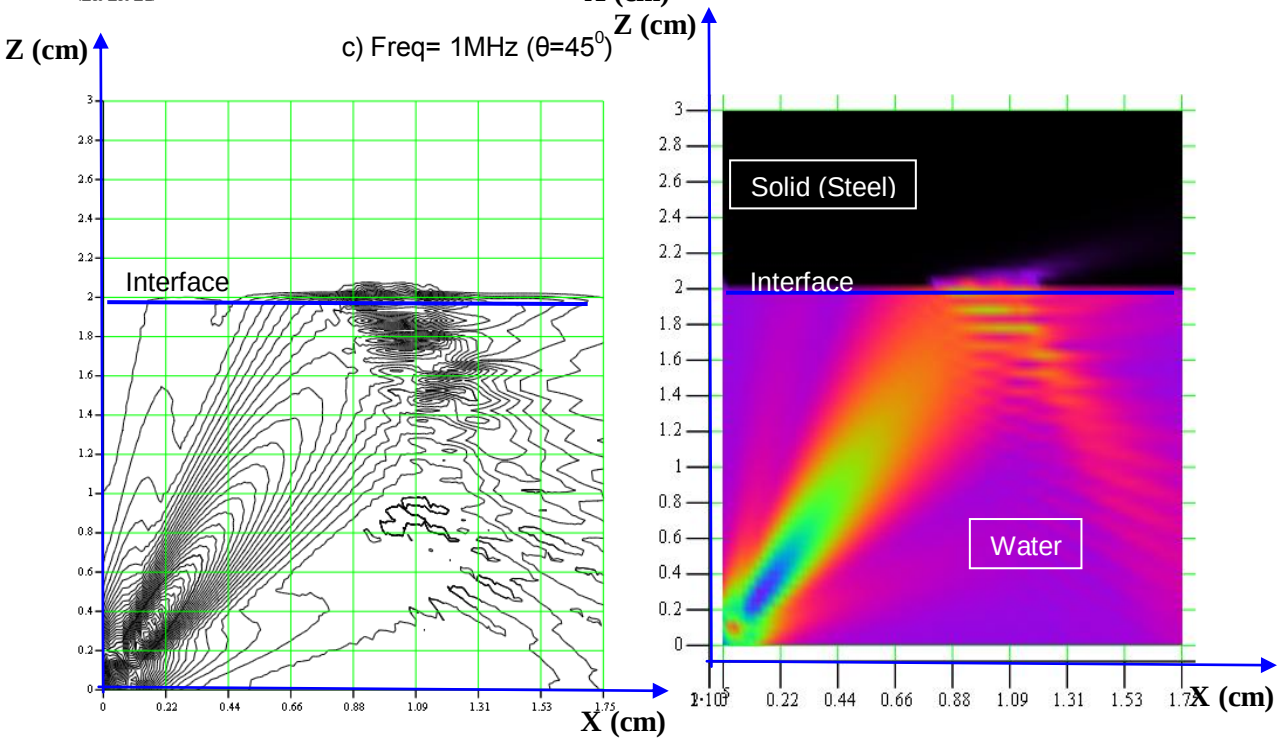

d) Freq=2.2 MHz(θ=45^0)

Figure 5.39 Pressure And Stress Plot for Varying Angles at Different Frequencies

5.6 Rayleigh Waves

Rayleigh waves can be generated by choosing critical angle of incidence at the interface. MathCAD programming has been done for modeling Raleigh waves in plates. The basic assumption used is to increase number of points at interface such that there effect can be

calculated for a larger area and hence simulating Rayleigh waves, which travel through surface with little penetration equals to wavelength of wave.

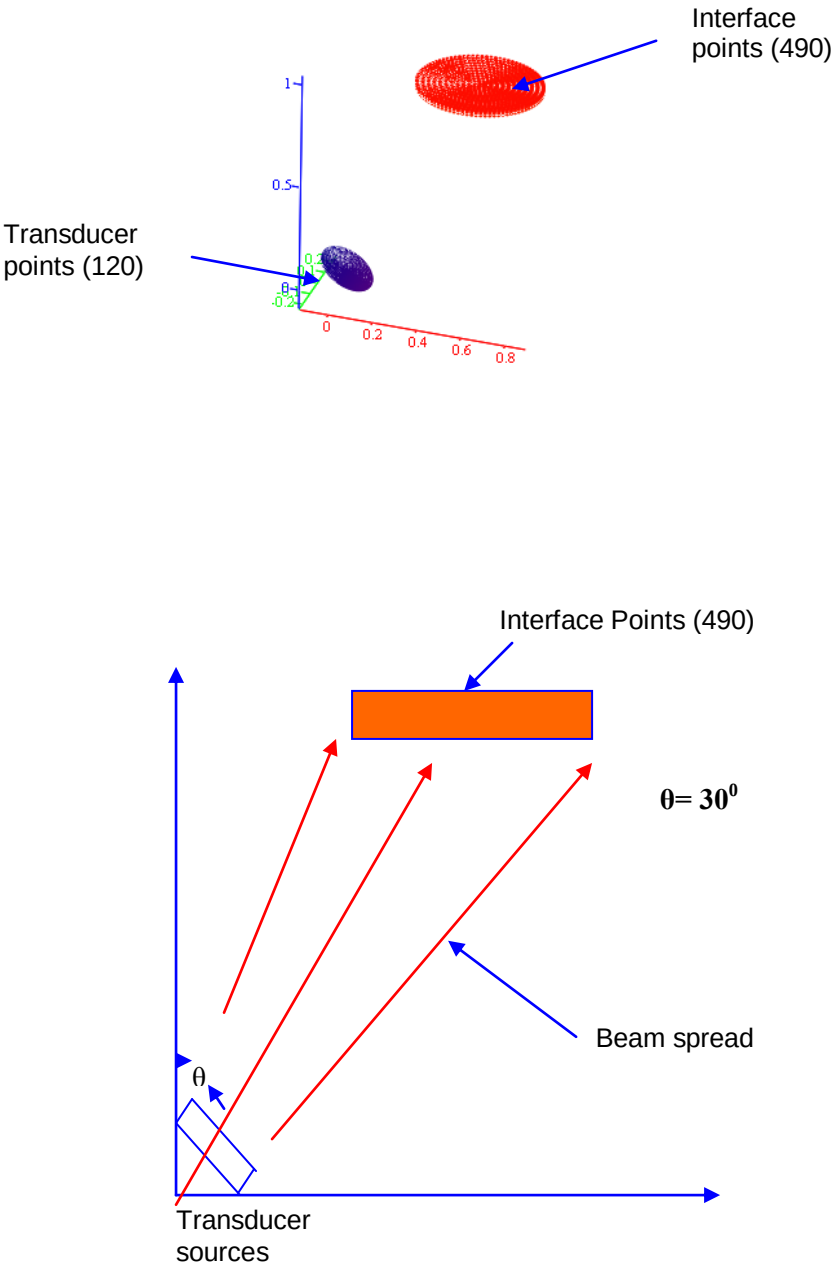

Figure 5.40 Rayleigh Wave Source and Target points Definition

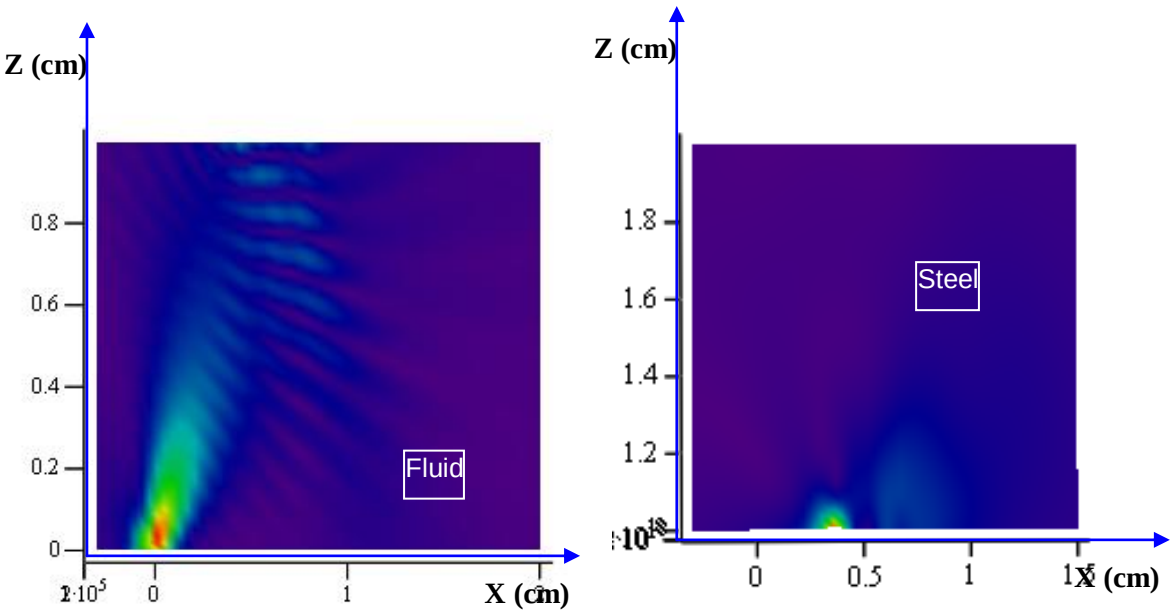

a) Pressure distribution in fluid b)Displacement in solid

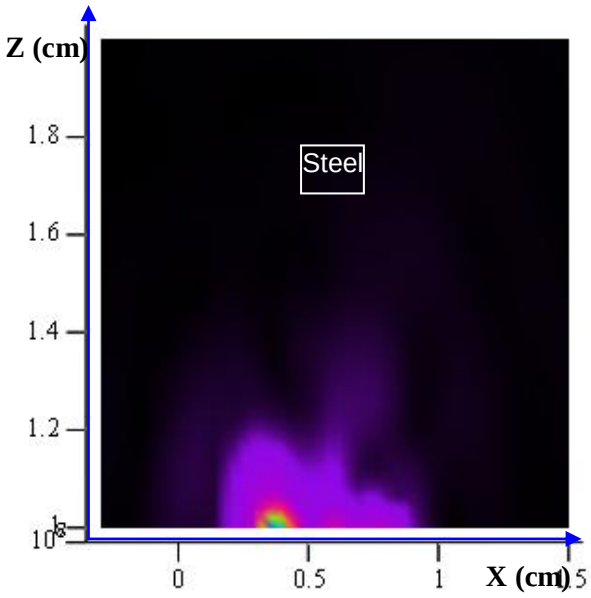

c) Stress distribution in solid

Figure 5.41 Rayleigh Waves- Pressure, Displacement and Stress Distribution at 30.2^0 for Aluminum

The above graphs clearly indicate how Raleigh wave will propagate inside a solid. When transducer is inclined at critical angle of incidence the waves which formed at interface are Rayleigh waves. In the above graph showing the stress and displacement distribution inside the plate the waves sees to travel along the interface much but if we look at the previous cases the stress distribution is completely different.

5.7 Wave propagation in plates

The analysis of plates has been done using interface boundary condition discussed in chapter 4 for fluid solid interface. Following cases has been considered while modeling ultrasonic field in plates.

5.7.1 When two transducers are emitting energy into the plate:

The first case consists of modeling of plate when two transducer are placed on both sides of plates. It is like two simultaneous energy emitting sources working together on series of plates.

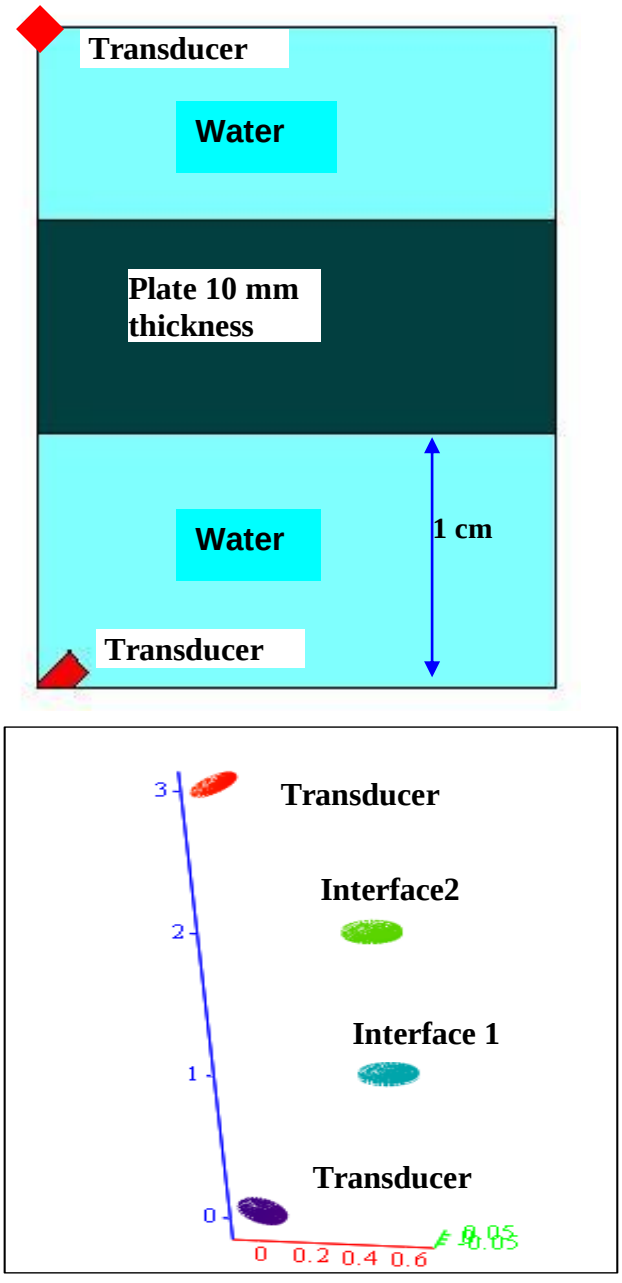

Figure 5.42 Source and Target Definition for a Plate Completely Submerged in Water

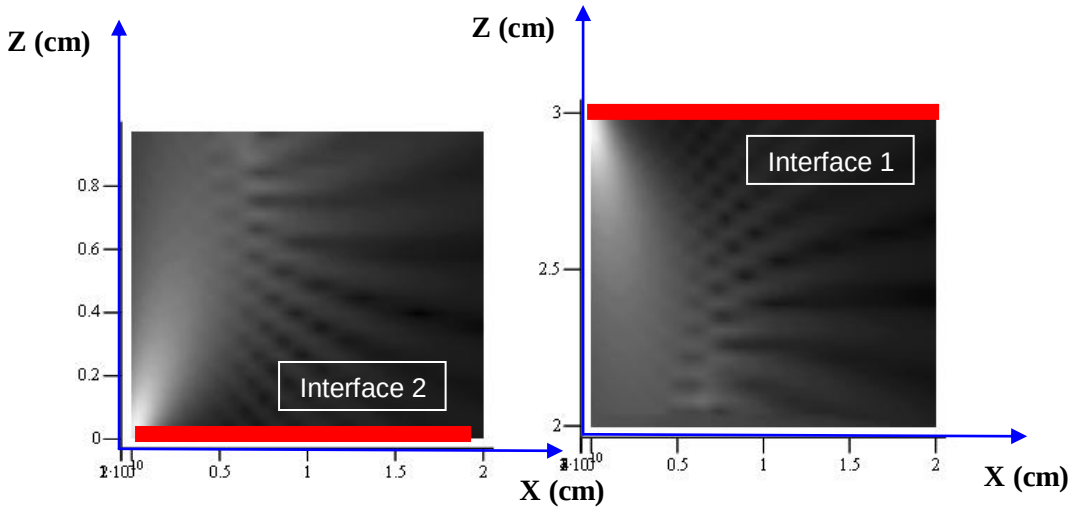

a) pressure distribution in fluid both sides

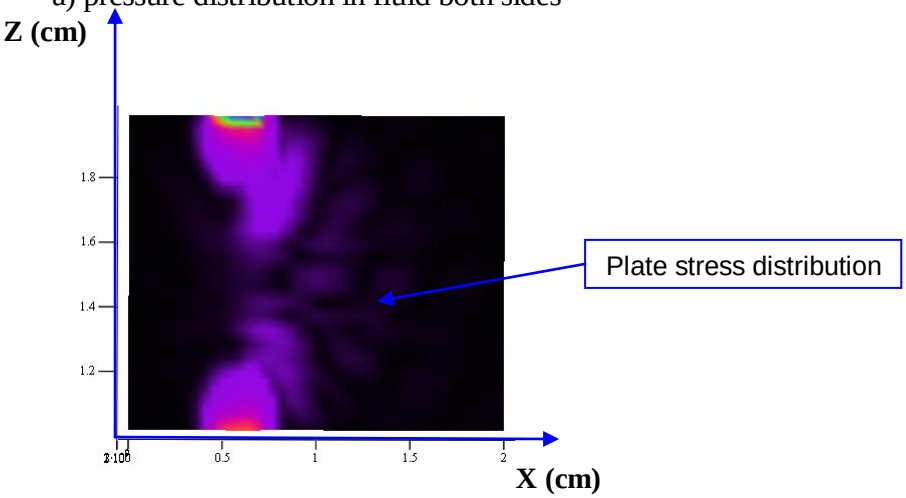

b)Stress distribution in solid plate

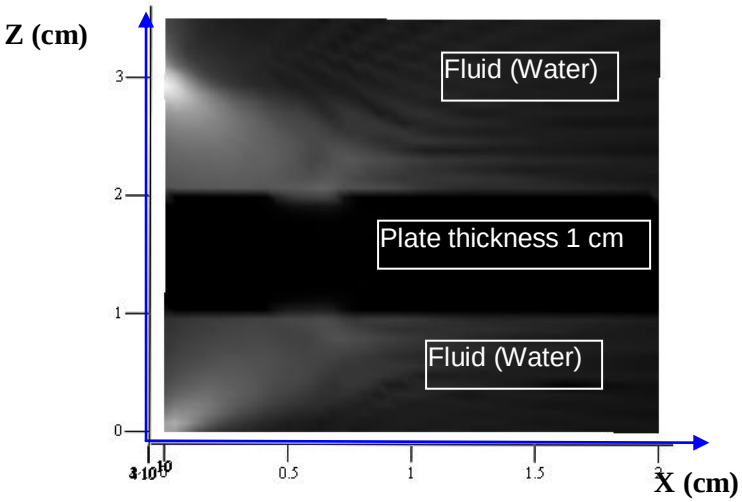

c) Pressure and Stress combine plot for plate

Figure 5.43 Pressure and Stress Variation in Plate (freq = 1 MHz)

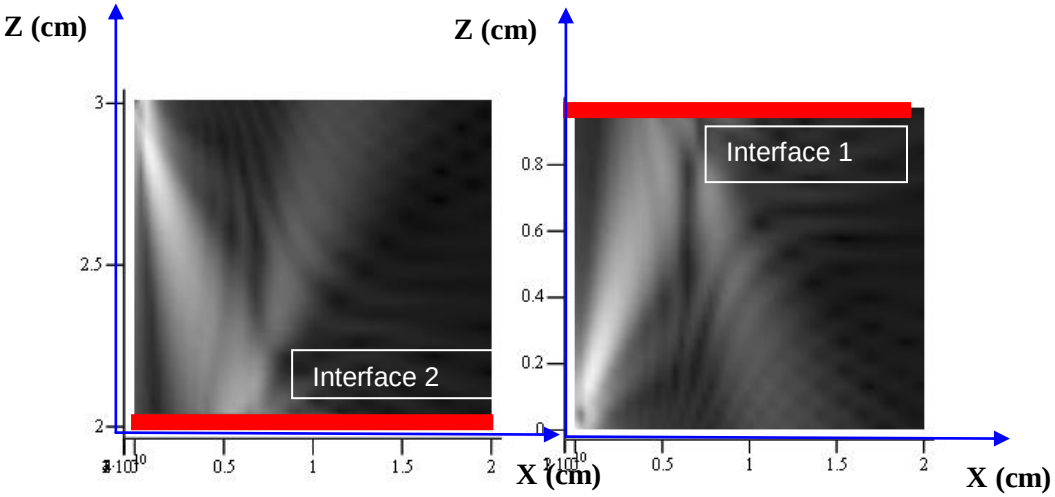

a) Pressure variation in fluid

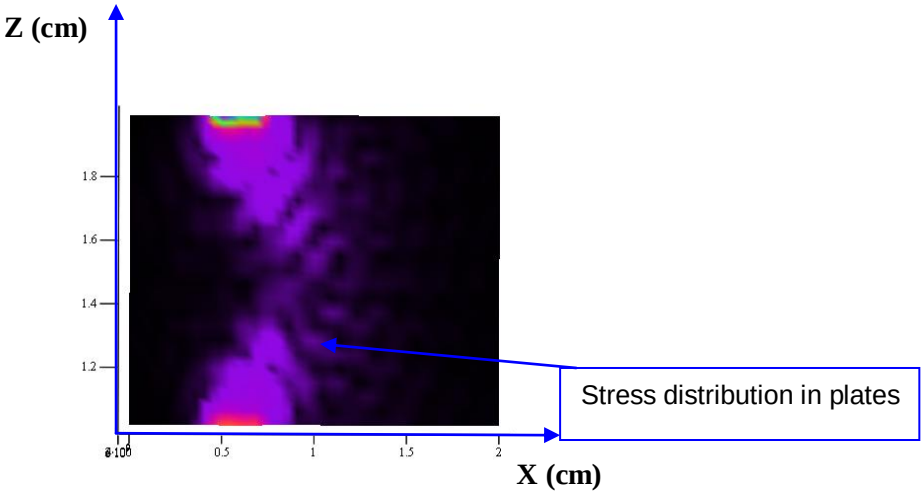

b) Stress distribution in solid

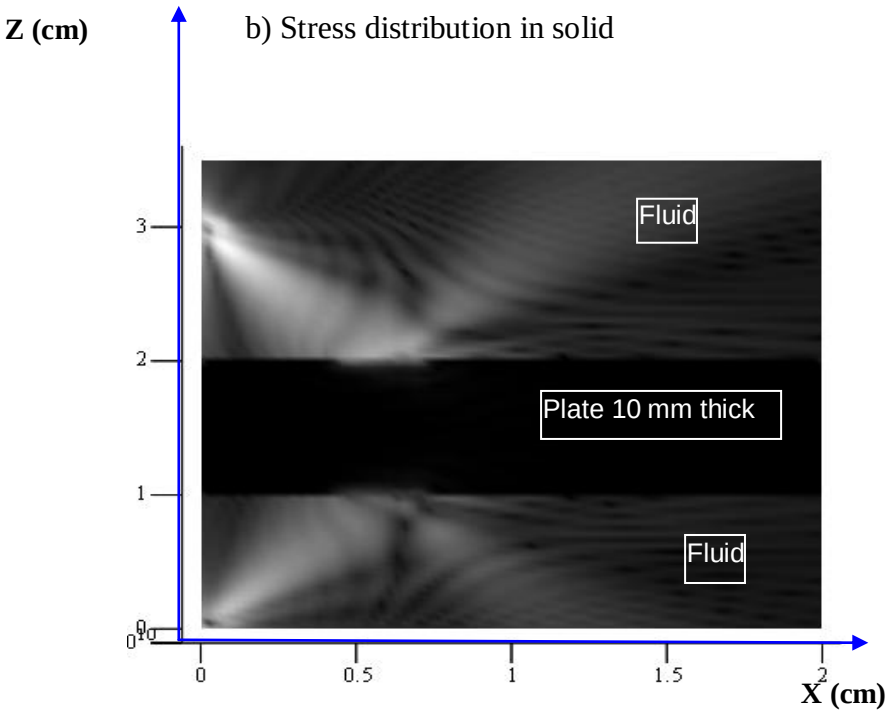

Figure 5.44 Pressure and Stress Variation (freq = 2.2 MHz)

From the above results for plates having active transducers on both sides of plate it can be concluded that stress plots and displacement plots are symmetrical and significant loss of energy is occurred near both interfaces. The active sources are assumed to have same initial velocity and based on this assumption all the results have been calculated.

5.7.2 Single transducer is acting as source

In last case when two transducer are used as energy sources the graphs tends to be symmetric because of geometry of the plate, but while doing experimental testing of plates generally one transducer is used as source and other transducer acts as a receiver to plate. Following results shows the pressure and stress distribution plots when only one source is present in the system. Plate with transducer at one end and the whole energy is transferred to the system by that single transducer instead of two transducer as taken in last case. The modeling of system is same as that of case when two transducers were considered as sources; the only change which will be occurring is in MATV matrix. The size of matrix will be decreased(refer to chapter 4 section4.5).

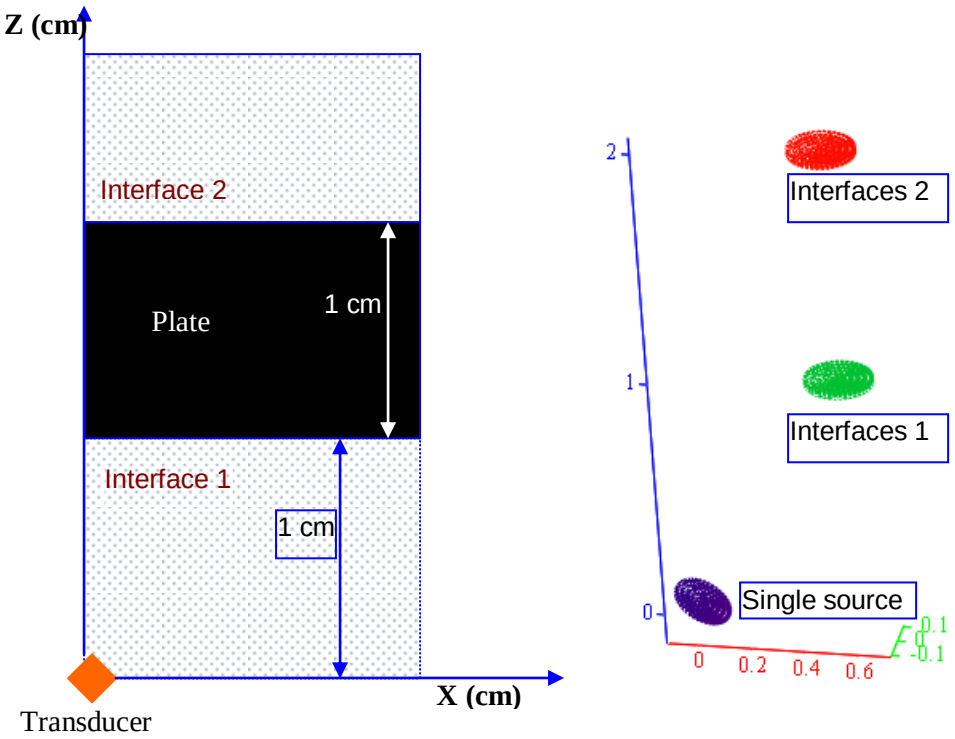

Figure 5.45 Source And Target Point Definition for one Active Transducer

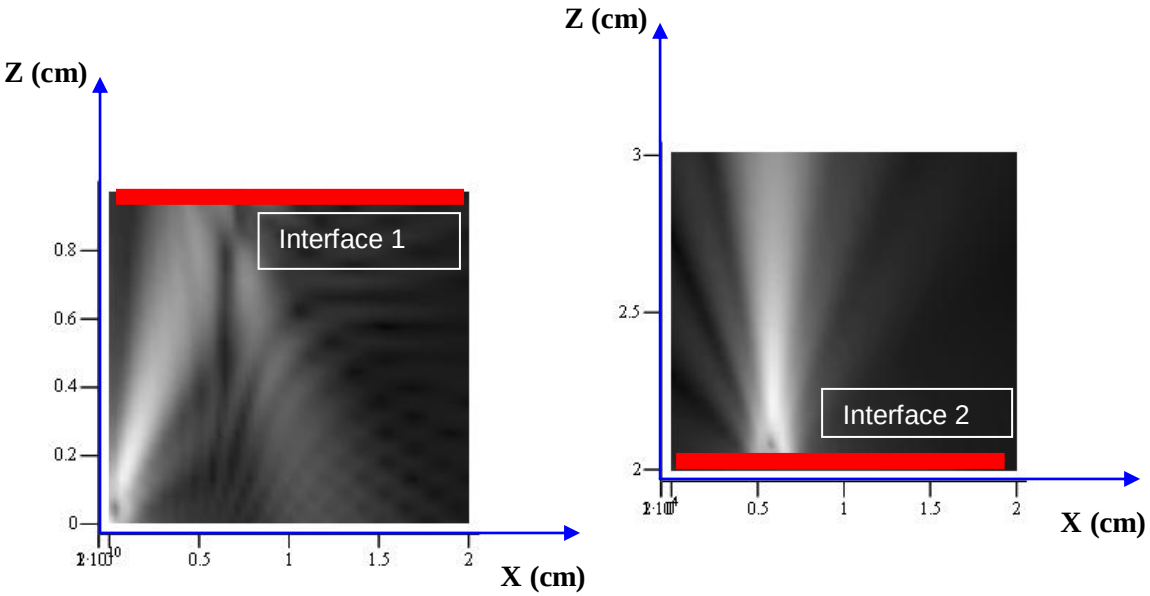

a)Pressure distribution in fluid above and below plate

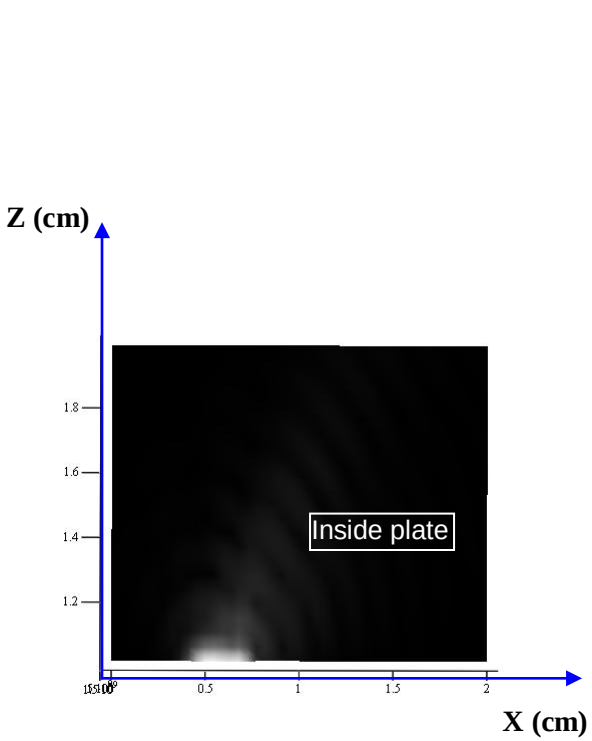

b)Stress distribution in plate

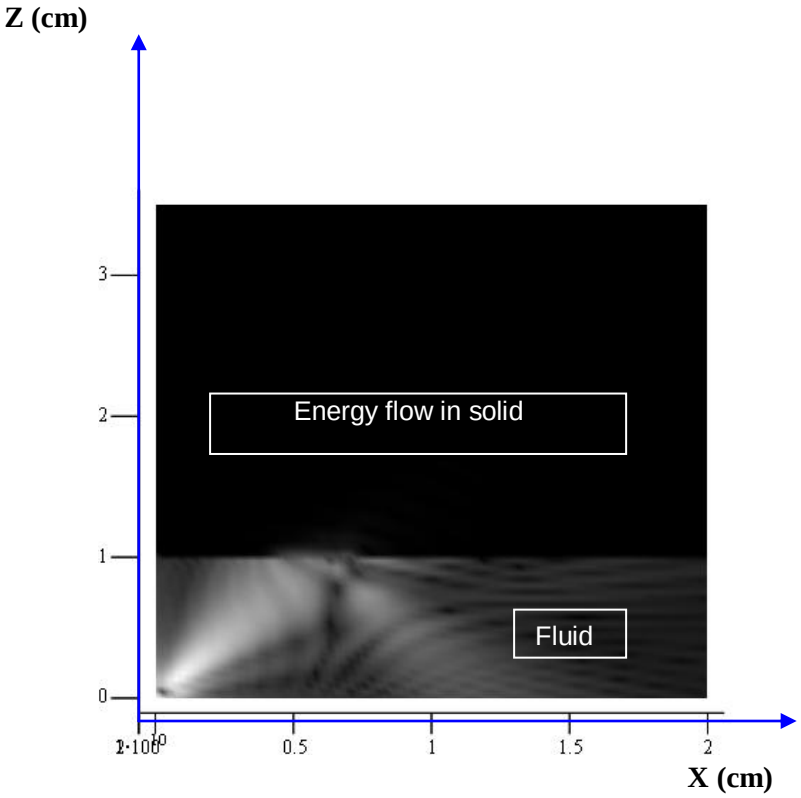

c)Combine stress and pressure plot

Figure 5.46 Single Source Plate Analysis (Freq= 2.2 MHz)

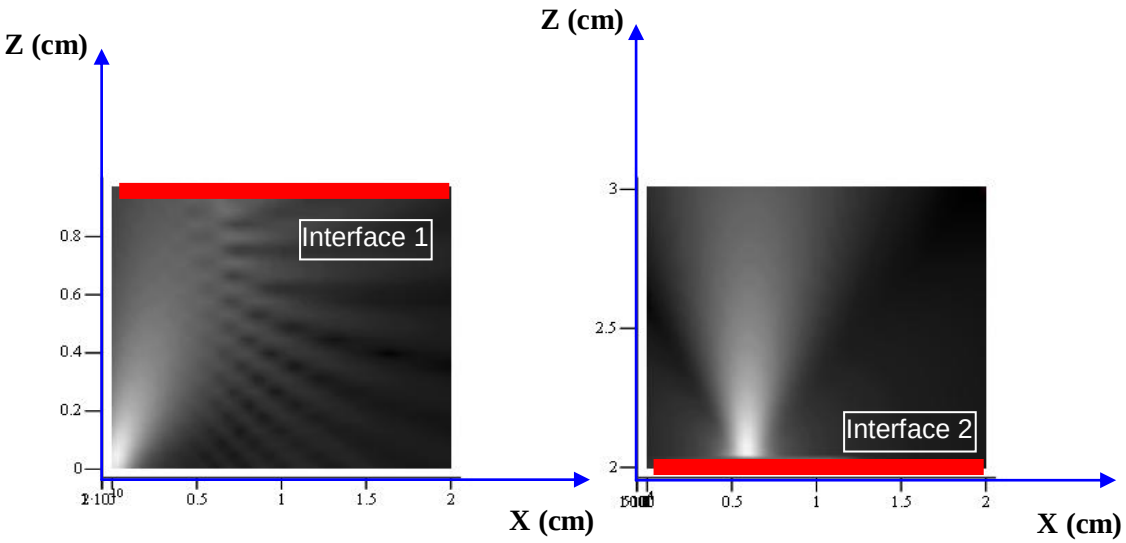

a)Pressure distribution in fluid above and below plate

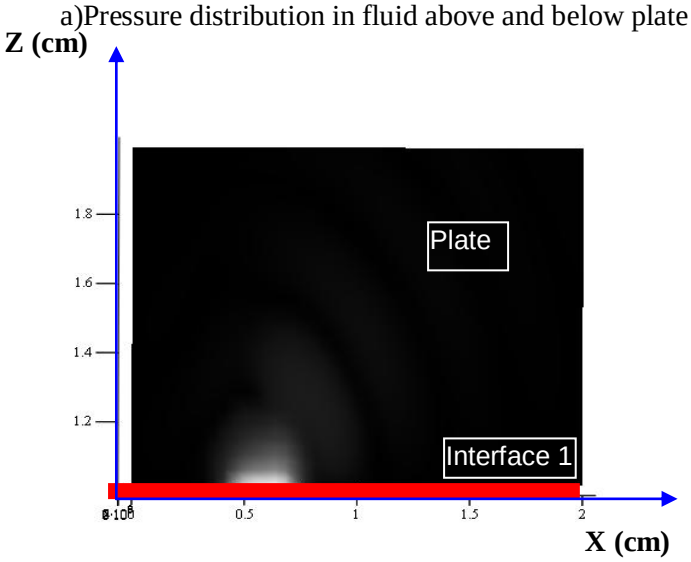

b) Stress distribution in plate

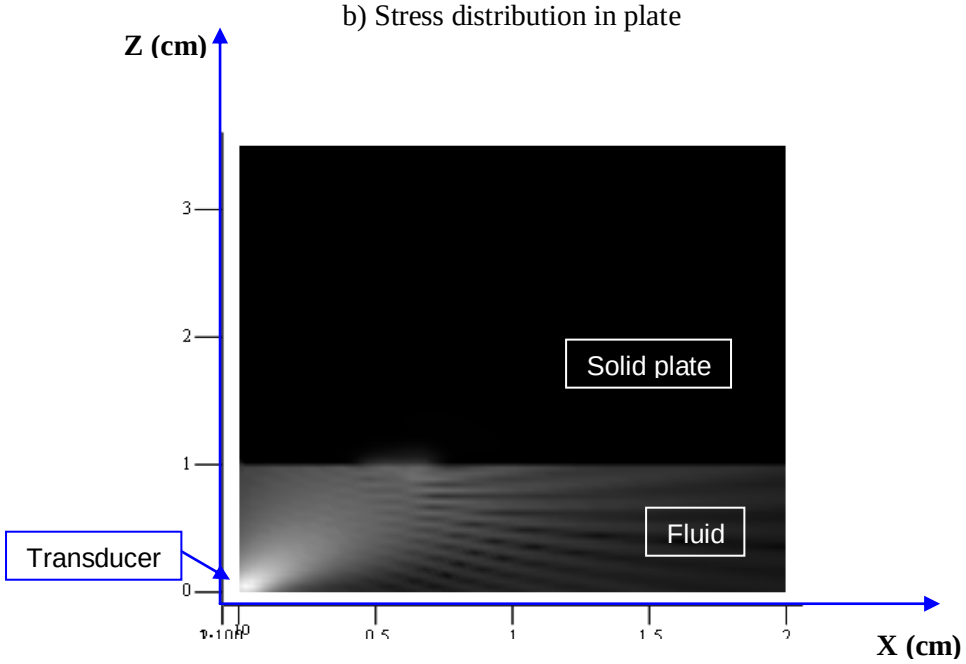

c) Combine plot for pressure in fluid and stress in solid plate

Figure 5.47 Single Source Plate Analysis (Freq= 1 MHz)

5.8 Ultrasonic field modeling when plate is defective

Defect in the plate can be of any shape size keeping the scope of present study in mind rectangular slot has been modeled using DPSM technique. The only difference in modeling the plate with defect as compared to modeling without defect, are the boundary condition where while calculating stress in plate the crack source also interfere with the active and passive sources at interface. The theory of modeling of plates with and without defect has already been discussed in chapter 4

Following graphs shows the stress distribution in plate when the defect geometry is changed.

Case 1,

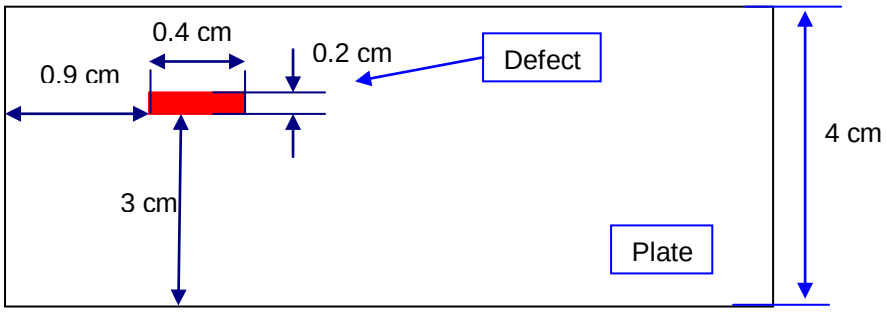

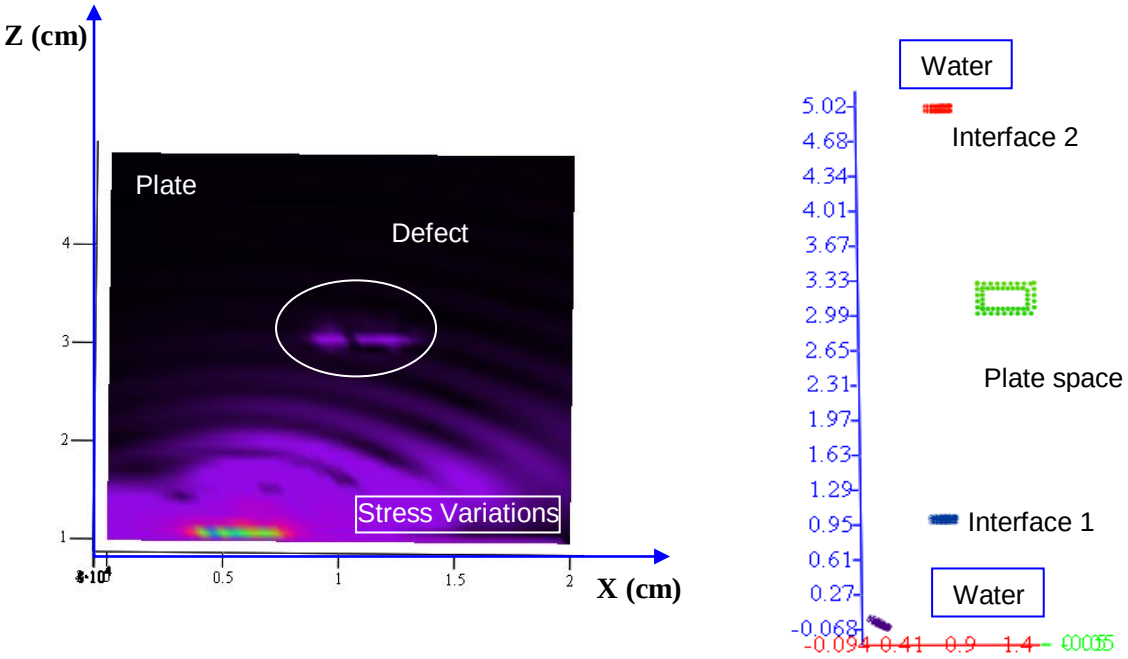

a) Stress distribution in plate with defect at location 1

Case 2, defect shape changes

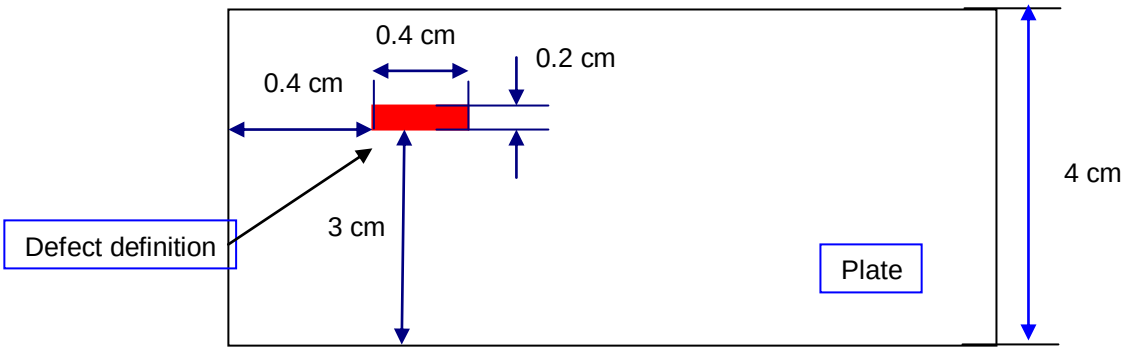

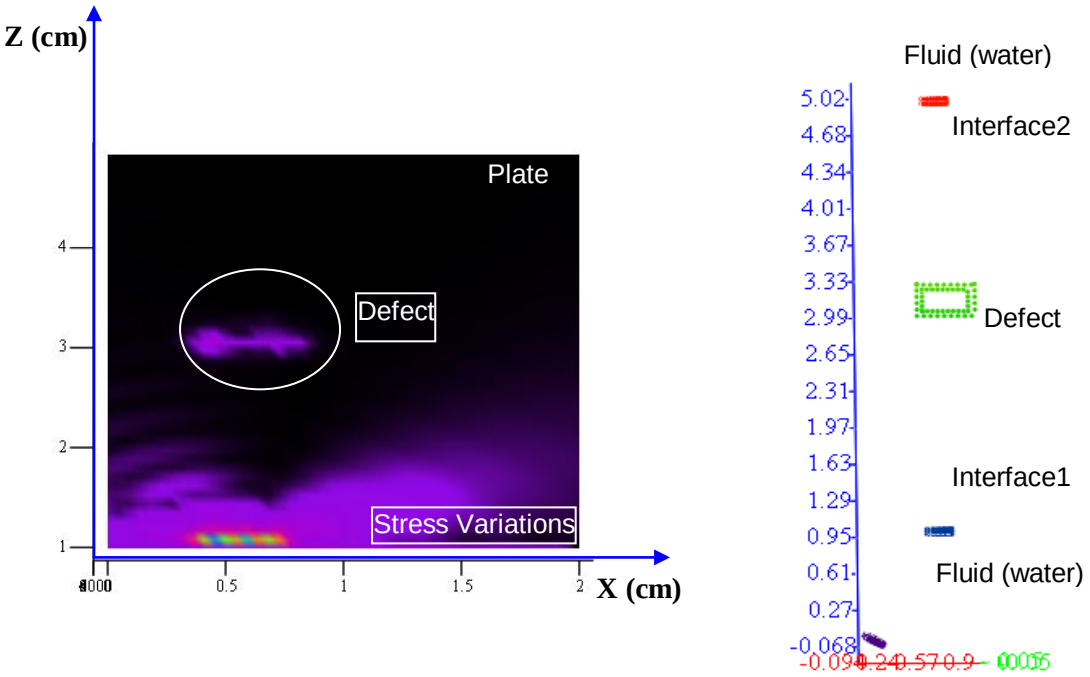

b) Stress distribution in plate with defect at location 2

Case 3, location and shape both changed

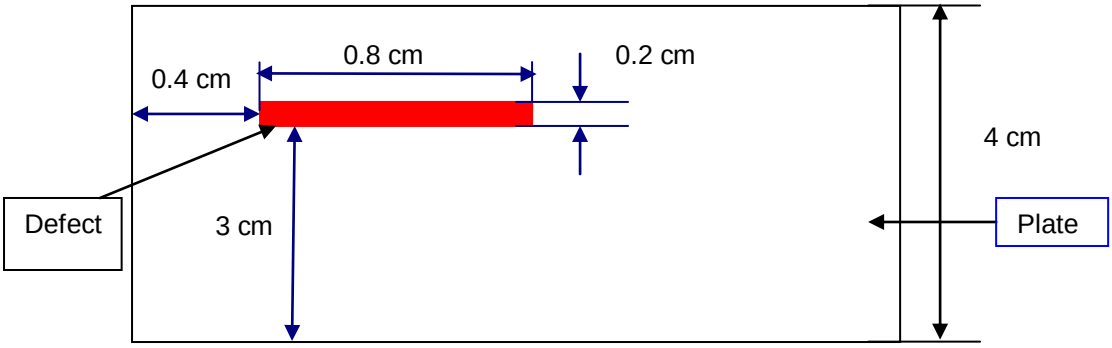

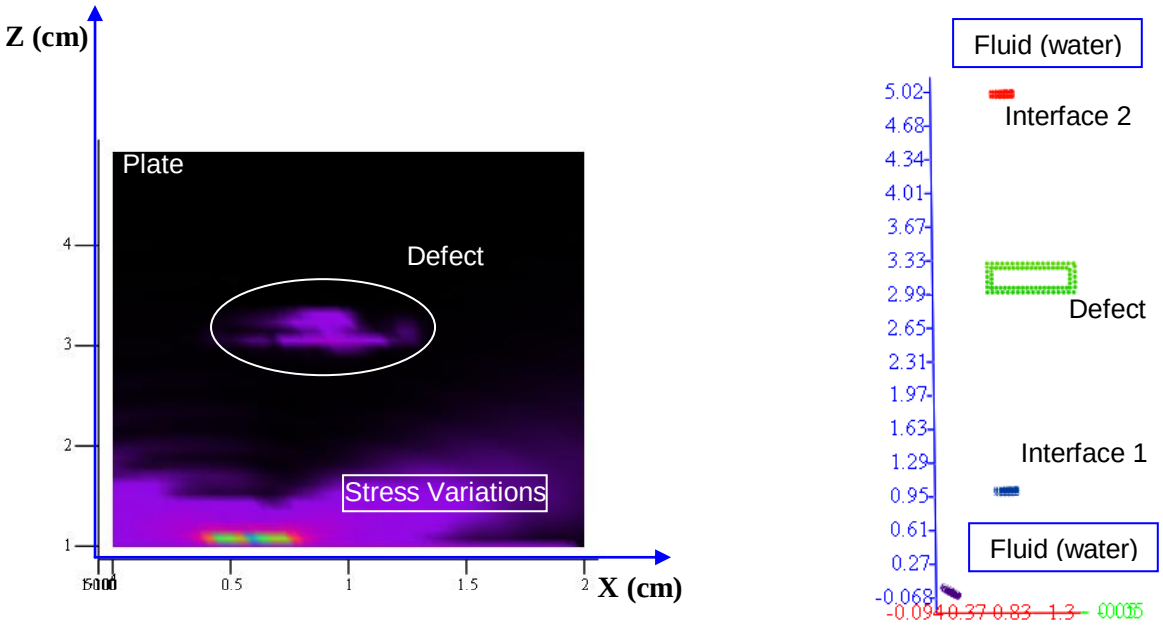

c) Stress distribution in plate with defect at location 3

Case 4, Shape and Location 4

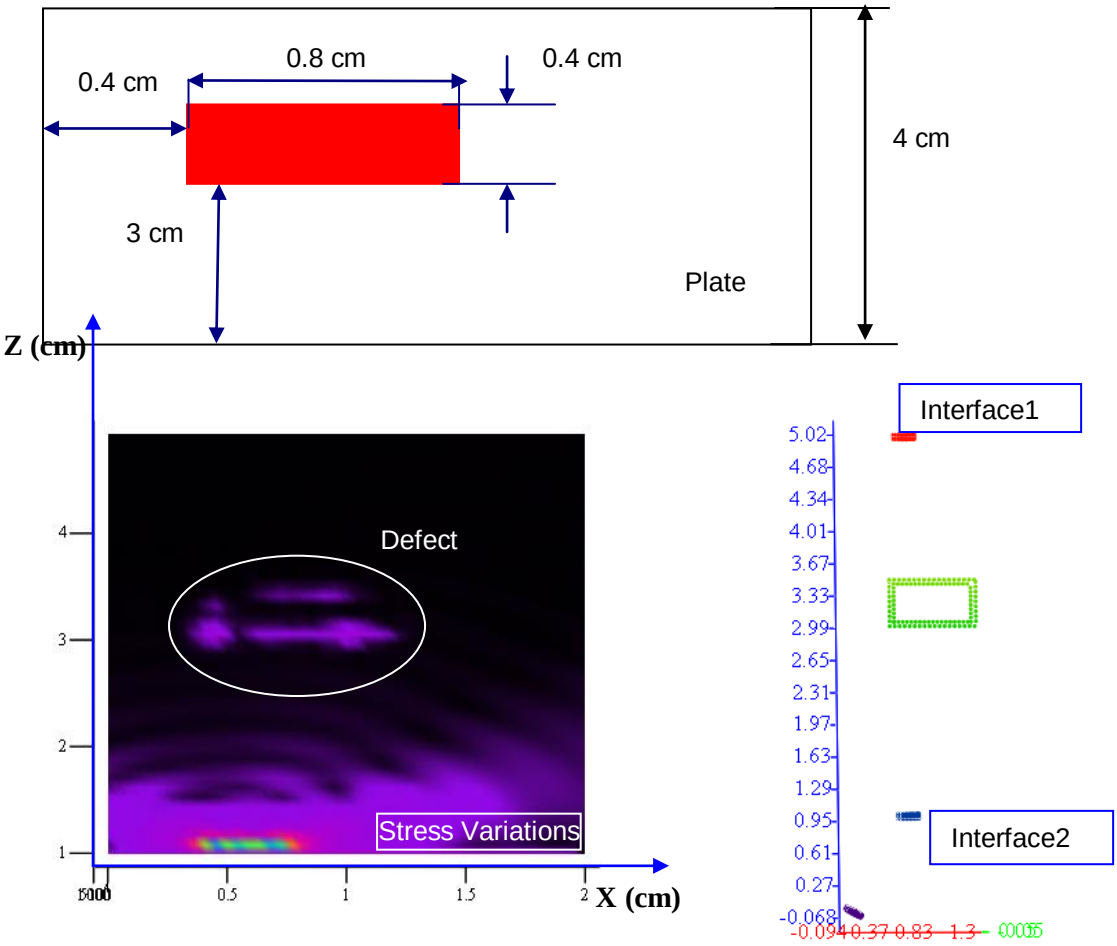

d) Stress distribution in plate with defect at location 4

Figure 5.48 Stress Distribution Graphs in Plates with Defects of Different Shape and Size and at Different Locations

5.10 Transient wave propagation while considering fluid solid interface.

5.10.1 Wave propagation in water:

For transient analysis of waves the same flow chart (refer fig 5.16) has been used.in this section only fluid space is considered. The input signal is tone burst (refer fig 5.17).in case of fluid the shear stress can not be generated hence pressure analysis has been done at different locations of target points.

At point 0 cm from transducer

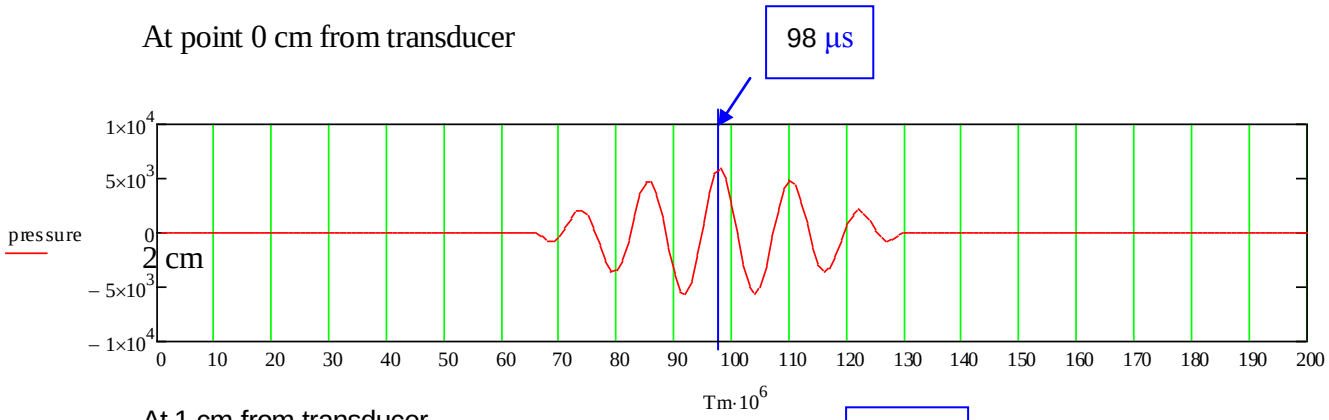

At 1 cm from transducer

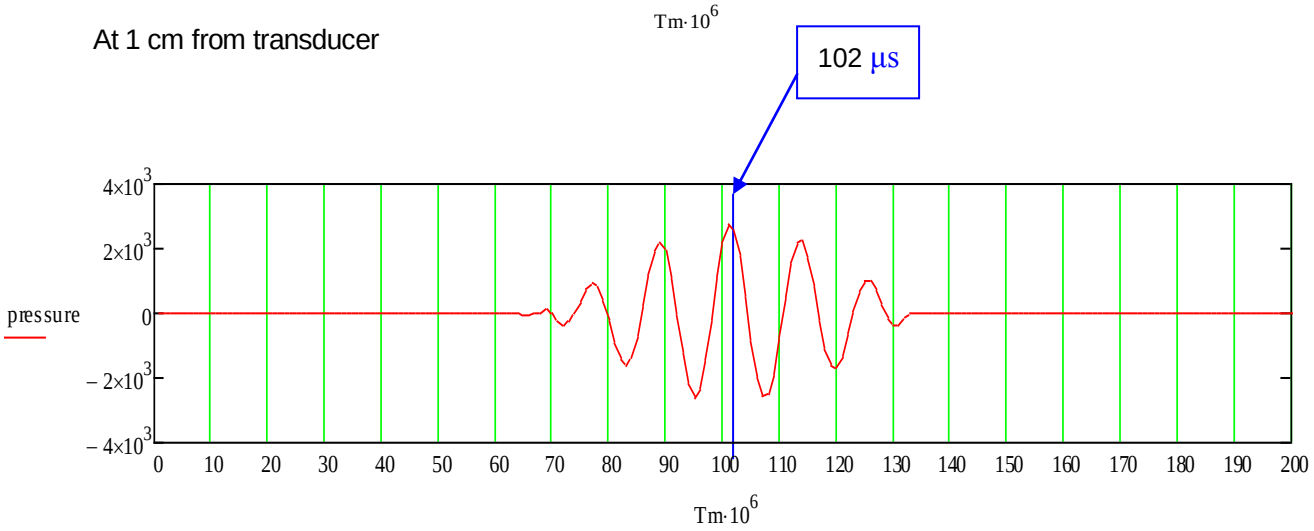

At 2 cm from transducer

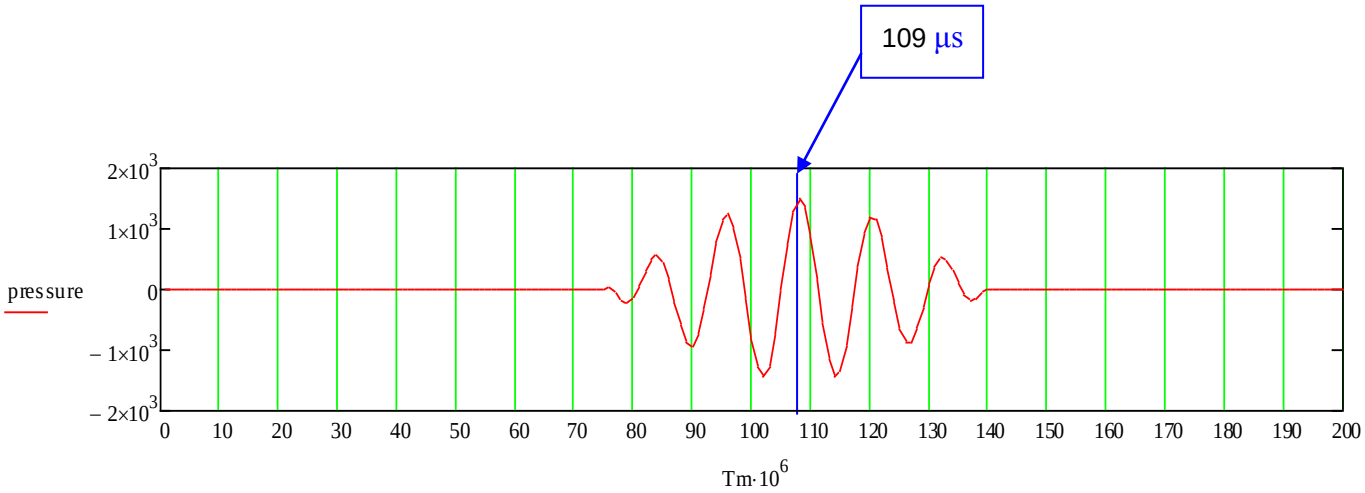

At 5 cm from transducer

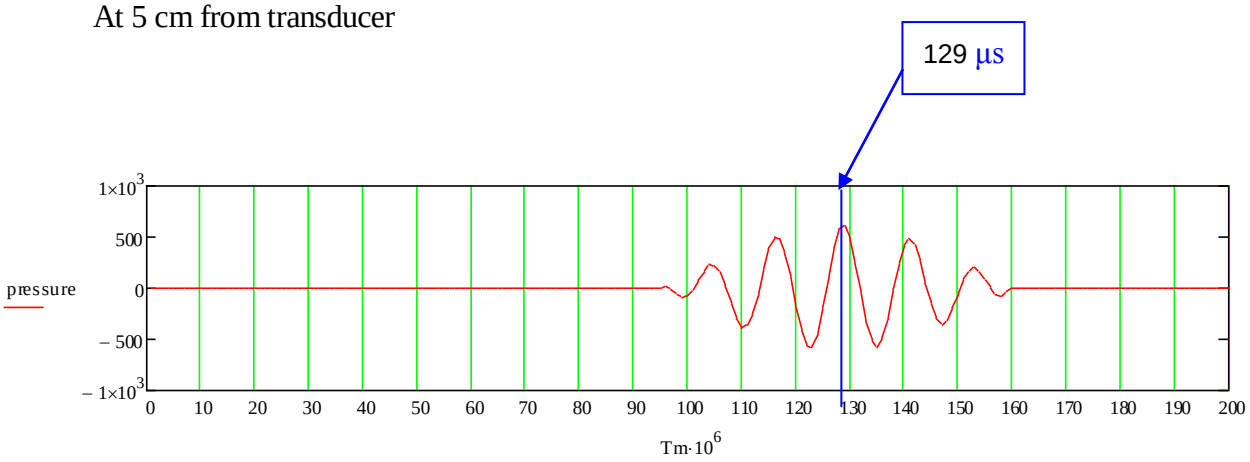

Figure 5.49 Transient Wave Propagation in Fluid

Method	Analytical	DPSM
Z=0 cm	-------	97 µs
Z=1 cm	102.6 µs	102 µs
Z=2 cm	109.45 µs	109 µs
Z=5 cm	129.2 µs	129 µs

Table 5.15 Transient Time Validation in Fluid When Fluid Solid Interface is considered

At 0. 2 cm above interface (interface is at 1 cm from transducer)

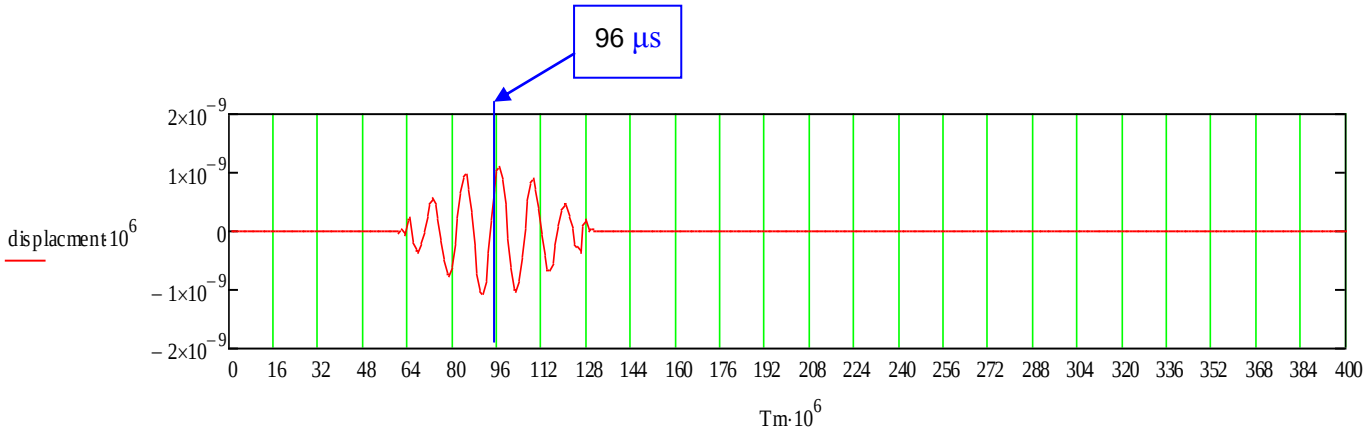

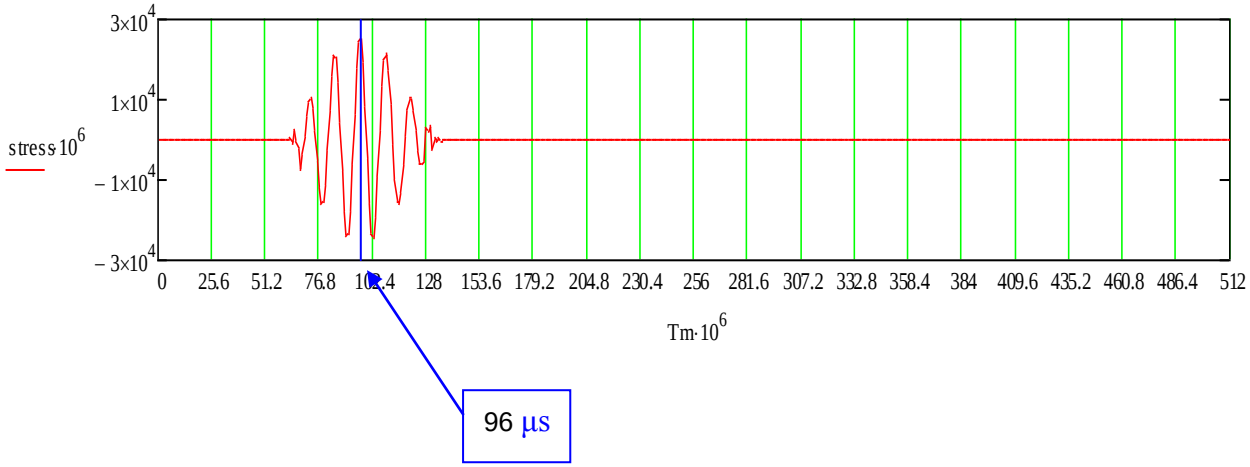

20 cm above interface (interface is at 1 cm from transducer)

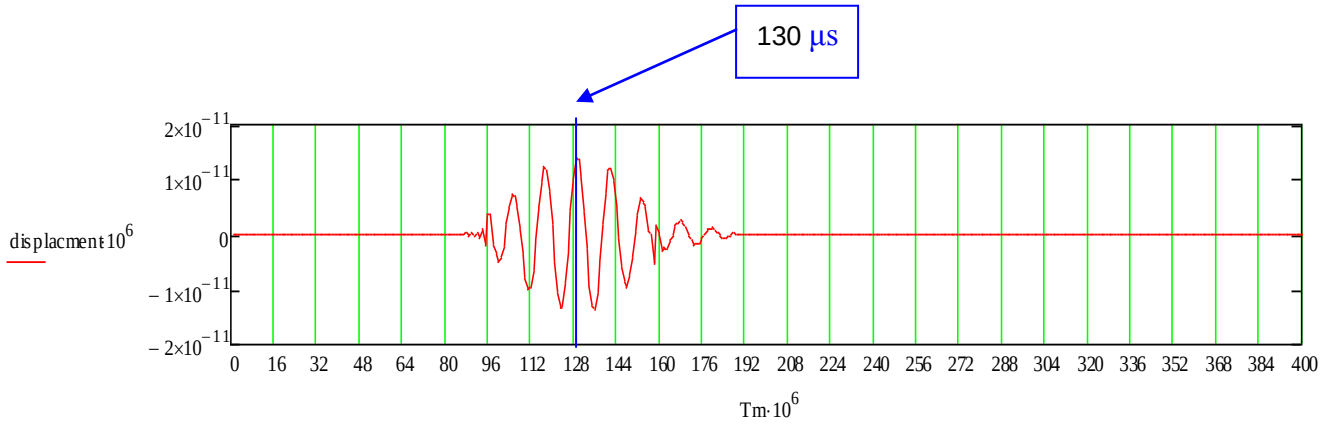

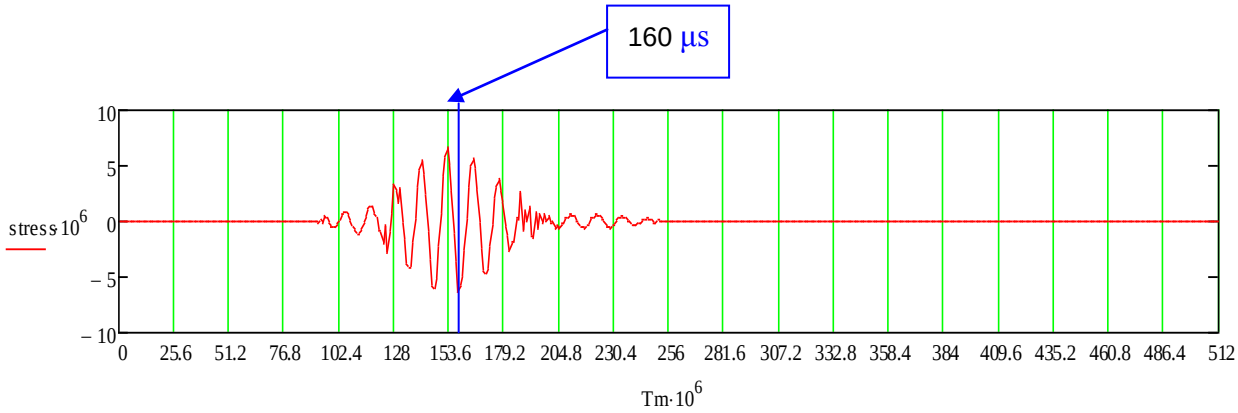

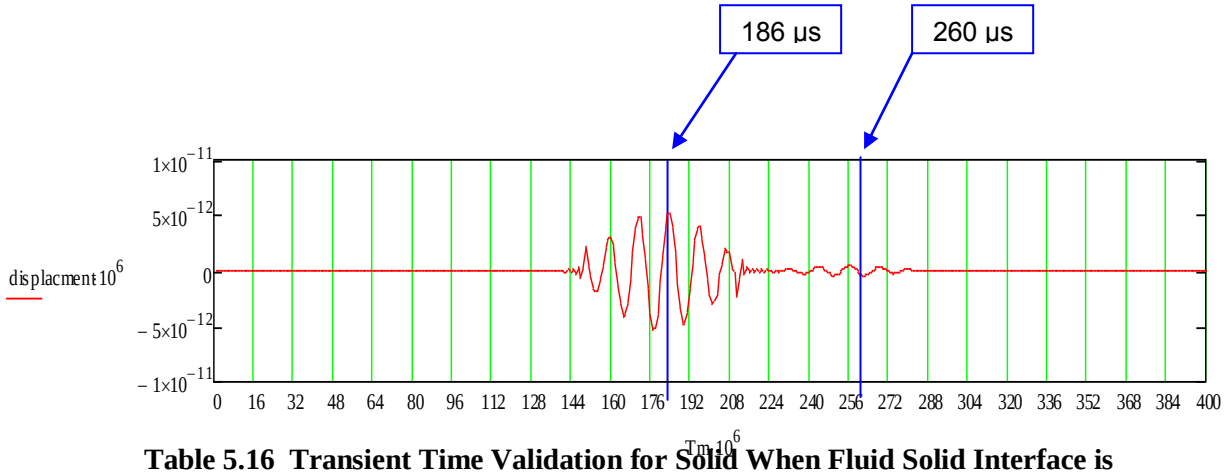

Table 5.16 Transient Time Validation for Solid When Fluid Solid Interface is considered

Method	Cp=5.66 km/sec	Cs =3.05 km/sec(STRESS)
Analytical (Z=20 cm)	200/5.66+98 = 131.2 μs	200/3.05+98=162 μs
DPSM	130 μs	160 μs
Analytical (Z=50 cm)	500/5.66+98 = 188.8 μs	500/3.05+98=260 μs
DPSM	186 μs	259 μs

Table 5.17Time Validation For Fluid/Solid Interface

Conclusion

The DPSM modeling presented in this work outlines an efficient technique for modeling homogeneous fluid, layered fluids, homogeneous solids, submerged plates with cracks, cavities and inclusions in half-space and plate structures. To model the ultrasonic waves in the solid structures are generated by finite size transducers directly attached incase of solid or immersed in the coupling fluid as in plates. Computed results clearly show that the propagating waves are significantly affected by the frequency, angle and diameter of transducers. While modeling fluids (homogeneous and non homogeneous) the transducers are kept at non normal incidence and its effects are calculated. In homogeneous solid field has been modeled with two different types of transducers (circular and rectangular) and the results clearly shows that the shape of transducer effects the distribution of stress in steady state but in transient state while conforming actual time of wave with the analytical time both tends to be same. Modeling near fluid solid interface has also been done in both steady and transient state. Once modeling of interface is done the study has been extended to its real world application. So interface modeling is effectively used to model field in plates completely submerged in water. Plates with and without anomalities are studied in both steady and transient state

Future Scope of work

- DPSM is a semi analytical technique therefore experimental validation is most important element. So the above developed model can be used for experimental validations for plates(with and without crack)
- For testing plates submerged in water guided waves are generated and recorded by reciever.Present model can also be used to validate the experimental results with theoretical results for testing of plates when both emitter and receiver are on one side of plate.
- The present model can be extended for modeling ultrasonic fields in corrugated plates.
- Can be used in petroleum exploring effectively.

REFRENCES

[1] Joseph L. Rose (2004) "*Ultrasonic Guided Waves in Structural Health Monitoring*" Trans Tech Publications, Switzerland

[2] Schmerr, L. W (1998) "*Fundamental of Ultrasonic Non-destructive Evaluation-A Modelling Approach"* (Plenum Press, New York)

[3] Bruck, H. A(2000) *"A one-dimensional model for designing functionally graded materials to manage stress waves"*, International Journal of solids and Structures.

[4]Ahmad, R., Kundu, T., Placko, D(2005) "*Modelling of Phased Array Transducers".* Journal of the Acoustical Society of America, Vol. 117, pp. 1762-1776

[5]Farrar, Charles R.; Keith Worden (2006). "*An introduction to structural health monitoring*". Philosophical Transactions of the Royal Society A (London: Royal Society Publishing)

[6] Christian Boller et al(2007) "*Fatigue in aero structures—where structural health monitoring can contribute to a complex subject"*philosophical transaction of raoyal society.

[7] Kim, J.-H., H.-S. Jeon, and C.-W. Lee, "Application of the modal assurance criteria for detecting and locating structural faults," in *Proc. 10th International Modal Analysis Conference*.

[8] Abrahams, I. D., Wickham, G. R., (1992), Scattering of elastic waves by a small inclined surface-breaking crack, *Journal of Mech. Phys. Solids*,

[9] Biwa, S., Yamamoto, S., Kobayashi, F., Ohno, N., (2004), Computational multiple scattering analysis for shear wave propagation in unidirectional composites,*International Journal of Solids and Structures*, 41, 435–457

[10] Joshi, S., Mukherjee, A., and Schmaudar S (2003) *"Numerical*

characterization of functionally graded active materials under electrical and thermal fields", Smart Materials and Structures, 12, 571-579

[11] Krawczuk, M., Palace, M., Ostachowicz, W., (2004), Wave propagation in plate structures for crack detection, *Finite Elements in Analysis and Design*.

[12] Samadhiya, R. And Mukherjee, A (2006*) "Functionally graded piezoceramic ultrasonic transducers",* Smart Materials and Structures.

[13] Ahmad, R., Kundu, T., Placko, D(2003) *"Modeling of the Ultrasonic Field of Two Transducers Immersed in a Homogeneous Fluid Using Distributed Point SourceMethod"*. I2M (Instrumentation, Measurement and Metrology) Journal; Vol.3, pp.87-116

[14] Ahmad, R., Kundu, T., Placko, D(2005) "*Modeling of Phased Array Transducers"*.Journal of the Acoustical Society of America, Vol. 117, pp. 1762-1776

[15] Banerjee, S., Kundu, T., Placko, D(2005) "*Ultrasonic Field Modelling in Multilayered Fluid Structures Using DPSM Technique",* ASME Journal of Applied Mechanics

[16] Banerjee, S., Kundu, T.,Alnuaimi.N,(2007) *"DPSM technique for ultrasonic field modeling near fluid-solid interface",* Journal of ultrasonics ,46,235-250.

[17] Banerjee, S., Kundu, T.(2007) "*Ultrasonic field modeling in plates immersed in fluid*", International Journal of solids and Structures,44,6013-6029

[18] Banerjee, S., Kundu, T.(2007) "*Ultrasonic field modeling in plates immersed in fluid with internal anomalies in it*", science direct, July 2007